

**Identifying genetic targets of *Tau* toxicity in Frontotemporal
Dementia *Drosophila* model**

Eve G. Lowenstein

A Dissertation in partial fulfillment of the requirements for the degree
of Doctor of Philosophy

Presented to the Department of Molecular and Medical Genetics
Oregon Health & Science University
School of Medicine

July 2024

School of Medicine
Oregon Health & Science University

Examination Committee

Doris Kretzschmar, PhD	Co-Mentor
Andrew Adey, PhD	Co-Mentor
Lucia Carbone, PhD	Committee Chair
Vivek Unni MD, PhD	Committee Member
Cheryl Maslen, PhD	Committee Member
Ian Martin, PhD	Committee Member

Table of Contents

List of Figures	vi
List of Tables	x
List of Abbreviations	xi
Acknowledgements	xiii
Abstract	xvii
Chapter 1: Introduction	1
Frontotemporal Dementia	2
Modeling Tauopathy	7
<i>Drosophila</i> Tauopathy Models	9
Actin Dynamics in Aging and Tauopathy	12
Neurodegeneration and the Nucleus	16
Single-cell Genomics in Dementia Research	21
Overview	24
Chapter 2: Materials and Methods	28
Data Presentation	29
<i>Drosophila</i> Stocks and Care	29
Single-cell combinatorial indexing ATAC-seq.....	35
Nuclei Isolation.....	35
Nuclei Tagmentation (Tn5) and Combinatorial Indexing using PCR	37
Sequencing Data Processing	38
Analysis.....	40
Single-nuclei RNA-seq	42

Nuclei Isolation and 10X Chromium	42
Analysis.....	42
Phototaxis.....	43
Western Blot.....	44
Sleep	45
Neurodegenerative vacuoles	46
Rough eye	46
Body Weight, Lipid Droplets and Metabolic Map	47
Chapter 3: Expression of actin-related gene, Fhos, in the fat body modifies behavioral toxicity of FTD-associated K369I Tau mutation.....	49
Introduction	50
Results	52
Disease-associated FTD mutants alter levels of heterochromatin protein 1	52
Chromatin accessibility and gene expression changes in FTD-associated mutants	55
FTD mutant hTau ^{K369I} has reduced locomotor drive in aged females	66
Fhos overexpression in the fat body induces decreased locomotor drive in aged flies....	66
Fhos manipulation in fat body alters locomotor drive in hTau flies	68
Sleep fragmentation and decreased nighttime sleep in aged hTau ^{K369I} flies.....	73
Fhos manipulation modifies sleep fragmentation in hTau ^{K369I}	74
Discussion	79
Supplemental.....	84
Chapter 4: Additional studies on candidate genes from single-cell genomics sequencing.....	95
4.1 Validation of cell-type specific behavioral effects in Tau and Fhos genetic interaction.....	96

Experimental Rationale	96
Results and Discussion	97
Fos manipulation in glial cells	97
Fos manipulation in neurons	113
4.2 Patterns of Neurodegeneration in hTau^{K369I} FTD mutant	124
Experimental Rationale	124
Results and Discussion	126
4.3 Screening differentially expressed candidate genes for genetic interaction with FTD-associated hTau^{V337M} mutant	130
Experimental Rationale	130
Results and Discussion	132
4.4 Model of Fat Body Metabolic Dysregulation in hTau^{K369I} FTD mutant.....	145
Experimental rationale	145
Results and Discussion	146
Glycolysis and Oxidative Phosphorylation	146
Glutathione.....	146
Lipogenesis, Lipolysis and Insulin Signaling	147
Alterations in body weight of hTau ^{K369I} flies	151
Conclusion	159
Chapter 3: Summary and Future Directions	160
Chapter 4: Summary and Future Directions	164
In sum.....	169
References	171

List of Figures

Figure 1: FTD mutants recapitulate disease phenotypes seen in patients with aging.	12
Figure 2: Schematic of single-cell genomics candidate discovery and validation through genetic interaction behavioral experiments.	26
Figure 3: Overview of dissertation by experimental assay and age of flies.	27
Figure 4: Tissue-specific expression using the UAS/GAL4.	30
Figure 5: Temporal tissue-specific expression with the UAS/GAL4/GAL80ts system.	32
Figure 6: Recombination crossing scheme to create AkhR-Gal4 or loco-Gal4 with hTau transgenic lines.	33
Figure 7: Schematic of single-cell experimental workflows.	36
Figure 8: hTau^{K369I} variant increases the levels of HP1α in 30-day old flies.	54
Figure 9: Cell-typing of single-cell genomics of FTD-associated mutants in Drosophila model.	61
Figure 10: Differentially accessible peaks and gene expression in FTD-associated mutants compared to hTau^{WT} in day 5 shows changes within the fat body cluster.	63
Figure 11: Early change in chromatin accessibility at day 5 within hTau^{K369I} in the Fhos gene translates to increased expression, specifically in the fat body and neuronal clusters.	65
Figure 12: <i>Fhos</i> overexpression and knockdown alters locomotor drive in the fat body.	72

Figure 13: Overexpression and knockdown of <i>Fhos</i> results in changes in sleep fragmentation in aged female flies.	79
Supplemental Figure 1: Quality control metrics for sciATAC-seq and snRNA-seq experiments.	85
Supplemental Figure 2: Coverage of sciATAC-seq reads within the dTau locus.	86
Supplemental Figure 3: Number of accessible peaks by cell type for each strain compared to hTau^{WT} heterozygous in 5-day old heads.	88
Supplemental Figure 4: Increased accessibility within <i>Fhos</i> gene in hTau^{K369I} homozygous and dTaudel in fat body of aged flies.	89
Supplemental Figure 5: Heterozygous hTau^{K369I} flies display decreased locomotor drive and fragmented sleep quality in aged females.	91
Supplemental Figure 6: <i>Fhos</i> overexpression in the fat body increases daytime sleep in aged females.	92
Supplemental Figure 7: <i>Fhos</i> knockdown in the fat body increases daytime and decreases nighttime sleep in hTau^{K369I} in aged males.	93
Figure 14: Heterozygous hTau^{K369I} females have reduced locomotor drive when aged at 29°C.	104
Figure 15: <i>Fhos</i> overexpression and knockdown in glia reduces locomotor drive in aged flies.	106
Figure 16: <i>Fhos</i> knockdown in glia leads to increased sleep fragmentation in hTau^{K369I} aged flies.	108

Figure 17: <i>Fhos</i> overexpression in glia increases daytime sleep in aged females.....	109
Figure 18: <i>Fhos</i> overexpression in glia increases daytime sleep and knockdown in glia decreases nighttime sleep in the hTau^{K369I} mutant males.	111
Figure 19: Knockdown of <i>Fhos</i> in neurons decreases locomotor drive in aged flies.	118
Figure 20: Overexpression and knockdown of <i>Fhos</i> in neurons worsens sleep fragmentation in females.	121
Figure 21: Duration of sleep is minimally impacted by <i>Fhos</i> overexpression and knockdown in neurons in aged females.....	122
Figure 22: <i>Fhos</i> knockdown in neurons can impact nighttime sleep duration in aged hTau^{WT} males.....	123
Figure 23: Neuroanatomical organization of <i>Drosophila</i> adult brain.	125
Figure 24: Neurodegenerative vacuoles in hTau^{WT} and hTau^{K369I} <i>Fhos</i> flies.	129
Figure 25: Schematic of expression system for rough eye screen.....	131
Figure 26: <i>Fhos</i> overexpression exacerbates hTau^{V337M} retina neurotoxicity.	137
Figure 27: Apolipoproteins <i>apolpp</i> and <i>apoltp</i> do not alter hTau^{V337M} retina neurotoxicity.	138
Figure 28: Insulin receptor <i>InR</i> modifies hTau^{V337M} retina neurotoxicity... 	139
Figure 29: <i>Gyf</i> overexpression rescues hTau^{V337M} retina neurotoxicity. ...	140

Figure 30: <i>Xrp1</i> overexpression results in glazed rough eye phenotype, which is worsened with hTau^{V337M} co-expression.	141
Figure 31: <i>klar</i> overexpression may increase rough eye phenotype in hTau^{V337M}	142
Figure 32: Candidate genes from differential expression analysis in the fat body cluster with subtle or no rough eye phenotype.	143
Figure 33: Metabolic map of differentially expressed genes in hTau^{K369I} fat body cells from 5-day old flies with genes involved in insulin signaling, lipid dynamics, glycolysis, and mitochondrial function.	150
Figure 34: hTau^{K369I} mutation modifies body size in females and males... ..	156
Figure 35: <i>Fhos</i> overexpression in the fat body increases body weight in aged female hTau^{K369I} mutant.....	157

List of Tables

Table 1: List of genotypes and descriptions.	34
Table 2: Marker gene list for cell-type identification.	41
Table 3: Rough eye phenotypes in differentially expressed genes in hTau^{K369I} from the fat body cluster.....	136

List of Abbreviations

AD - Alzheimer's disease

AkhR - Adipokinetic hormone receptor

ALS - amyotrophic lateral sclerosis

ArchR - single-cell chromatin analysis software

bvFTD - behavioral variant FTD

cDNA - complementary DNA

CRISPR/Cas9 - Clustered Regularly Interspaced Short Palindromic Repeats/
CRISPR-associated protein 9

CS - Canton-S

DA – differential accessibility

DE – differential expression

DNA - deoxyribonucleic acid

dTau - Drosophila Tau

dTaudel - Drosophila Tau deletion

F-actin - filamentous actin

FC - fold change

FDR - false discovery rate

FHOD - Mammalian Formin Homology 2 Domain Containing

Fhos - Drosophila Formin homology 2 domain containing

FTD - Frontotemporal dementia

G-actin - globular actin

GAL80ts - GAL80 temperature sensitive

H3K9me3 - histone 3 lysine 9 trimethylation

HP1 α or HP1 - Heterochromatin Protein 1

hTau - human Tau

hTau^{K369I} - human Tau with amino acid 369 lysine to isoleucine mutation

hTau^{P301L} - human Tau with amino acid 301 proline to leucine mutation
hTau^{V337M} - human Tau with amino acid 337 valine to methionine mutation
hTau^{WT} - human Tau wildtype
iPSC - induced pluripotent stem cell
LINC complex - linker of the nucleoskeleton and cytoskeleton complex
mRNA - messenger RNA
NIB - nuclei isolation buffer
PCR - polymerase chain reaction
RFP - red fluorescent protein
RNA - ribonucleic acid
RNAi – RNA interference
SAHF - senescent-associated heterochromatin foci
sciATAC-seq - single combinatorial indexing assay for transposase-accessible chromatin with sequencing
SEM - standard error of the mean
seq - sequencing
snRNA-seq - single-nuclei RNA sequencing
Tau 1N4R - Tau isoform with one N domain and 4 R domains
Tau or MAPT - Microtubule-associated protein tau
Tn5 - transposase used in sciATAC-seq
TSS - transcription start site
UAS/GAL4 - tissue-specific expression driver
UAS/GAL4/GAL80ts – tissue- and temporal-specific expression driver
UMAP - uniform manifold approximation and projection
UTR - untranslated region
WT - wildtype

Acknowledgements

For all the fruit fly enthusiasts and fruit flies out there. At times I was a *nwk*, but the lessons you learn in graduate school are *tim_{per}*. Many experiments were *fru*, but we are taught to be like Dory from Finding *nmo* to not get *drl*. It was *ro* this past year but for the most part, it was pretty *pain* thanks all of you. First, I would like to thank my mentors, Doris Kretzschmar and Andrew Adey, for letting me follow my interests, and allowing a young untested graduate student to start a joint lab project in areas outside her expertise. Thank you to Amanda McCullough and Mushui Dai for making the genetics program a welcoming and compassionate environment. Special thanks to Amanda, who checked throughout COVID to make sure both myself and my project were running smoothly, as well as always bringing me gluten free goodies. Thank you to Monica Hinds for securing funding so that I could attend OHSU. Lastly, Cheryl Maslen, Vivek Unni, and Lucia Carbone for helping me think critically about my work, for being understanding when my project flipped on its head, for understanding that my career path was ever evolving, and thank you to Ian Martin, my external reader. Emily Hillhouse, thank you for encouraging me. Similarly, without Zoe Speidel's wise words, I would have been in writing purgatory for much longer. Jackie Wirz, for her guidance and help finding my way. Amy Forester, for the Training Future Faculty program and ongoing support.

I was extremely lucky to work with so many fantastic people. Special thanks to Dani for running the sleep studies and providing many hours of their time to help me. Alex, for all your knowledge and of course for birding with me. There is no better way to procrastinate preparing for my seminar presentation than staking out

for a Rose Breasted Grosbeak. One day I will find the Scissor Tailed Flycatcher. Rachel, thank you. All of us need someone to commiserate with and help us through those mundane days in lab, I'm so glad you joined. To the whole Kretzschmar lab, I love that we spent comparable time talking about science as we did our dogs in lab meeting. As we should. Ryan and Casey, you were the best lab mates that anyone could hope for, thank you for sharing your scripts as well as answering all questions and putting my worries about quals in perspective. Andrew Nishida, I cannot fully emphasize how much you helped and guided me. Thank you for the many hockey games, feeding me through the Rad Pantry and the countless hours of analysis help sessions. Kevin, thank you for your friendship and sharing your bioinformatics acumen. Andy, thank you for everything, especially your patience with me in lab. Thank you to Sonia and Cierra for bringing the labs together. Lauren, although we haven't known each other long, your help with my manuscript storyboarding helped me overcome my writers block and get started. Lastly, thank you to all the students who have worked with me in the lab (Lyla, Erin, Anneliese and Andres).

Thank you to Stephen Moore for creating a wonderful environment to learn in journal club, which has been a constant source of laughs and support. Cheers to Elephants Mimosas. Anne, Michael, and Shannon, thank you for adopting me into your cohort and your willingness to engage and discuss *Drosophila* genetics. Homma, Tyler, Lauren, Thomas, and Colin (and Taylor), you are all amazing humans, and I am so privileged to have gone on this journey with you. Thank you for the Thai Yummy lunches, working with me to set up the Student Learning

Center, and the boardgame lunches. Special thanks to Colin for being willing to read my writing and helping me improve my presentation skills. Lastly, thank you to all GRU executives for all their thankless work.

I have been spoiled by wonderful teachers who have shaped my values and interest in science. Mr. D, I am nervous for my defense, but I will reframe it as an OTP. Veronica, I didn't know it in high school, but you were preparing me for my PhD. Iva and Paul, I would have peaced out after Calc III. Thank you for creating a plan for me to pursue math and encouraging me but not frosting a cardboard cake and sticking a smile on it. Casey and Dr. Kuo, OChem was the best and it isn't opposite day, and I haven't had a Pabst. Also, Dr. Kuo, thank you for stopping by my "office" space in Olin to chat. Yung-pin and Janis, thank you for showing me that exams can be fun and challenging. Norma, your enthusiasm and patience for me and my project was the main reason I pursued a PhD. Without your tremendous dedication to my education and future, I would not be here. You showed me how to think as a scientist while also encouraging my development as a mathematician. Thank you for guiding me through my honors thesis and supporting me in the loss of my peers. Forever thankful that we met at the cookie table at community chorale.

Gloria and Jeannette, your wisdom and guidance has changed how I see myself as a teacher and human. Thank you for bolstering my confidence and always lending an ear when grad school was all consuming. And of course, to all the Budz, Good Vibes to the Evening. Emily, Dani, and Shannon, you all inspired me to keep putting words on the page when I thought there was nothing worth saying. Thank you, Emily, for the long hours at Jola while I wrote this dissertation,

keeping me on track and your eternal positive energy. Mehtab, a lot has happened since our first days at OHSU and I'm so glad we were able to support each other as we navigated our programs. I am so grateful for your friendship. Thank you to all my remarkable friends from LC: Emily, Mehtab, Naomi, Mako, Burnley, Marianne, Amanda, Erin, and Riley. To Erin and Riley, I aspire to live everyday with the curiosity that you brought to lab and everything you pursued. Riley said it best, "Catch you on the flau flau."

I have received so much love and support from my family and friends. Dad, thank you for bestowing me with a love of learning. Mom, thank you for all the phone calls, check-ins, and dog photos to keep me smiling through the hard days of graduate school. Sarah, thank you for being the absolute best, believing in me, feeding me, and I owe you for life for bringing me Olive. I love you all so much! To my grandparents, you live a life again within all of us. To all the dogs who have given me so much unconditional love.

David and Olive, thank you for holding everything together and for helping me not take things too seriously. Especially Olive, for cleaning the yoga mats every night. I'm unbelievably happy with the life we have created together and can't wait for our next chapter. David summed up this dissertation when helping me photograph the rough eye phenotype: "so you messed with the flies and the flies got messed up." Thank you, David, for giving me the perfect elevator speech for my job interviews.

Abstract

Frontotemporal dementia (FTD) is a neurodegenerative disease associated with mutations in the microtubule binding protein Tau. The clinical presentation of FTD is heterogeneous with patients exhibiting a range of parkinsonism, dementia, atrophy in the temporal lobes, and personality changes. Treatments are limited to mitigation of behavioral changes associated with FTD, but nothing exists to slow the progression of disease. In our lab, we model FTD using *Drosophila*, which allows us to conduct longitudinal studies to observe FTD progression throughout the adult lifespan. Our FTD models show pathogenic phenotypes associated with tauopathies. Recent work in model systems and post-mortem tissue has shown that expression of FTD-associated mutant Tau may lead to epigenetic modifications that alter gene expression. In Chapter 3 of this dissertation, we utilize single-cell sequencing techniques to probe chromatin accessibility and gene expression to assess human Tau FTD mutations in young and aged adult *Drosophila*. Comparing the wildtype hTau to the FTD mutants revealed differentially accessible regions in all cell populations, and notably many in the fat body. *Fhos*, an actin nucleation gene, was increased both in accessibility and expression within the fat body of the hTau^{K369I} mutant. To validate our finding, we manipulated the expression of *Fhos* within the hTau^{K369I} mutant and characterized behavioral phenotypes. In Chapter 4, we highlight the cell-type specific *Fhos* phenotypes in the hTau^{K369I} mutant, present preliminary work on possible regions of neurodegenerative susceptibility, screen additional hits from the sequencing experiments and review the metabolic changes that could be impacting neuronal function.

Chapter 1: Introduction

Frontotemporal Dementia

Cases of dementia are projected to triple by 2050 to 130 million worldwide (Prince et al., 2015). The identification of early markers and preventative care measures are necessary to alleviate the economic and personal burdens that accompany dementia. The progressive memory loss associated with dementia impacts patients' ability to function in daily life. Other symptoms also impact the quality of life for both patients and their families, including sleep disruption, depression, personality changes, apathy, hyperphagia and locomotor changes (Cardarelli et al., 2010). Current treatments can mitigate aspects of the behavioral changes associated with FTD; however, no therapies are available to slow the progression. Therefore, increasing our understanding of early biomarkers of disease progression will be key to creating targeted therapies to help slow the progression of disease.

Frontotemporal dementia (FTD) is a broad classification for three main neurodegenerative diseases based on atrophy in the frontal and temporal lobes of the brain: behavioral variant FTD (bvFTD), semantic dementia, and progressive non-fluent aphasia. The frontal and temporal lobes of the brain are responsible for our executive functioning, which includes planning, organizing, personality, movement, speech, emotions, and memory (Ghetti et al., 2015). The clinical presentation of FTD is heterogeneous with patients exhibiting a combination of parkinsonism, dementia, depression, hyperorality, sleep disturbances and personality changes (sleep disturbances are expanded on in Box 1; McCarter et

al., 2016). With an insidious onset and similarity to other neurodegenerative and psychiatric disorders, diagnosis of FTD can be difficult (Elahi and Miller, 2017).

Box 1: Sleep disturbances in dementia patients

Sleep disturbances are common in patients with mild cognitive impairment (Beaulieu-Bonneau and Hudon, 2009). Sleep disruption in dementia patients is a strain on caregivers and negatively affects quality of life for many dementia patients. Sleep is one of the most cited reasons for families choosing to move elderly relatives into care facilities, which increases the economic burden of the disease (Pollak and Perlick, 1991). Sleep is important in memory consolidation and for clearance of metabolites from the brain (Kang et al., 2009; Rasch and Born, 2013; Roh et al., 2012). Sleep disturbances have been shown to lower the effectiveness of metabolite clearance in mice leading to increased amyloid beta accumulation in the brain (Kang et al., 2009; Roh et al., 2012). Therefore, researchers have postulated that perhaps sleep disturbances could precede neurodegeneration. Whether sleep could be harnessed for preventative care is unclear but hopefully, the dissection of how sleep modulates disease progression could help lead to earlier detection. Targeted therapies to improve sleep hygiene and monitoring of the aging population for sleep disruptions could help to mitigate the dementia crisis in the coming decades and improve quality of life for patients living with these disorders.

There are known causal genes associated with FTD (*MAPT* or *Tau*, *C9orf72*, *GRN*, *TBK1*, *SQSTM1*, *TARDBP*), as well as a host of risk genes that have been implicated in FTD (Sirkis et al., 2019). *C9orf72* (20-30%), *Tau* (5-20%) and *GRN* (5-25%) have the highest mutation frequency in familial FTD (Sirkis et al., 2019). These estimates are likely to change in the coming years as more patients are sequenced across the world and our ability to connect these mutations to diagnostic labels improves. A 2020 metaanalysis of case studies and patient data from centers involved in the Frontotemporal Dementia Prevention Initiative found that the disease diagnosis, age of onset and age of death varied for patients with mutations in *Tau*, *GRN* and *C9orf72* (Moore et al., 2020). The most common disease diagnosis for patients with *Tau* mutations was bvFTD (44.8%) followed by

unspecified dementia (34.6%) and then Parkinson's disease (4.9%). Patients with *GRN* mutations were also diagnosed with bvFTD and unspecified dementia (37.8% and 30.6%, respectively), but the next highest classifications were non-fluent variant primary progressive aphasia (9.1%) and Alzheimer's disease (AD; 8.2%). In contrast, the *C9orf72* genetic group had 30.3% of patients diagnosed with either amyotrophic lateral sclerosis (ALS) or FTD/ALS. These data highlight the spectrum of patient symptoms and variability of diagnosis even within the same genetic grouping. Patients with mutations in *Tau* exhibited the lowest age of onset and death compared to the *GRN* and *C9orf72* patients. The average age of onset for FTD patients with a *Tau* mutation is 49 years of age with a life expectancy of 8.5 years after diagnosis (Ghetti et al., 2015). However, both age of onset and death is highly variable depending on the genetic group and mutation, as well as whether patients have ALS or parkinsonism pathology within the broader classification of FTD.

In this dissertation, we focus on FTD-associated mutations in *Tau*. There are more than 50 known *Tau* mutations that have been found associated with FTD (Sirkis et al., 2019). In healthy brains, *Tau* aids in microtubule assembly and stabilization to maintain axonal integrity and transport (Sotiropoulos et al., 2017). *Tau* is found hyperphosphorylated and aggregated in neurofibrillary tangles of FTD and AD patients (Ghetti et al., 2015). *Tau* has six isoforms and some FTD mutations effect splicing of exons 2, 3 and 10, and thus dictate which isoforms are expressed (Ghetti et al., 2015). Part of the clinical variability of FTD is thought to depend on to which isoform of *Tau* is expressed (Ghetti et al., 2015). In the adult

brain, the ratio of isoforms with either three or four microtubule binding regions are roughly equal (3R or 4R; Ghetti et al., 2015). In FTD, this ratio can be altered depending on the *Tau* mutation (Liu and Gong, 2008). The mutations can also alter phosphorylation of Tau and interfere with microtubule binding (Sotiropoulos et al., 2017). Even within the same mutation, there is inconsistency in clinical symptoms, age of onset and life expectancy in patients. Published case studies of familial and sporadic cases of FTD emphasize the variability of clinical presentation between patients. In this dissertation, we focus on three clinically distinct *Tau* mutations (P301L, V337M and K369I). Case reports for each mutation are described in Box 2.

Box 2: Case reports of FTD patient disease progression

Case A: Patient with P301L *Tau* mutation with initial symptom of apathy.

One case report from Japan in 2018 describes a patient with the P301L mutation in *Tau* that was sequenced post-mortem (Miki et al., 2018). Upon autopsy, the pathology showed ballooned neurons with 4R *Tau* positive inclusions. Originally, the patient exhibited apathy at age 51, which then resulted in him losing his job. He had no indications of memory impairment, parkinsonism, loss of inhibition/insight or change in living conditions, but was found to have frontal lobe atrophy. At age 55, he developed speech impairment and parkinsonism. The patient died of pneumonia at age 60 with a diagnosis of unspecified dementia. Miki et al. (2018) underscores that the clinical symptoms until the middle stage of the disease were inconsistent with FTD, but were more similar to a psychiatric disorder. Other clinical cases with P301L mutations from the literature outlined by Miki et al., (2018) showed personality changes, disinhibition, parkinsonism, memory impairment, speech changes, depression, or apathy as initial symptoms.

Case B: Family with V337M *Tau* mutation with variability onset and duration.

Over four generations, there were 18 affected family members with an average age of onset of 51.5 years and average duration of illness of 13.8 years (Poorkaj et al., 1998; Domoto-Reilly et al., 2017). The initial symptoms were “social withdrawal and reclusiveness, suspiciousness and paranoid ideas, auditory hallucinations, and bizarre compulsive activities sometimes associated with aggressive behavior” (Domoto-Reilly et al., 2017). Later symptoms included “hyper oral behaviors, increased muscle tone, mutism, and myoclonic jerks” (Domoto-Reilly et al., 2017). Domoto-Reilly et al. (2017) followed up on family member III-5 and her son. She showed personality changes at age 47, which included loss of inhibition. In her late 50s, she could no longer perform daily tasks with reduced communication and cooperation, which resulted in her moving in with family. By age 80, she was non-verbal and non-mobile. She died at 92 of pneumonia, 45 years after disease onset. Her son exhibited anxiety symptoms in his late 50s and has remained in the normal range for the mental status exam at age 67. These cases demonstrate the varied nature of FTD even within a single family with the same mutation.

Case C: K369I *Tau* mutation with initial depressive symptoms.

At age 50, she was treated for depression and retired two years later becoming socially isolated, paranoid and withdrawing from family (Neumann et al., 2001). Within a few years, she was not able to complete daily tasks with memory impairment, mood changes and loss of insight. She had slight coordination phenotypes, but no parkinsonism. She was diagnosed with presenile dementia and died of bronchopneumonia at age 61. At autopsy, there were Pick body-like inclusions with positive *Tau* staining and temporal lobe atrophy.

Modeling Tauopathy

Researchers have utilized FTD-associated mutations in *Tau* to understand how Tau dysregulation leads to neurodegeneration. Tau is particularly interesting as it is found aggregated in both primary and secondary tauopathies (Frost et al., 2023). Primary tauopathies are classified as diseases where Tau is the causative factor while secondary tauopathies are those where Tau is dysregulated later in disease progression. Since patient sample procurement is restricted to post-mortem tissue, our understanding of the progression and underlying pathogenic mechanisms of these diseases are limited. Therefore, to address these issues requires the use of model organisms and cell culture systems. Here, we discuss an overview of some of the models used to study the cellular mechanisms of tauopathy.

Given the high variability of patient symptoms and pathology, creating a single model system for neurodegenerative diseases that recapitulates the human condition is difficult (Ahmed et al., 2017). Each of the Tau models, across multiple model systems, have served different purpose in our understanding of FTD. Optimal models have disease progression over time, which allows for the study of early phenotypes and identification of biomarkers. Post-mortem tissue aids in our understanding of late-stage pathology but does not allow for the study of disease progression at the cellular level due to the inability to biopsy the brain. Therefore, to maintain the patient specific mutations in a human cell line, induced pluripotent stem cells (iPSC)-derived cortical neurons have been used to understand the cellular mechanisms *in vitro*. Fibroblasts derived from skin biopsies of non-

demented controls and FTD/AD patients are reprogrammed to cortical neurons or other cell types of interest (Fong et al., 2013; Paonessa et al., 2019; Lee and Huang, 2017; Sposito et al., 2015). These cell culture systems are used to assess Tau isoform expression, phosphorylation, aggregation, cellular/nuclear morphology changes, drug discovery and more. However, these systems lack the complexity of an *in vivo* system both in terms of cellular diversity and the inability to study behavioral changes.

There are dozens of *in vivo* tauopathy models using mice, zebrafish, *C. elegans* and *Drosophila melanogaster* (referred to as *Drosophila*). Mouse models of FTD have used both wildtype human *Tau* and FTD-associated mutations to study the function of Tau *in vivo*. These transgenic mouse models vary in the promoter used to express the human *Tau* (Dujardin et al., 2015). Therefore, each model has a unique subset of brain regions with *Tau* expression, differences in expression level and in phenotypes observed (Dujardin et al., 2015). The models vary in neurofibrillary deposition timing (process of tangle formation) ranging from one month to 12-24 months and some models with none detected. The advantage of using mice over other model systems is the ability to test higher complexity behaviors, such as memory, anxiety, social interaction, eating behavior, muscle wasting and parkinsonism-like features. A disadvantage of these Tau models is the extended timeline, expense, and inability to quickly screen for modifiers of disease.

Zebrafish is another vertebrate model used for studying tauopathies with many established expression systems and quick breeding. One limitation of

zebrafish is the duplication of the Tau gene in the zebrafish genome. This means that there are multiple copies of zebrafish *Tau* as well as the expression of human *Tau*, which may lead to overexpression phenotypes. Phosphorylation, cell death, locomotion and Tau inclusions have all been assayed in the zebrafish model (Giong et al., 2021). *C. elegans* have also been used to study aging and tauopathies based on the ease of genetic manipulation, short lifespan, RNA interference (RNAi) screening and a mapped cell lineage (Giong et al., 2021). In these models, researchers have found decreased lifespan, abnormal phosphorylation, synaptic defects, locomotion changes, cell loss, microtubule, and mitochondrial phenotypes (Giong et al., 2021). No single model presents with all characteristics of FTD from the molecular to behavioral levels. Thus, our understanding of the mechanisms behind specific phenotypes necessitates the use of multiple models within and across model organisms (Ahmed et al., 2017).

***Drosophila* Tauopathy Models**

The humble fruit fly has earned its place in the lab for over a century. Originally used due to their prolific procreation, it has provided researchers with many fruitful discoveries. Although the *Drosophila* brain could fit on the tip of a needle, it is responsible for complex behaviors, such as flight, odor sensing, locomotion, sleep and has many of the same basic functional regions as vertebrates. The field of behavioral neurogenetics began in *Drosophila* in Seymour Benzer's lab and has evolved into an extensive field with the creation of many

behavioral tests to assay learning and memory, locomotion, sleep, feeding preference and more.

Drosophila have been used to study Tau-induced neurodegeneration for over 20 years. Most of the models utilize the UAS/GAL4 system, originally discovered in yeast (**Figure 4**; used in Chapters 3 and 4; Brand and Perrimon, 1993). This system allows for the expression of short hairpin RNAi or cDNA constructs in a tissue specific manner. Similar systems modifying the basic UAS/GAL4 system allow for temporal- and tissue-specific expression (GAL80ts) of the desired construct (**Figure 5**; used in Chapter 4.1). Many of the *Drosophila* tauopathy models use this system to overexpress specific isoforms of human *Tau* (hTau) either pan-neuronally, in the mushroom body (memory center of the brain) or in the peripheral nervous system. The most common phenotypes tested are memory, locomotion, microtubule stability, neuronal death, and phosphorylation (Giong et al., 2021). One downside to the UAS/GAL4 system is that the spatial expression and dosage are not consistent with the endogenous *Drosophila Tau* (dTau). Even expression of wildtype hTau can lead to phenotypes when using the UAS/GAL4 system (Giong et al., 2021). This system, however, is amenable to creating double mutants to test for modifiers of Tau toxicity. A *Drosophila* screening system for genetic interactors uses the UAS/GAL4 system to overexpress *Tau* in the eye, which results in a rough eyed phenotype (used in Chapter 4.3). Co-expressing candidate gene knockdowns or overexpression constructs with *Tau* allows for quick assessment of potential modifiers. In the past few years, alternatives to the UAS/GAL4 system have been created using CRISPR. One used

CRISPR to edit the FTD-associated mutation into the orthologous nucleotide of the dTau locus (Bukhari et al., 2024). In this dissertation, we utilize a CRISPR model with hTau edited into the dTau locus allowing for the endogenous dTau promoter to control expression of the hTau construct (Cassar et al., 2020; Law et al., 2022).

Specifically, we modeled the P301L, V337M and K369I FTD-associated mutations using a CRISPR knock-in of 1N4R hTau into the dTau locus (**Figure 1A, B**). We focus on the heterozygous mutant model as mutations in *Tau* are autosomal dominant. One disadvantage to our model is the subtlety of phenotypes in the heterozygous mutants and thus, we can also analyze homozygous mutant phenotypes to evaluate the severity of the phenotype. Another limitation is the restriction to a single isoform of hTau, 1N4R. This is an issue with using transgenic animal models rather than iPSC lines. In our model, adult *Drosophila* expressing FTD-associated mutations in hTau have age-dependent neurodegenerative vacuoles, axonal changes, locomotion defects and impaired memory. Control flies expressing normal wildtype hTau did not exhibit these phenotypes or displayed phenotypes to a lesser extent than the mutants (**Figure 1C**; Cassar et al., 2020; Law et al., 2022). This model has a slower development of phenotypes compared to the previously described models (most UAS/GAL4 systems display phenotypes at 10-days of age). The slower development of phenotypes allows us to conduct longitudinal studies to observe disease progression throughout the adult lifespan. For context, *Drosophila* reach sexual maturity within a day of eclosing from the pupa and can live about 2-3 months (Sun et al., 2013). Prior to this study, we had found memory impairment phenotypes in the heterozygous mutants occurring in

adulthood at 14-days old, sleep and locomotion changes by 30-days old and neurodegeneration at 60 days of age (**Figure 1C**; Cassar et al., 2020; Law et al., 2022).

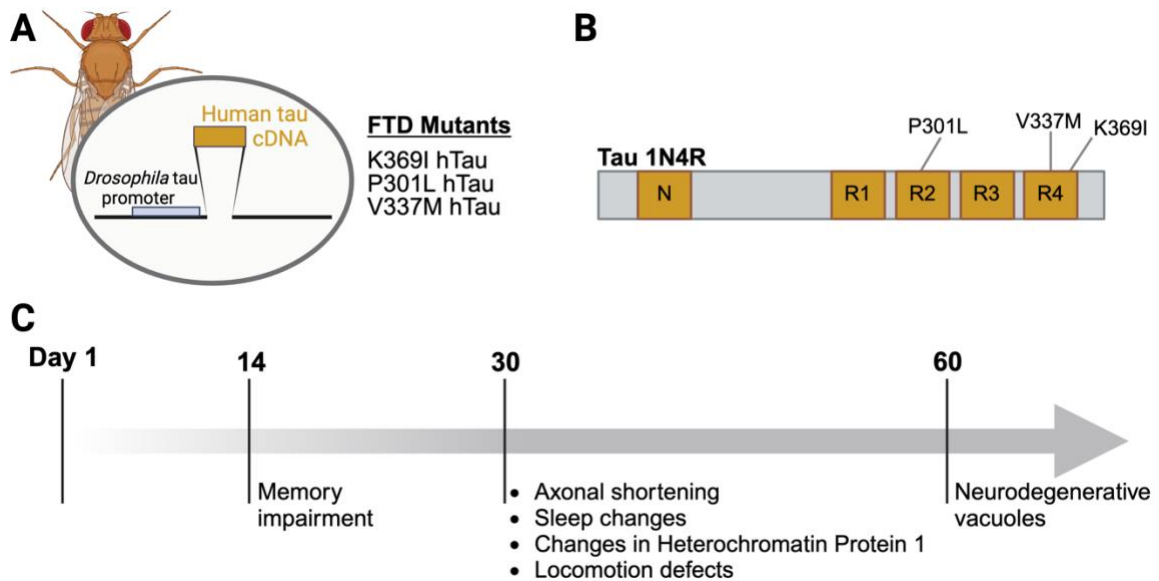


Figure 1: FTD mutants recapitulate disease phenotypes seen in patients with aging.

(A) The 1N4R isoform of human *Tau* was inserted into the *Drosophila* locus using CRISPR for wildtype and three-FTD associated mutations (K369I, P301L, and V337M). (B) Schematic of 1N4R isoform with four microtubule binding domains and the location of the three FTD-associated mutations used in this dissertation. (C) Timeline of disease phenotypes in the FTD-associated mutant adult flies (Cassar et al., 2020; Law et al., 2022). Day 1 indicates eclosion from pupa.

Actin Dynamics in Aging and Tauopathy

Tauopathy animal and cell culture models allow for the study of molecular mechanisms that drive neurodegeneration. One of the molecular mechanisms that has been tied to neurodegenerative diseases is breakdown of regulation in the

cytoskeleton. Actin is an essential component of the cytoskeleton, with roles in cell signaling, gene transcription, mitochondrial function, autophagy, axonal pathfinding, trafficking of organelles, and many more cellular processes (Dogterom and Koenderink et al., 2019; Kast and Dominguez, 2017; Illescas et al., 2021; Weston et al., 2012). Actin regulation genes work in concert to facilitate polymerization, depolymerization, and actin bundling. Actin nucleation and elongation is the process that allows for F-actin (filamentous actin) assembly from G-actin monomers (i.e., formins, Spire, WASP). Actin polymers can also be depolymerized by actin severing proteins (i.e., gelsolin and cofilin). It is well accepted that the actin cytoskeleton is altered in aging and age-related diseases (Lai and Wong, 2020). To understand how actin dynamics regulate aging, it is necessary to dissect which actin processes can modulate age-related phenotypes.

Since this study utilizes the *Drosophila* tauopathy model, this section will focus on the actin dynamic changes that have been discovered in aging and in neurodegenerative models within the *Drosophila* system. Researchers have observed abnormal actin rod formation, which increases with age in *Drosophila* brains (Schmid et al., 2023 preprint). Adult neuronal-specific knockdown of actin nucleation gene, *Fhos* (Formin homology 2 domain containing; FHOD in humans), reduced age-associated action rods, increased survival, and enhanced olfactory memory and locomotion (Schmid et al., 2023 preprint). Reducing *Fhos* levels also improved autophagosome maturation and mitophagy. Actin dynamics are also altered in dementia models. Investigation of alpha-synuclein cellular phenotypes, a Parkinson's risk gene, found trafficking deficiencies in autophagy and decreased

mitochondrial fission tied to dysregulation of actin dynamics (Ordonez et al., 2018; Sarkar et al., 2021). Knockdown of *Fhos* (to decrease actin nucleation) and overexpression of *gelsolin* (to increase actin depolymerization) in neurons expressing alpha-synuclein rescued the mitochondrial defects (Ordonez et al., 2018). These studies demonstrated that altering actin dynamics can influence age- and disease-related autophagy and mitochondrial function phenotypes. This is particularly relevant to this dissertation as *Fhos* is found to be transcriptionally dysregulated in our model of FTD and is a focus of this work (Chapter 3 and 4.1).

Similar to the work in alpha-synuclein, many studies have assessed how Tau interacts with the cytoskeleton. Actin inclusions, called Hirano bodies, are found in some tauopathies suggesting that actin dynamics could be involved in neurodegenerative pathology. Pan-neuronal expression of human Tau FTD-associated mutant, R406W (hTau^{R406W}), with the UAS/GAL4 system has been primarily used to test these mechanisms. Levels of F-actin and F-actin bundles were increased in the hTau^{R406W} brains (Fulga et al., 2007). Tau protein was also found in F-actin precipitates suggesting that Tau interacts with filamentous actin (Fulga et al., 2007). Staining of Hirano bodies in patients has revealed both actin and actin-related proteins, such as cofilin, are present in the inclusions (Maciver and Harrington, 1995). *Drosophila* hTau^{R406W} mutants and a mouse model of the FTD-associated mutation P301L have also displayed “actin-rich rod structures” with actin and cofilin mimicking Hirano bodies found in patients (Fulga et al., 2007). Lastly, researchers have also used the rough eye phenotype to look for *Tau* disease modifiers. Using the hTau^{V337M} mutant and wildtype hTau overexpressed

in the eye, *actin* overexpression with the *Tau* mutant or wildtype exacerbated the rough eye phenotype, while overexpression of *cofilin* (actin severing) partially rescued the phenotype (Fulga et al., 2007). Similarly, *cofilin* overexpression rescued F-actin levels, rod-inclusions, neuronal loss, and neurodegenerative vacuoles (Fulga et al., 2007). Overall, these studies confirmed that Tau can induce actin related phenotypes within multiple models, actin severing gene overexpression can minimize phenotypes and that the mechanism could be due to a direct interaction between Tau and F-actin. This work laid the groundwork for future studies to assess how Tau mutations impact known actin-dependent downstream systems such as mitochondrial dynamics and autophagy (Bardai et al., 2018; Duboff et al., 2012; Ordonez et al., 2018).

Actin and actin-related proteins also have roles in the nucleus and at the nuclear envelope (Weston et al., 2012). Both the mammalian FHOD1 and *Drosophila* Fhos, which are known to enable actin nucleation, have been found to translocate into the nucleus in response to programmed cell death (Anhezini et al., 2012; Ménard et al., 2006). Mammalian FHODs have also been associated with nuclear positioning and binding to the outer nuclear membrane protein, Nesprin (Msp300 in *Drosophila*), a part of the LINC complex. The LINC complex spans the nuclear membrane interacting with actin in the cytoplasm and Lamin in the nucleus (Antoku et al., 2023). Lamin is key to the structural integrity of the nucleus and lines the inner nuclear membrane. Increased actin polymerization by overexpression of *spire* and *wasp* decreased Lamin levels and increased nuclear invaginations (an abnormal nuclear membrane structure) in *Drosophila* brains

(Frost et al., 2016). This was phenocopied when FTD-associated mutant hTau^{R406W} was expressed pan-neuronally and rescued when actin-severing *gelsolin* was overexpressed in the hTau^{R406W} brains (Frost et al., 2016). F-actin was also shown to surround the nucleus near nuclear blebs in the hTau^{R406W} brain (Frost et al., 2016). Knockdown of Nesprin ortholog, *Msp300*, in the hTau^{R406W} brain rescued Lamin levels and neuronal loss (Frost et al., 2016). This suggests a mechanism that could connect the actin and Tau to the nuclear phenotypes associated with aging and age-related diseases discussed in the next section.

Neurodegeneration and the Nucleus

Organization of chromatin within the nucleus contributes to the regulation of gene expression. Chromatin is organized into euchromatic or heterochromatic regions, which results in the activation or repression of DNA elements, respectively. Heterochromatin is a highly condensed chromatin and is characterized by methylation of the histone 3 lysine 9 (H3K9) within the nucleosome protein complex and the presence of Heterochromatin Protein 1 (HP1). HP1 is a chromodomain protein, which binds H3K9 tri-methylation (H3K9me3) and facilitates the spread of the heterochromatin domain by recruiting H3K9 methyltransferase complexes. These heterochromatic regions are transcriptionally silent and heavily populated with repeat and transposable elements. Within the nucleus, heterochromatin is localized to the nuclear periphery and associates with nucleoskeleton proteins, such as Lamin (Romero-Bueno et al., 2019). This nuclear architecture is necessary to maintain proper gene

expression, mRNA transport and nuclear organization. With aging, the tight regulation of nuclear organization begins to break down, which is especially problematic in tissues with post-mitotic cells, such as the brain. Epigenetic regulation is an active area of aging research and changes have been found in DNA methylation, non-coding RNAs, histone modifications, and chromatin condensation (Fenoglio et al., 2018; Liu et al., 2018; Maloney and Lahiri, 2016; Winick-Ng and Rylett, 2018).

In 1997, Bryant Villeponteau proposed that aging was due to a progressive loss of heterochromatin. Villeponteau hypothesized that heterodomains shrink with age due to telomere shortening, replication and DNA damage. This shrinking results in transcriptional dysregulation and expression of genes that would otherwise be repressed (Villeponteau, 1997). The phenomenon of heterochromatin loss with age has been found in *C. elegans*, *Drosophila*, and human cultured cells collected from aged individuals (Haithcock et al., 2005; Larson et al., 2012; Scaffidi and Misteli, 2006).

In *C. elegans*, Haithcock et al. (2005) found decreased heterochromatin at the nuclear periphery in muscle, along with nuclear membrane structural changes in muscle, hypodermal and intestinal cells with the progression of age. The nuclear periphery within the nervous system, however, remained stable throughout aging (Haithcock et al., 2005). Notably, *C. elegans* with decreased levels of Lamin had markedly reduced lifespans compared to wildtype (Haithcock et al., 2005). Heterochromatin loss with aging was also observed in *Drosophila* with decreased levels of H3K9 methylation (Larson et al., 2012). *Drosophila* with increased HP1 α

expression lived longer, and HP1 α mutants heterozygous for a loss of function allele had shorter life spans than wildtype (Larson et al., 2012). These data support the role of heterochromatin in aging. This was further confirmed in human fibroblasts collected from humans greater than 68 years of age, which exhibited decreased H3K9 methylation and HP1 levels compared with young individuals (Scaffidi and Misteli, 2006). These results demonstrate the importance of heterochromatin in longevity.

Researchers have also investigated the link between neurodegenerative diseases and heterochromatin integrity. In addition to the synaptic and transport functions, Tau has a role in maintaining heterochromatin integrity in the nucleus (Sotiropoulos et al., 2017). Recent work has revealed abnormal nuclear membrane structure and heterochromatin condensation as possible drivers of epigenetic dysregulation in AD and FTD. Researchers have utilized FTD-associated *Tau* mutants to investigate the nuclear role of Tau in dementia. Tau FTD-associated mutant *Drosophila* (hTau^{R406W}) and mice (hTau^{P301L}) both displayed decreased H3K9 methylation and HP1 α levels, which are markers for heterochromatin (Frost et al., 2014). When post-mortem human AD brain tissue was tested for heterochromatin changes, there was a decrease in H3K9 methylation within sorted neurons (Frost et al., 2014). This suggests that heterochromatin is decreased in AD and tauopathy models.

Although studies have found decreased heterochromatin in FTD models and AD patient cortical tissue, this is not universal in the field. Lee et al. (2020) found an increase in the heterochromatin mark H3K9 methylation in post-mortem

cortical AD tissue compared with normal controls. The heterochromatin foci in AD patients appear clumped to one side of the nucleus in cortical neurons. This appears contrary to other evidence of decreased heterochromatin in aging and tauopathy models (Frost et al., 2014; Haithcock et al., 2005; Larson et al., 2012; Scaffidi and Misteli, 2006). However, senescent-associated heterochromatin foci (SAHF) have been reported with aging and suggest that, even with a loss of global heterochromatin, there can be foci enriched for HP1, H3K9 methylation and alternative histone macroH2A markers of SAHF (Sen et al., 2016).

Frost et al. (2016) speculated that the underlying cause of heterochromatin changes in *Tau* mutants could be due to dysfunctional Lamin, the main structural component of the nuclear envelope. This has been shown in progeria (premature aging disease), where the Lamin A precursor is not cleaved, which prevents Lamin A from interacting with other nuclear envelope proteins (Romero-Bueno et al., 2019). To mimic this phenotype, Frost et al. (2016) removed the nuclear membrane localization signal of Lamin and found decreased H3K9 methylation and HP1 α in the adult *Drosophila* brain. In the FTD-associated hTau^{R406W} *Drosophila* mutant, there was decreased levels of Lamin and increased nuclear invaginations (Frost et al., 2016). In addition, with Lamin knocked down in the hTau^{R406W} mutant, neuronal death was exacerbated (Frost et al., 2016). Nuclear invaginations have also been characterized in FTD-associated *Tau* mutants in iPSC-derived excitatory cortical neurons (MAPT IVS10+16, MAPTP301L; Paonessa et al., 2019). Disruptions in the nuclear lamina have also been found in AD and FTD post-mortem brain tissue (Frost et al., 2016; Paonessa et al., 2019).

How Tau alters Lamin to influence the relaxed heterochromatin state is still being investigated. However, the working hypothesis is that mutant Tau stabilizes F-actin, which in turn destabilizes the nuclear lamina through the LINC complex resulting in invagination and dysregulation of gene expression through disruption of heterochromatin (discussed in previous section; Frost et al., 2016).

In addition to changes in heterochromatin and nuclear invaginations, microtubule invasion of the nuclear membrane is increased as well as the localization of Tau to cell bodies (rather than axonal localization) in FTD-associated *Tau* mutants (Paonessa et al., 2019). Further work by Paonessa et al. (2019) suggests that these morphological changes in the nuclear membrane influence RNA export and nucleocytoplasmic transport. Paonessa et al. (2019) showed that disruption of nucleocytoplasmic transport in *Tau* FTD-associated mutants was eliminated with microtubule polymerization inhibition. *Tau* FTD-associated mutant *Drosophila* also display accumulation of polyadenylated RNA at the invaginated regions (Cornelison et al., 2019). Inhibition of RNA export reduced *Tau* FTD-associated toxicity (Cornelison et al., 2019). This further supports that abnormal nuclear architecture in *Tau* mutants results in toxicity in the brain. Based on these epigenetic alterations in *Drosophila* tauopathy models, we decided to investigate genomics changes in our knock-in human FTD model (Chapter 3).

A recurring mystery in aging research is *why some people develop dementia while others do not?* These studies suggest that heterochromatin alterations can modulate longevity and are associated with neurodegenerative

diseases. The differences in the heterochromatin state across dementia models and post-mortem tissue could be due to a multitude of reasons: pathological severity, age of individuals/animals, differences across species, the underlying genetic mutations, or variations across different cell types/brain regions. Also, heterochromatin changes are just one component of epigenetic aging. No single epigenetic change underlies aging. Further research is needed to fully delineate how other epigenetic marks along with other aging factors, such as caloric intake and oxidative damage, integrate to influence the aging epigenome.

Single-cell Genomics in Dementia Research

Most FTD research has focused on neuronal cell types, anatomical and pathological phenotypes. However, neurons are not operating in isolation. Neuronal function is highly reliant on glia for metabolic and synaptic support, as well as metabolic tissues for energy homeostasis (Volkenhoff et al., 2015). Therefore, it is important to understand the interaction between the neurons with glia and other metabolic tissues within disease models. Interrogation of the cell-type specific gene expression and chromatin state changes will help reveal how the epigenome controls aging and age-related diseases.

Single-cell genomics is one way of investigating cell-type specific changes within complex systems, like the brain, at a molecular resolution. The high dimensionality of the data provides a broad view of the system allowing for characterization of each cell type through the cell-type specific transcripts/genomic regions. One of the main advantages of single-cell genomics is the ability for

hypothesis generation. Another is the ability to use any animal model or patient tissue sample so long as nuclei or cell isolation is robust. There have been many studies using post-mortem tissue to look at gene regulatory network changes in hopes of finding mechanisms of disease (Luquez et al., 2022). However, as mentioned above, these are late-stage disease samples and do not reveal the progression of the disease. Given that prevention or slowing of progression is the aim, we need to use animal models as well to probe earlier timepoints for mechanisms of action.

Given the genetic trackability of the *Drosophila* system, single-cell genomic technologies and analysis techniques were quickly adapted for use in *Drosophila*. There have been two major efforts to characterize aging in *Drosophila* using single-cell RNA-seq (Davie et al., 2018; Lu et al., 2023). The first was focused on the brain transcriptome and found that there was a decrease in oxidative phosphorylation genes with aging (Davie et al., 2018). This work was expanded in 2023 to include the whole *Drosophila* body as part of the Aging Fly Cell Atlas project (Lu et al., 2023). Single-cell RNA-seq has also been used to probe the mechanisms of FTD-associated *Tau* mutations. Single-cell transcriptome analysis of the UAS/GAL4 pan-neuronally expressed hTau^{R406W} mutant and human AD samples found cell-type specific enrichment of immune response genes in neurons and glia (Wu et al., 2023). Bulk RNA-seq of whole heads in the UAS/GAL4 pan-neuronally expressed hTau^{R406W} mutant also found upregulation of innate immune response, synapse, cytoskeleton, and endocytosis (Mangleburg et al., 2020). These studies used the UAS/GAL4 system expressing *Tau* pan-neuronally.

Therefore, there could be artifacts in the single-cell dataset due to overexpression phenotypes. However, given the amount of research that has been conducted to dissect the mechanisms of *Tau* in this system, it is still interesting to compare these molecular signatures to known phenotypes. Recently, Bukhari et al. (2024) utilized CRISPR to introduce the P301L *Tau* mutation into the *Drosophila* locus (equivalent mutation: P251L) and conducted single-cell RNA-seq on dissected 10-day old fly brains. Similar to the hTau^{R406W} mutant, the dTau^{P251L} mutant showed dysregulation in the glia cell clusters. Specifically, changes in metabolism and actin cytoskeleton from the protein interaction network analysis and learning from the gene ontology enrichment.

When setting out on this project, we were primarily interested in understanding differences in neuronal subtypes and glia within our FTD model. An unanticipated benefit of using whole heads to isolate nuclei for the single-cell assays was the inclusion of the fat body, which lines the head capsule. The fat body is a multifunctional system that performs the functions of the human liver, adipose tissue, and the innate immune system. This dissertation outlines some of the key changes we see in the fat body and exemplifies the benefit of single-cell genomics. Especially relevant to this dissertation, the Aging Fly Atlas found that the adult fat body and pericerebral fat body ranked in top three for aging markers (Lu et al., 2023). Specifically, decline of cell identity, number of differentially expressed genes, nuclear changes and genes expressed with aging (Lu et al., 2023). In addition, there are a high number of sex-specific differential genes expressed between females and males in the adult fat body (Lu et al., 2023). From

the Aging Fly Atlas, one can search for the expression profile of any gene across the major *Drosophila* tissues. Similar references exist for human tissue, and both the *Drosophila* and human atlases show that *Tau* is expressed in a wider variety of cell-types than is typically discussed. Most notably for this dissertation, there is low expression of *Tau* in adipose tissue and glial cells. Single-cell approaches provide a glimpse of possible molecular mechanisms across cell-types allowing for unbiased discovery.

Overview

Dissecting the mechanisms of neurodegeneration can be difficult due to the cellular diversity in the brain and the interorgan communication. Single-cell technology allows us to investigate the molecular mechanism within specific cell types, which is not always apparent in bulk genomics. This dissertation has been completed through the collaborative effort of the Adey and Kretzschmar labs, bringing together expertise in single-cell technology development and neurodegeneration, respectively. From the previous literature discussed in the introduction, I hypothesized that FTD mutant *Tau* alters heterochromatin distribution, which leads to disruption in gene expression and chromatin structure early in disease progression producing or contributing to the behavioral and neurodegenerative phenotypes seen in FTD pathology. In addition, I hypothesized that the gene regulatory networks will vary depending on the FTD mutation as each mutation is clinically distinct. I tested these hypotheses with the following aims: (1) Use single-cell omics to assess how human *Tau* FTD mutations alter chromatin

accessibility and gene expression in the young and aged adult *Drosophila* brain, (2) Determine the role of novel candidate genes in our FTD *Drosophila* model through genetic interaction tests. The experimental outline is presented in **Figure 2** and **Figure 3**. Utilizing single-cell technology allowed us to understand how mutant Tau affects distinct cell types and identify cell-type-specific candidates. This approach led our investigation to an unexpected cell type, the fat body.

In this dissertation, I outline the reasoning for why the fat body is a worthwhile organ to interrogate further in our model system and how it could apply to human health and FTD. All strains used in this dissertation are listed in **Table 1** as well as how the strain is described in the text for reference. Chapter 3 presents the fat body as a tissue of interest and focuses on the discovery of a key gene, *Fhos*, that is altered in the fat body specifically in the hTau^{K369I} mutant. In Chapter 4.1, we show further validation of the unique role of *Fhos* in the fat body by comparing behavioral effects from *Fhos* expression manipulation in neurons and glia. In Chapter 4.2, we present preliminary data on potential regions of interest to look for neurodegeneration in future experiments with *Fhos*. In Chapter 4.3, we screened other potential candidates for future investigation based on candidate genes from Chapter 3. Lastly, we propose a possible metabolic map based on changes seen in gene expression in the hTau^{K369I} mutant. Overall, this dissertation touches on many of the proposed mechanisms in the field – from changes in metabolism in FTD patients to Tau’s interaction with the actin network.

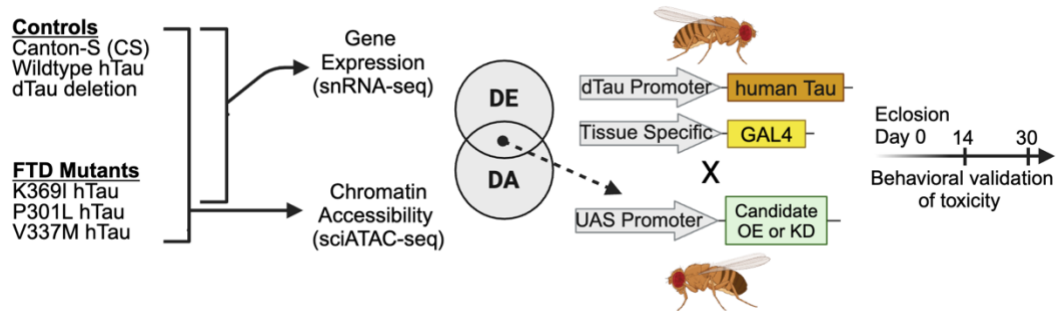


Figure 2: Schematic of single-cell genomics candidate discovery and validation through genetic interaction behavioral experiments.

Concordant candidates from chromatin accessibility and gene expression analyses were validated using the behavioral assays as a read out for toxicity. (DE – differential expression, DA – differential accessibility). Double mutants with hTau and candidate gene expression manipulation were created with the UAS/GAL4 system described in the methods (**Figure 4, Figure 6**).

	Age (days)						
	5	10	11	14	15	30	45
Chromatin Accessibility	Single-cell ATAC-seq with hTauK369I, hTauV337M, hTauP301L					Single-cell ATAC-seq with hTauK369I, hTauV337M, hTauP301L	
Gene Expression	Single-cell RNA-seq with hTauK369I						
Phototaxis				hTauK369I		hTauK369I	
				Fat body Genetic Interaction with hTauK369I + Fhos		Fat body Genetic Interaction with hTauK369I + Fhos	
				Neuron genetic Interaction hTauK369I + Fhos		Neuron genetic Interaction hTauK369I + Fhos	
		Glia Genetic Interaction with hTauK369I + Fhos			Glia Genetic Interaction with hTauK369I + Fhos		
Sleep						hTauK369I	
						Fat body Genetic Interaction with hTauK369I + Fhos	
						Neuron genetic Interaction hTauK369I + Fhos	
					Glia Genetic Interaction with hTauK369I + Fhos		
Rough Eye	Genetic Interaction with hTauV337M and candidate genes from snRNA-seq						
Body Weight			hTauK369I			hTauK369I	
			Fat body Genetic Interaction with hTauK369I + Fhos			Fat body Genetic Interaction with hTauK369I + Fhos	
Neurodegeneration							Fat body Genetic Interaction with hTauK369I + Fhos

Figure 3: Overview of dissertation by experimental assay and age of flies.

Age (days) indicates number of days of adulthood. Each experiment discussed in the dissertation is shown with the corresponding age, FTD-associated mutation and candidate gene tested.

Chapter 2: Materials and Methods

Data Presentation

All figures were created in BioRender.

Drosophila Stocks and Care

Knock-in Tau lines were created by removing the dTau coding region and replacing it with the cDNA of the human Tau 1N4R isoform using CRISPR/Cas9 genomic editing (Cassar et al., 2020; Law et al., 2022). We have validated the knock-in of hTau and loss of dTau by PCR and Western blots (Cassar et al., 2020; Law et al., 2022). The knock-in background was originally w1118, but the lines were backcrossed to CS when necessary for behavior. Flies were fed standard fly food and kept at 25°C in a 12:12 hour light:dark cycle. Wildtype Canton S (CS), provided by M. Heisenberg (University Würzburg), was used as a control. The UAS-EGFP-Fhos-FL (Lammel et al., 2014) was provided by C. Klämbt (University of Münster). The UAS-Fhos RNAi stock (#51391) was acquired from the Bloomington Stock Center. The crossing scheme for the *Fhos* overexpression and knockdown with the UAS/GAL4 system is outlined in **Figure 4** and **Figure 5**. Double mutants with hTau and candidates of interest (if construct was on the third chromosome) were created by first recombining hTau with the necessary GAL4 driver (**Figure 6**). All genotypes and reference for how the fly is referred to in the text can be found in **Table 1**. All stocks used in Chapter 4.3 were ordered from Bloomington and the stock numbers are listed in the figures.

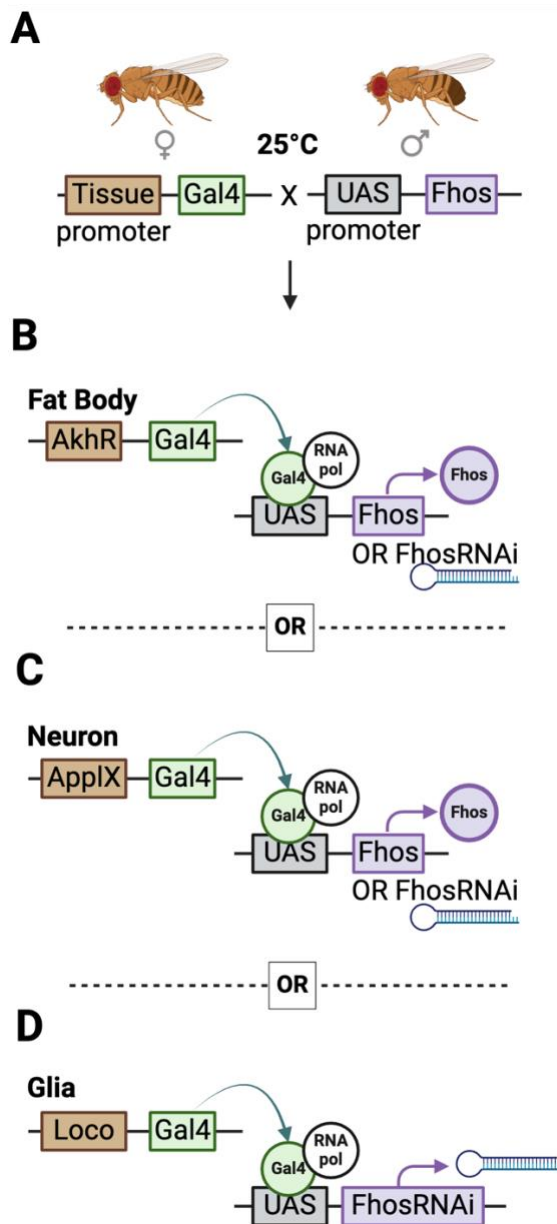


Figure 4: Tissue-specific expression using the UAS/GAL4.

(A) Overexpression or knockdown constructs can be expressed in a tissue-specific manner using the UAS/GAL4 system. Here, we use the gene *Fhos* as an example for how the UAS/GAL4 system works. (B) In the offspring of the cross in A, the GAL4 transcription factor is expressed in the fat body by controlling expression with the AkhR promoter. Therefore, in the fat body, GAL4 can bind to the UAS-Fhos (or Fhos-RNAi) to allow for expression. (C) Same as B but the expression of the *Fhos* gene (UAS-Fhos or UAS-Fhos-RNAi) is in neuronal tissue using the Appl

promoter. (D) In glia, we expressed only the UAS-Fhos-RNAi using the loco promoter for GAL4, which is further explained in Chapter 4.

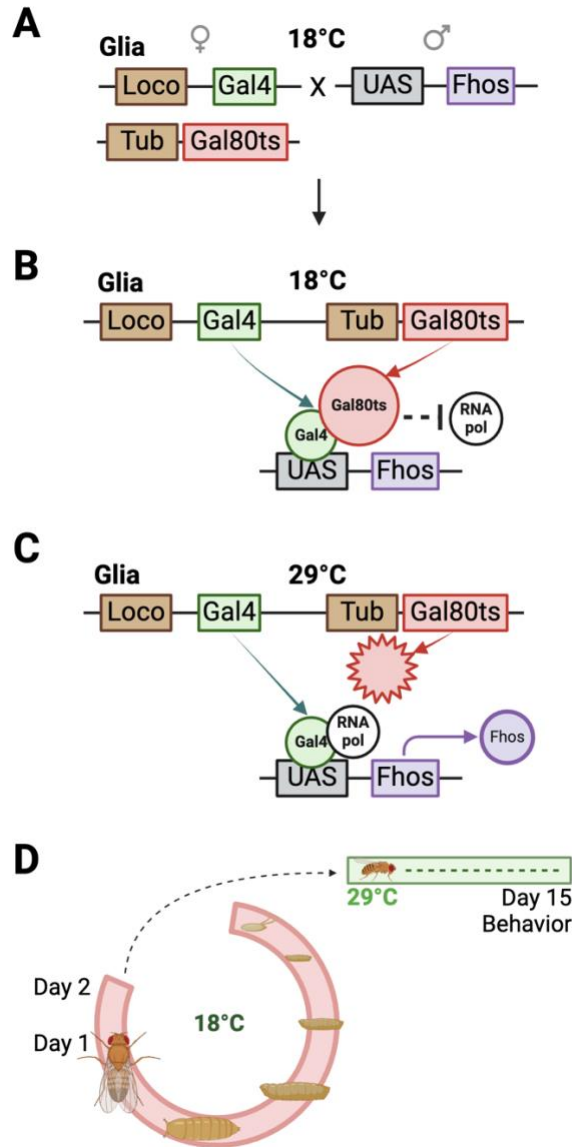


Figure 5: Temporal tissue-specific expression with the UAS/GAL4/GAL80ts system.

(A) The UAS/GAL4/GAL80ts system allows for both tissue-specific and temporal control of construct expression using the *Fhos* gene. (B) In the offspring of the cross in A, the GAL4 transcription factor is expressed in glia by controlling expression with the *loco* promoter but at 18°C, GAL4 is blocked from activating transcription by GAL80ts. (C) When the flies are grown at 29°C, the GAL80ts is temperature sensitive and can no longer block GAL4 and thus the *Fhos* construct can be transcribed. (D) Flies were grown at 18°C for development to prevent lethality from *Fhos* overexpression and moved to 29°C between 1-2 days old to allow for the expression of *Fhos*. Behavioral tests were conducted at 10-days of age for young and 15-days of age for the old timepoint.

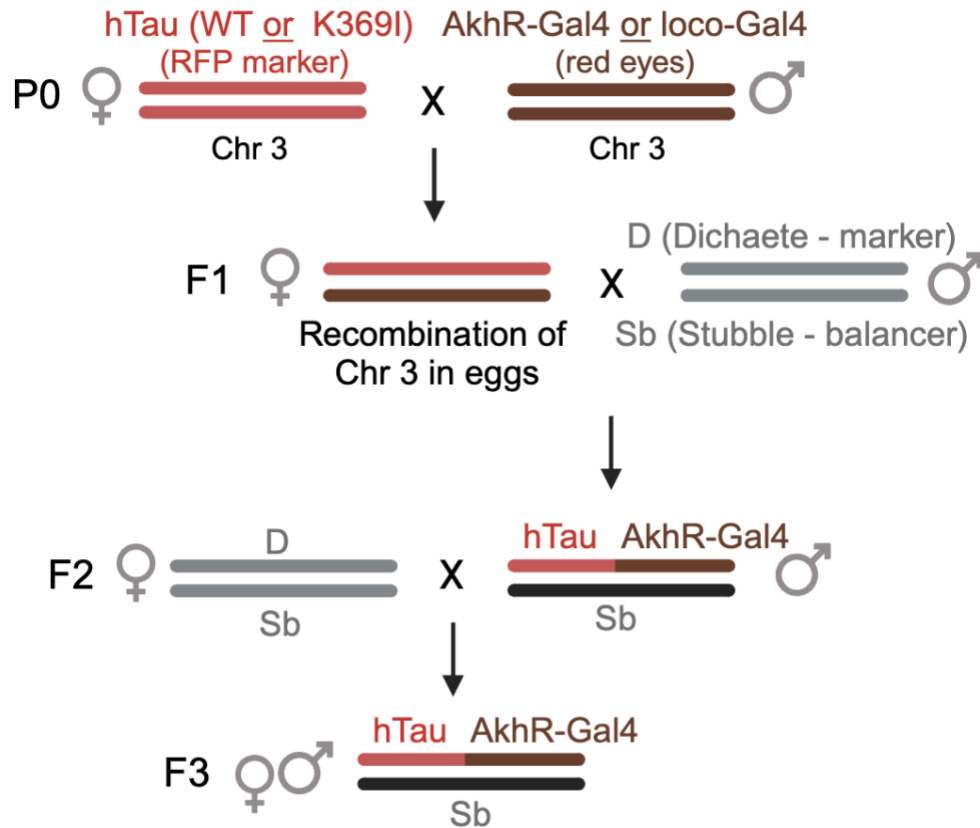


Figure 6: Recombination crossing scheme to create AkhR-Gal4 or loco-Gal4 with hTau transgenic lines.

The *hTau* cDNA construct and the *AkhR-GAL4/loco-GAL4* are on the third chromosome. This necessitated using recombination to then be able to create a double mutant with the candidate genes from Chapter 3. The *hTau* and *GAL4* lines were crossed, and recombination of the chromosomes occurred in the germline of the F1 generation. The virgin female F1 offspring were crossed to males from a balancer strain with *Dichaete* (wing marker) on one chromosome and the *Stubble* (bristle hairs) balancer on the other. Balancers prevent recombination due to inversions within the chromosome. A single male F2 offspring was crossed with the balancer strain virgin females to create a homogenous strain with a single recombination event. RFP and red eyes were used to ensure that both the *hTau* and *GAL4* were present in the line.

Table 1: List of genotypes and descriptions.

Genotype	Description	Referred to in text as
Canton-S	unedited control	CS
::hTau ^{WT}	wildtype hTau control	hTau ^{WT} /hTau ^{WT} homozygous hTau ^{WT} /CS heterozygous
::hTau ^{K369I}	K369I mutant	hTau ^{K369I} /hTau ^{K369I} homozygous hTau ^{K369I} /CS heterozygous
::hTau ^{P301L}	P301L mutant	hTau ^{P301L} /hTau ^{P301L} homozygous hTau ^{P301L} /CS heterozygous
::hTau ^{V337M}	V337M mutant	hTau ^{V337M} /hTau ^{V337M} homozygous hTau ^{V337M} /CS heterozygous
::dTau ^{del}	dTau deletion using CRISPR line	dTau ^{del} homozygous
::AkhR-GAL4/CS	Fat body promotor for GAL4 expression	driver control
::UAS-EGFP-FHOS-FL CS	Fhos expression construct with UAS promotor	Fhos overexpression construct control (UAS-Fhos)
:: <u>AkhR-GAL4</u> CS ::UAS-EGFP-FHOS-FL	Fhos overexpression in fat body using AkhR-GAL4	Fhos overexpression in fat body (Fhos alone)
:: <u>AkhR-GAL4,hTau^{WT}</u> CS	hTau ^{WT} with AkhR-GAL4 construct	hTau ^{WT} driver control
:: <u>AkhR-GAL4,hTau^{K369I}</u> CS	hTau ^{K369I} with AkhR-GAL4 construct	hTau ^{K369I} driver control
:: <u>AkhR,hTau^{WT}</u> ::UAS-EGFP-FHOS-FL	Fhos overexpression in fat body in hTau ^{WT} flies	hTau ^{WT} Fhos overexpression
:: <u>AkhR,hTau^{K369I}</u> ::UAS-EGFP-FHOS-FL	Fhos overexpression in fat body in hTau ^{K369I} flies	hTau ^{K369I} Fhos overexpression
::P{TRIIP.HMJ21037} attp40, CS (UAS-Fhos-RNAi)	Fhos knockdown construct driven by UAS	UAS-Fhos-RNAi Fhos knockdown construct control
:: <u>UAS-Fhos-RNAi</u> , <u>AkhR-GAL4,hTau^{WT}</u> +	Fhos knockdown in fat body in hTau ^{WT} flies	hTau ^{WT} Fhos knockdown
:: <u>UAS-Fhos-RNAi</u> , <u>AkhR-GAL4,hTau^{K369I}</u> +	Fhos knockdown in fat body in hTau ^{K369I} flies	hTau ^{K369I} Fhos knockdown
:: <u>loco-GAL4</u> CS	Glia promotor for GAL4 expression	hTau ^{K369I} Fhos knockdown
:: <u>UAS-Fhos-RNAi</u> , <u>loco-GAL4,hTau^{WT}</u> +	Fhos knockdown in fat body in hTau ^{WT} flies	hTau ^{WT} Fhos knockdown
:: <u>UAS-Fhos-RNAi</u> , <u>loco-GAL4,hTau^{K369I}</u> +	Fhos knockdown in fat body in hTau ^{K369I} flies	hTau ^{K369I} Fhos knockdown
:: <u>TubGAL80^{ts}</u> , <u>loco-GAL4</u> +	Glia promotor for GAL4 expression under temperatur sensitive control of GAL80 ^{ts}	driver control
:: <u>TubGAL80^{ts}</u> , <u>loco-GAL4,hTau^{WT}</u> +	hTau ^{WT} with loco-GAL4 construct	hTau ^{WT} driver control
:: <u>TubGAL80^{ts}</u> , <u>loco-GAL4,hTau^{K369I}</u> +	hTau ^{K369I} with loco-GAL4 construct	hTau ^{K369I} driver control
:: <u>TubGAL80^{ts}</u> , <u>loco-GAL4</u> + ; <u>UAS-EGFP-Fhos-Fhos-FL</u> ;	Fhos overpression in Glia controlled by incubator temperature (29° C)	Fhos overexpression (Fhos alone)
:: <u>TubGAL80^{ts}</u> , <u>loco-GAL4,hTau^{WT}</u> + ; <u>UAS-EGFP-Fhos-Fhos-FL</u> ;	Fhos overpression in Glia controlled by incubator temperature (29° C) in hTau ^{WT} flies	hTau ^{WT} Fhos overexpression
:: <u>TubGAL80^{ts}</u> , <u>loco-GAL4,hTau^{K369I}</u> + ; <u>UAS-EGFP-Fhos-Fhos-FL</u> ;	Fhos overpression in Glia controlled by incubator temperature (29° C) in hTau ^{K369I} flies	hTau ^{K369I} Fhos overexpression
<u>Appl-GAL4</u> , CS	Neuronal promotor driving GAL4 expression in hTau ^{K369I} flies	driver control
<u>Appl-GAL4</u> , CS ; <u>UAS-EGFP-Fhos-FL</u> +	Fhos overexpression in neurons	lethal
<u>Appl-GAL4</u> , CS ; <u>hTau^{WT}</u> ; <u>UAS-EGFP-Fhos-FL</u>	Fhos overexpression in neurons in hTau ^{WT} flies	hTau ^{WT} Fhos overexpression
<u>Appl-GAL4</u> , CS ; <u>hTau^{K369I}</u> ; <u>UAS-EGFP-Fhos-FL</u>	Fhos overexpression in neurons in hTau ^{K369I} flies	hTau ^{K369I} Fhos overexpression
:: <u>GMR-GAL4</u> , CS	GMR promotor for GAL4 expression	GMR control
<u>UAS-hTau^{V337M}</u> , CS ; <u>GMR-GAL4</u> , CS	hTau ^{V337M} overexpression in eyes	hTau ^{V337M} overexpression (hTau ^{V337M} alone)

Single-cell combinatorial indexing ATAC-seq

Nuclei Isolation

Flies (5-7 days and 30 days old) were frozen at -80°C and frozen heads were collected using a sieve on dry ice (20-60 heads; **Figure 7A**). The heads were gently sheared open using a Teflon homogenizing stick in 150µl of cold Nuclei Isolation Buffer (NIB) (10 mM HEPES-KOH, pH 7.2 [Fisher, Cat. BP310-1], 10 mM NaCl [Fisher, Cat. M-11624], 3 mM MgCl₂ [Sigma, Cat. M8226], 0.1% IGEPAL [v/v; Sigma, I8896], 0.1% Tween-20 [v/v, Sigma, Cat. P7949], and 1x protease inhibitor [Roche, Cat. 11836170001]). All contents were transferred to a 1mL Dounce-homogenizer with 300µl of cold NIB and left for 5 minutes. The A (loose) pestle was used 3-4 times to achieve a turbid solution then left to incubate for 15 minutes on ice. The B (tight) pestle was then used 3-4 times until the heads were sheared and left to incubate for 15 minutes on ice. The solution was strained using a 35 µM cell strainer and the nuclei concentration was determined using a hemacytometer.

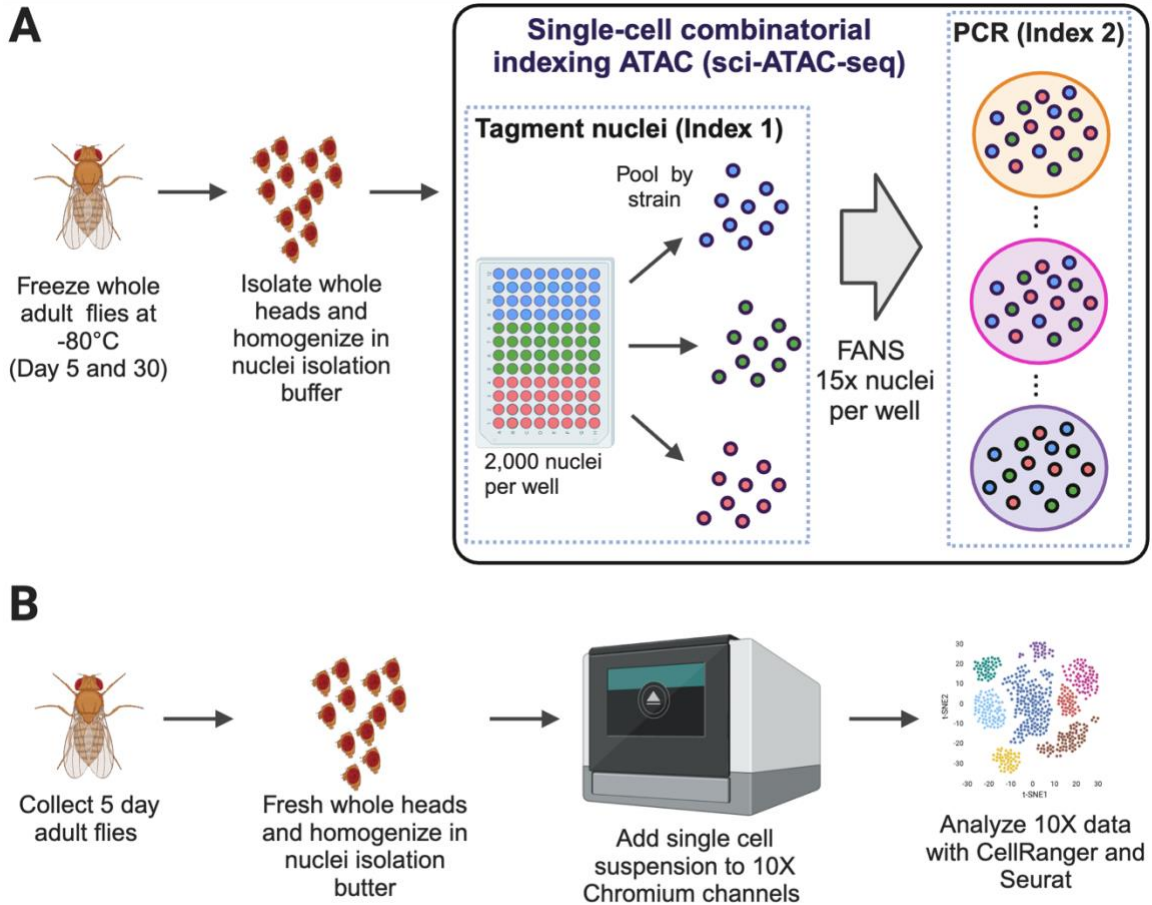


Figure 7: Schematic of single-cell experimental workflows.

(A) For sciATAC-seq, flies were frozen at -80°C at either 5 or 30 days of age. Heads were removed and homogenized in nuclei isolation buffer. The nuclei were then tagmented to introduce the first index and then pooled by strain. Pooling by strain ensured that we end with a comparable number of nuclei for each strain. The nuclei were sorted based on the combinatorial indexing protocol that allows for each cell to receive a unique set of barcodes. The PCR introduces the second index for the two-barcode system. (B) For snRNA-seq, flies were collected at 5-days of age and the fresh heads were homogenized in nuclei isolation buffer. The 10X Chromium platform was used to introduce cell specific barcodes and analyze the data.

Nuclei Tagmentation (Tn5) and Combinatorial Indexing using PCR

Single cells were uniquely labeled using two rounds of indexing (combinatorial indexing). The first round utilized transposase to introduce an index into open regions of chromatin. Each 96 well plate used had a unique index oligo pre-loaded into the Tn5. Fresh 4X TAPS buffer was diluted with cold NIB to 1X and used to dilute nuclei to desired concentration of 200 nuclei/ μ l (132 mM TAPS (N-[Tris(hydroxymethyl)methyl]-3-aminopropanesulfonic acid) pH=8.5, 264 mM potassium acetate, 40 mM magnesium acetate, and 64% dimethylformamide). 10 μ l of nuclei solution and 1.5 μ l 8 μ M uniquely indexed transposase was added to each well on ice (Picelli et al. 2014 transposase synthesis). The 96-well tagmentation plates were then incubated on a thermomixer at 55°C with gentle shaking at 300 rpm for 15 minutes. Once completed, the plates were immediately returned to ice to prevent over-transposition and nuclei lysis. All wells for each strain or experimental condition were pooled on ice. Each condition was pooled separately to limit sorting bias to control conditions as was found in preliminary workflow establishment tests. Nuclei were stained with DAPI (5mg/mL) prior to sorting with the BD FACS Diva software (v8.0.1) on a Sony SH800 FACS machine. Sorting 96-well plates with Transposase Neutralization Buffer (8.5 μ l/well) were prepared in advance and placed on ice (0.25 μ l BSA [NEB, Cat. B9000S], 0.5 μ l 1% SDS, 7.75 μ l dH₂O per well). Indexed PCR primers were added prior to sorting (2.5 μ l of 10 μ M i5 indexed PCR Primer and 2.5 μ l of 10 μ M i7 indexed PCR Primer. For each condition, 15 events per 96-well plate were sorted per PCR plate (e.g. if two Tn5 96-well plates were used for condition 1, then 30 events of condition 1

nuclei would be sorted into each well of the PCR plates; **Figure 7A**). After sorting, the transposase was denatured, and nuclei were lysed at 55°C for 20 minutes in the SDS Transposase Neutralization Buffer. The plates were spun down and frozen at -20°C. The second index was added via PCR on the BioRad CFX real-time cycler running CFX Manager (v3.1) software. 11.5 µl of PCR Master Mix was added to each well of the 96-well nuclei sorted plates (5 µl 5x KAPA HiFi Buffer (GC Buffer), 0.75 µl 10mM KAPA dNTP mix, 0.5 1U/µL KAPA HiFi DNA Polymerase, 0.25 µl 100X SYBR Green I, 5µl dH₂O). The real time PCR was performed with the following setup: 72°C 5min, 15-21 cycles of 98°C 30sec, 63°C 30sec, 72°C 1min, Plate Read, 72°C 20sec. The plate was pulled at the 72°C 20 second step when the plate reached a plateau, which was dependent on the number of nuclei per well, which varied based on the number of initial Tn5 plates (between 85-135 nuclei). The libraries were stored at -20°C after spin down. 10µl from each PCR reaction was pooled and DNA was concentrated using the Nucleospin Gel and PCR Clean-up kit and size selection using 1X SPRI beads (DNA >200 bp). The DNA concentration was quantified using the Qubit 2.0 fluorometer High-Sensitivity kit and then diluted to 1ng/µl for library fragment size and concentration measures using the Agilent TapeStation using a D1000 or D5000 tape.

Sequencing Data Processing

The NextSeq 550 was used for all sequencing runs using custom chemistry (Thornton et al., 2019). The “scitools” software (github.com/adeylab/scitools) was

used to process the sequencing runs. The following “scitools” commands were used to process the runs: fastq file creation (Nextseq2fastq -R, wrapper for bcl2fastq (Illumina Inc., v2.19.0)), index assignment (fastqdump, hamming distance of 2), alignment (fastq-align -r 10 -n -t 25 to dm6), merged bams by age (samtools merge -n), remove PCR duplicates (bam-rmdup -n -t 10), check for sequencing saturation and quality (plot-complexity), merged ages (5 and 30 day), and filtered bam for cells with at least 1000 reads (scitools bam-filter -N 1000). MACS3 callpeak was used for peak calling with the following settings: --call-summits --shift -100 --extsize 200 --nomodel --keep-dup all (Cusanovich et al., 2018). The peaks file was subtracted from the dm6 TSS file (utilized ensemble dm6 tss bed files) to create a background file for TSS enrichment. All cells with TSS lower than 2 were removed for downstream analysis (scitools filter-bam). Peaks were called using macs3 callpeak with the filtered bam and read groups were added to assign reads to the strain, age, and experiment indicator (scitools bam-addrg). Bams were split by experiment (scitools bam-filter) for doublet removal in ArchR (Granja et al., 2021). ArchR was utilized for all downstream analysis with the following used to create a custom genome: BSgenome.Dmelanogaster.UCSC.dm6,TxDb.Dmelanogaster.UCSC.dm6.ensGene (Granja et al., 2021). ArrowFiles were created for each experiment date with the following parameters: minFrag=0, maxFrag=10000000, minTSS=0, gsubExpression=":.*",addTileMat=T,addGeneScoreMat=T,excludeChr=c("chrM","chrX_DS483995v1_random","chrY_DS483742v1_random","chrY_DS483875v1_random","chrY_DS483931v1_random","chrY_DS484142v1_random","chrY_DS48

4530v1_random", "chrY_DS484530v1_random", "chrY_DS484909v1_random", "chrY_DS485423v1_random", "chrY_DS485523v1_random", "chrY_DS485938v1_random", "chrUn_CP007081v1", "chrUn_CP007102v1", "chrUn_CP007120v1", "chrUn_DS483646v1", "chrUn_DS483910v1", "chrUn_DS484581v1", "chrUn_DS484898v1"), nChunk = 20, cleanTmp = T, force=T.

Analysis

R version 4.0.4 and 4.1.2 were used for following analyses depending on the package compatibility. ArchR was used for all downstream analyses (Granja et al., 2021). For dimensionality reduction, `addIterativeLSI`, `addClusters`, and `addUMAP` were used with the following settings: `excludeChr=c("X","Y")`, `iterations=3`, `useMatrix="TileMatrix"`, `varFeatures=25000`, `totalFeatures=200000`, `resolution=2`, `sampleCells=10000`, `maxClusters=9`, `nNeighbors=30`. `addCellColData` was used to add annotations for experiment date, age, and strain. MAC3 peakset was added using `addPeakSet`. The ATAC and RNA datasets were integrated to assist with identifying cell classes. `addGeneIntegrationMatrix` with the `GeneScoreMatrix` was used to predict the mapping between the ATAC and RNA clusters. To visualize the integration, the confusion matrix was plotted with the fraction of total cells in the ATAC cluster that mapped to the given RNA cluster using the `confusionMatrix` and `pheatmap` functions. At least 86% of the ATAC cells mapped to the RNA clusters assigned using unconstrained integration. Curated marker lists were used to assign cluster identity for ATAC and RNA sequencing (**Table 2**). Differential accessibility was calculated using the `getMarkerFeatures`

function with the Wilcoxon test and TSSEnrichment and log10(nFrag) bias for both the GeneScoreMatrix and PeakMatrix. plotBrowserTrack was used to look at accessibility tracks and plotMarkerHeatmap was used to plot curated marker gene list.

Table 2: Marker gene list for cell-type identification.

Gene	CELL TYPE	Reference
repo	glia	Janssens et al., 2024
Gat	glia	Freeman et al., 2015
moody	glia	Janssens et al., 2024
nrv2	glia	Górska-Andrzejak et al., 2009
almr	glia	Stork et al., 2012; Janssens et al., 2024
wrapper	glia	Coutinho-Budd et al., 2017
AdamTS-A	glia	DeSalvo et al., 2014 (as CG14869)
Indy	glia	DeSalvo et al., 2014; Janssens et al., 2024
Gs2	glia	Kato et al., 2020
Mhc	muscle	Aging Atlas (ASAP, Lu et al., 2023); Janssens et al., 2024
up	muscle	Aging Atlas (ASAP, Lu et al., 2023)
sls	muscle	Aging Atlas (ASAP, Lu et al., 2023); Janssens et al., 2024
Hml	hemocyte	Janssens et al., 2024
srp	hemocyte	Ghosh et al., 2015
AkhR	fat body	Bharucha et al., 2008; Janssens et al., 2024
bmm	fat body	Grönke et al., 2005
fit	fat body	Sun et al., 2017
to	fat body	Dauwalder et al., 2002
Yp2	fat body	Abrahamsen et al., 1993
Yp1	fat body	Abrahamsen et al., 1993
ninaE	photoreceptor	Zhu et al., 2009
ninaA	photoreceptor	Xu et al., 2004
ninaC	photoreceptor	Janssens et al., 2024
Rh3	photoreceptor	Senthilan et al., 2019
Rh4	photoreceptor	Senthilan et al., 2019
Rh5	photoreceptor	Senthilan et al., 2019
Rh7	photoreceptor	Senthilan et al., 2019
elav	neuron	Janssens et al., 2024
Syt1	neuron	Janssens et al., 2024
nSyb	neuron	Weaver et al., 2020
Gad1	neuron	Nassel et al., 2008; Enell et al., 2007
VGlut	neuron	Daniels et al., 2006
VACHT	neuron	Boppana et al., 2017
ple	neuron	White et al., 2010
ChAT	neuron	Yasuyama et al., 1996
brp	neuron	White et al., 2010

Single-nuclei RNA-seq

Nuclei Isolation and 10X Chromium

Fresh fly heads (from 5-7 day old) were collected into 1xPBS (phosphate-buffered saline) on ice (~20 heads) and gently homogenized using a Teflon homogenizing stick in 150µl of cold Nuclei Isolation Buffer (NIB) (10 mM Tris HCl, pH 7.4, 10 mM NaCl [Fisher, Cat. M-11624], 3 mM MgCl₂ [Sigma, Cat. M8226], 0.1% IGEPAL [v/v; Sigma, I8896], 0.5% RNase Inhibitor Murine NEB [M0314S]). The contents were transferred to a 1mL Dounce-homogenizer with 350 µl of cold NIB and left for 5 minutes (**Figure 7B**). The A (loose) pestle was used 4 times to achieve a turbid solution then left to incubate for 15 minutes on ice. The B (tight) pestle was then used 4 times until the heads were sheared and left to incubate for 15 minutes on ice. The solution was strained using a 35 µM cell strainer and spun at 500 rcf at 4°C for 10 minutes. The nuclei were twice washed with 400µl of the NIB without IGEPAL. The nuclei concentration was determined using a hemacytometer. The Chromium Single Cell 3' v3 protocol was used for index introduction, library construction and sequencing.

Analysis

R version 4.0.4 and 4.1.2 were used for following analyses. The snRNA-seq data was pre-processed using the CellRanger 6.1.2 software suite. The Ensembl *Drosophila_melanogaster*.BDGP6.28.dna.*.fa.gz version was used to create the genome assembly. The Adey Lab unidex was used to demultiplex the sequencing runs (github.com/adeylab/unidex). Count matrices were created using

cellranger count --expect-cells=10000 --include-introns --chemistry=SC3Pv3 for each sample. To reduce noise, cellranger reanalyze --force-cells 10000 was used prior to running Scrublet for doublet detection and removal with the expected doublet rate of 7.6% based on the 10X protocol (Wolock et al., 2019). Reanalyze was used to filter out doublets prior to running SoupX to remove ambient RNA (Young et al., 2020). All downstream analysis was done using Seurat 4.1.0 (Hao et al., 2021). The dataset was filter with the following: nFeature_RNA > 200, nFeature_RNA < 4000 and percent.mt < 5. FindMarkers with the Wilcoxon test was used for differential expression analysis. ID Converter (id.converter.R) was used to fix gene IDs to match between the ATAC and RNA dataset (github.com/hangoh/flybaseR).

Phototaxis

Flies were collected at day 1-3 then aged to 29-31 days (noted as 30 days in “Results”) with fresh food vials given every 6–7 days. Flies were then sorted by sex and starved overnight with damp tissue to provide water. The phototaxis countercurrent apparatus was used for the fast phototaxis assays. Benzer (1967) described the fast phototaxis behavioral test, which is conducted with a single light source in the dark. Experimental conditions are described in Strauss and Heisenberg (1993). The flies were allowed 6 seconds to make the transition towards the light source for five consecutive iterations. A numeric value was assigned to each fly based on which of the six vials it reached after the five iterations (0,20,40,60,80,100). Statistical analysis was conducted with R using the

Kruskal Wallis and Dunn's test post hoc with Holm's multiple comparisons adjustment. We used the Kruskal Wallis test for the phototaxis data as the data was not normal by the D'Agostino test and the conditions are independent. The test uses ranks instead of values and tests if the groups have the same median.

Western Blot

To detect HP1 α , 15 adult fly heads of mixed sex aged to 30 days were dissected on an ice-cold plate, homogenized in 80 μ l of 1.25X LDS Sample Buffer (ThermoFisher B0008) supplemented with 50 mM tris(2-carboxyethyl)phosphine (TCEP) as a reducing agent along with protease and phosphatase inhibitors (Cell Signaling Technology 5872S), and centrifuged at 10,000 \times g for 10 min at 4 $^{\circ}$ C. The supernatant was heated to 70 $^{\circ}$ C for 10 minutes to denature proteins. The equivalent of about two heads was electrophoresed through 8% bis-tris gels (ThermoFisher NW0082) to achieve separation of proteins, which were then transferred to PVDF membranes (Millipore ISEQ85R). Membranes were blocked with 10% nonfat dry milk dissolved in 1XTBST (Tris-buffered saline + 0.1% TWEEN-20) then probed with primary and secondary antibodies using standard western blotting procedures (mouse anti-HP1 α (1:100; Wallrath, L.L.; Developmental Studies Hybridoma Bank C1A9), mouse anti-GAPDH G-9 (1:1000; Santa Cruz sc-365062), goat anti-mouse peroxidase conjugate (1:10,000; Jackson ImmunoResearch 115-035-166)). Enhanced chemiluminescent substrate (Michigan Diagnostics FWPD02) was used to visualize bands. For the quantification of protein levels, the intensity of the HP1 α bands was measured and

normalized to GAPDH using Fiji (Schindelin et al., 2012). The HP1 α protein levels for each strain were then compared to the mean level of hTau wildtype (hTau^{WT}). Statistical analysis was done using measurements from at least four independent Western blots and GraphPad Prism with Kruskal-Wallis with Dunn's multiple comparisons to hTau^{WT}.

Sleep

Sleep was assessed starting at 28-33 days of age (AkhR-GAL4 and Appl-GAL4) or 16-19 day old (loco-GAL4) female and male flies of the specified genotypes using the *Drosophila* Activity Monitor Systems (DAMS). Flies were placed individually in glass tubes with standard *Drosophila* food placed in one end with a wax seal and the other end was sealed with a short piece of yarn. Tubes were placed in DAMS model DAM2 monitors (TriKinetics, Waltham, MA, USA) and activity data were recorded every minute for 3 full days in 12:12LD conditions. Sleep bout was defined as 5 or more consecutive minutes of inactivity (Hendricks and Sehgal, 2004). Activity is measured when the fly crosses a beam at the center of the vial. The number of sleep bouts per day and sleep bout length data were analyzed using ClockLab6 (version 6.1.02, Actimetrics, Wilmette, IL, USA). For statistical analysis, one-way ANOVA with Bonferroni's multiple comparisons tests were used to compare all genotypes using GraphPad Prism (v6.07; GraphPad Software Inc. La Jolla, CA, USA).

Neurodegenerative vacuoles

Adults at age 44-47 days were threaded into a collar with eyeless flies as markers for orientation. The protocol is described in depth in Sunderhaus and Kretzschmar (2016). The flies were fixed in Carnoy for 4 hours or overnight at room temperature (30 mL of 99% ethanol, 15 mL chloroform p.A. (C298-500, Fisher Chemical) and 5 mL acetic acid p.A (A38-500, Fisher Chemical). The flies were dehydrated at room temperature in 99% ethanol 2x30 minutes, 45 minutes in ethanol p.A. and overnight in Methyl Benzoate p.A. (126345000, Thermo Scientific). Next, the collars were placed into 1:1 Methyl Benzoate:Paraffin at <60°C for 1 hour. The paraffin (22900700, Fisher) was then exchanged 6x over a 3-hour period (every 30 minutes) at <60°C. The collars were then placed into paraffin molds and left at room temperature to solidify. The excess paraffin was cut away to allow for slicing of the heads using a Leica Model 2040 Autocut Microtome. The brains were sliced into 7µm thick ribbons. The paraffin was removed with SafeClear™ (23-314629, Fisher) 3x30 minutes at room temperature and the ribbons were mounted with Permount™ Mounting Medium (SP15-500, Fisher Chemical).

Rough eye

Flies between the ages of 5-10 days old were used to examine the rough eye phenotype. The GMR-GAL4 strain and UAS-hTau^{V337M}; GMR-GAL4 were crossed with Canton-S for heterozygous controls for each experiment date to control for variability of the rough eye phenotype. Each candidate gene stock

(knockdown or overexpression) was crossed to both the GMR-GAL4 line and the UAS-hTau^{V337M}; GMR-GAL4 to determine the effect of the candidate gene and the interaction between the candidate gene and hTau^{V337M} (**Figure 25**). Bloomington stock numbers for each cross are included in the figures (Xrp1 36 and 37 reference internal Kretzschmar Lab stock numbers). The Leica MZ75 dissecting microscope with 5x magnification was used to evaluate the phenotype and a Canon EOS 6D camera without a lens with the following settings: 1/640s exposure and ISO 3200.

Body Weight, Lipid Droplets and Metabolic Map

Females and males were weighed separately in groups of 4-10 flies at 11- and 30-days of age using the Mettler Toledo ME104 scale. For the lipid droplet pilot experiment, 45-day old adult fat bodies were dissected in 1xPBS with 0.1% Triton and fixed in 4% paraformaldehyde for 20 minutes. The preps were washed three times for 5 minutes each with 1xPBS and then stained with 1:1000 BODIPY (493/503, Cayman Chemical Company) in 1xPBS for 30 minutes. The wash steps were repeated, and the preps were mounted with glycerol and imaged immediately using the KEYENCE BZ-X inverted fluorescence microscope. The differentially expressed genes in hTau^{K369I}/CS compared to hTau^{WT}/CS were split into upregulated and downregulated based on the Log2FC. These lists were run through PANGEA (Pathway, Network and Gene-set Enrichment Analysis) A Multi-Species Enrichment Tool using the following gene set lists: *Drosophila* Gene Ontology sets (SLIM2 GO BP, SLIM2 GO CC, SLIM2 GO MF), FlyBase Gene Group, FlyBase signaling pathway (experimental evidence), and KEGG Pathway

D.mel (Hu et al., 2023). The gene grouping aided in selecting pathways to focus on in the metabolic map. The map does not contain all differentially expressed genes but highlights genes of interest based on known functions in metabolism.

Chapter 3: Expression of actin-related gene, *Fhos*, in the fat body modifies behavioral toxicity of FTD-associated K369I Tau mutation

Eve Lowenstein¹, Dani Long², Andrew Adey^{1,3,4,5}, and Doris Kretzschmar^{1,2}

¹Department of Molecular & Medical Genetics, Oregon Health & Science University, Portland, OR, USA. ²Oregon Institute of Occupational Health Sciences, Oregon Health & Science University, Portland, OR, United States. ³Cancer Early Detection Advanced Research Institute, Oregon Health & Science University, Portland, OR, USA. ⁴Knight Cardiovascular Institute, Oregon Health & Science University, Portland, OR, USA. ⁵Knight Cancer Institute, Oregon Health & Science University, Portland, OR, USA

In-preparation for submission to Aging Cell. Additional data added for this dissertation (Supplemental Figure 5-7).

Funding: NIA F31AG076251

Introduction

Aging is a major risk factor for many diseases, from cancer to neurodegenerative disorders. Over the past 20 years, studies have uncovered a complex model of epigenetic aging that includes heterochromatin loss, altered gene expression, aberrant DNA methylation, histone loss, changes in histone modifications, retrotransposition, and abnormal nuclear envelope structure (Booth and Brunet, 2016). Some or all of these age-associated changes in epigenetic regulation may provide a framework to explain why certain individuals develop dementia while others do not. Furthermore, the identification of specific epigenetic regulators that drive dementia may aid in the development of targeted therapies that go beyond symptom mitigation.

Frontotemporal dementia (FTD) is a neurodegenerative disease with no current disease-modifying treatments. Presentation of FTD in humans is heterogeneous, as patients exhibit a spectrum of clinical manifestations, including parkinsonism, dementia, atrophy in the temporal lobes, and personality changes (Ghetti et al., 2015). Mutations in the microtubule-stabilizing protein Tau have been implicated as a genetic cause of FTD (Ghetti et al., 2015). In the healthy brain, Tau is required for microtubule assembly and stabilization in the cytoplasm, which is critical for axonal integrity and transport (Sotiropoulos et al., 2017). However, Tau is also found in the nucleus and has been shown to have a role in heterochromatin distribution, potentially serving as a source of epigenetic dysregulation, which could lead to aberrant gene expression in FTD and Alzheimer's disease (AD) patients (Mansuroglu et al., 2016; Maina et al., 2018). Expression of FTD-

associated mutant Tau in *Drosophila* neurons and in induced pluripotent stem cell-derived excitatory cortical neurons leads to abnormal nuclear structure (nuclear invaginations) (Cornelison et al., 2019; Paonessa et al., 2019). Furthermore, *Drosophila* and mouse models with FTD-associated *Tau* mutations have decreased histone 3 lysine 9 methylation (H3K9me) and Heterochromatin Protein 1 (HP1) levels, which are markers for heterochromatin (Frost et al., 2014). In contrast, Lee et al. (2020) found an increase in heterochromatin H3K9me in post-mortem cortical AD tissue compared with normal controls (Lee et al., 2020). Taken together, these studies suggest a putative link between *Tau* mutations and pathogenic age-associated epigenetic alterations that may drive FTD and other forms of dementia.

While it has been established that FTD *Tau* mutant models have alterations in nuclear organization, a breakdown of the cell types that are dysregulated at the genomic level has not been thoroughly assessed. Recent work leveraging single-cell transcriptomics found immune-related changes in excitatory neuron and glia transcriptomes in *Drosophila* pan-neuronally expressing a human *Tau* with a FTD-associated mutation (R406W; Wu et al., 2023). Another has looked at the equivalent mutation to P301L in *Drosophila* and found changes in mitochondrial gene networks (Bukhari et al., 2024). Here, we investigate the impact of patient-associated FTD mutations in human *Tau* (hTau) at the single-cell level, using our established *Drosophila* FTD model that harbors the human *Tau* gene at the endogenous *Drosophila Tau* locus (Cassar et al., 2020; Law et al., 2022). We utilized *Drosophila* to model FTD because of the ease of genetic manipulation and

the availability of overexpression and knockdown fly lines to validate candidate modifier genes by genetic interaction. We have previously shown that flies heterozygous for FTD-associated mutations in hTau show disrupted axonal projection, sleep, locomotion, and memory impairment, which are features of FTD (Law et al., 2022). Using the knock-in model approach allowed us to look at epigenetic changes in all cell types where Tau is endogenously expressed. Here, we demonstrate that FTD-associated mutations elicit varied chromatin changes. Specifically, the variant hTau^{K369I} exhibits altered chromatin patterns and gene expression in the actin regulator gene, *Formin homology 2 domain containing (Fhos)*, within the pericerebral fat body cells. We confirmed that manipulation of Fhos expression in our FTD hTau^{K369I} model modifies behavioral disease-phenotype toxicity. This result agrees with the model of actin dysregulation in tauopathy.

Results

Disease-associated FTD mutants alter levels of heterochromatin protein 1

In our FTD *Drosophila* model, we leveraged CRISPR/Cas9 to create knock-in strains with the hTau gene inserted at the *Drosophila* Tau (dTau) locus (**Figure 8A**; Cassar et al., 2020; Law et al., 2022). This allows for control of hTau expression level by the endogenous dTau regulatory machinery (**Figure 8A**; Cassar et al., 2020; Law et al., 2022). We focused on three mutations in hTau that are associated with FTD in humans with clinically distinct phenotypes: P301L, V337M, and K369I (Cassar et al., 2020; Law et al., 2022). To control for presence

of exogenous hTau and genetic background, we also inserted the 1N4R wildtype hTau isoform (hTau^{WT}). We used Canton-S (CS) flies as the unedited strain control.

Changes in protein levels and nuclear distribution of heterochromatin markers, such as Heterochromatin Protein 1 (HP1), are one of the epigenetic changes seen in models of FTD/AD and patient tissue (Frost et al., 2014, Lee et al., 2020). Based on these findings, we examined whether *Drosophila* HP1 α levels were changed in our *Drosophila* model with FTD-associated mutations (hTau^{P301L}, hTau^{V337M}, and hTau^{K369I}). We first analyzed HP1 α protein levels from 30-day old hTau homozygous fly heads, which we would expect to elicit more severe phenotypes than heterozygous mutants (**Figure 8B, C**). We found that hTau^{K369I} and hTau^{V337M} had significantly higher HP1 α levels than hTau^{WT} (**Figure 8B, C**). In the heterozygotes, the hTau^{K369I} FTD mutant showed significantly increased HP1 α protein levels compared to hTau^{WT} (**Figure 8D, E**). This contrasts with previous results using hTau^{R406W} FTD *Drosophila* model, which showed decreased HP1 α and H3K9me (Frost et al., 2014). This difference could be due to the use of another FTD-associated mutation or the UAS/GAL4 system, which overexpresses the FTD mutant pan-neuronally, compared to our CRISPR model using the endogenous *Drosophila Tau* promoter. In contrast to Frost et al. (2014), a study of AD cortical tissue found increased H3K9me levels, but the work did not test HP1 levels (Lee et al., 2020). This inconsistency within the field could also be due to age of testing and/or a tissue specific mechanism. Nevertheless, the changes found in HP1 α in our model suggests that there could be chromatin accessibility

and gene expression changes in our knock-in FTD models, motivating our assessment of these properties.

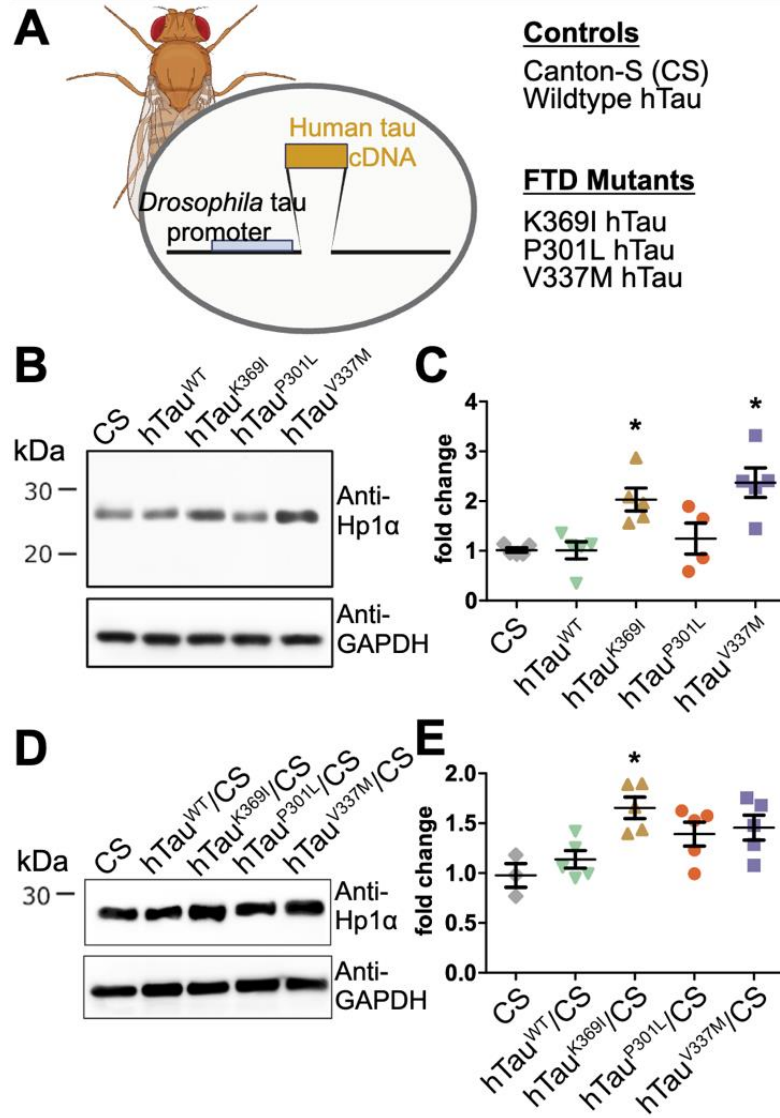


Figure 8: hTau^{K369I} variant increases the levels of HP1α in 30-day old flies.

(A) Human Tau (hTau) cDNA of 1N4R was inserted using CRISPR/Cas9 at the *Drosophila tau* promoter. CS was used as the control line with no insertions and hTau wildtype (hTau^{WT}) was used to control for presence of normal hTau. (B, D) Representative Western blots of HP1α with GAPDH loading control from homozygous (B) and heterozygous (D) hTau whole head lysates. (C) Homozygous hTau^{K369I} and hTau^{V337M} have significantly increased levels of HP1α. (E) Heterozygous hTau^{K369I} has significantly increased levels of HP1α. Quantification

was done from 4 or 5 independent biological replicates. SEMs are indicated. Kruskal-Wallis with Dunn's multiple comparisons to hTau^{WT} with *p<0.05. (Westerns run and analyzed by Alex Law).

Chromatin accessibility and gene expression changes in FTD-associated mutants

Due to the changes in HP1 α levels in our models, we tested whether the mutations affect chromatin accessibility and/or the transcriptome. The heterogeneity of clinical presentations across FTD patients led us to look at whether there were distinct epigenetic changes in chromatin state and gene expression depending on the mutation (**Figure 9A**). As *Tau* is expressed in a wide variety of cell types, including neurons, glia, and fat cells based on the Single-Cell Fly Atlas and Human Protein Atlas, we employed single-cell genomics to allow for analysis of cell-type specific changes (**Supplemental Figure 1G**). Specifically, we leveraged Single-Cell Combinatorial Indexing Assay for Transposase Accessible Chromatin (sciATAC-seq) to examine whether patient mutations exhibited different epigenetic states within specific cell types. These efforts were carried out alongside Single-Nuclei RNA sequencing using the 10X Genomics platform to assess transcriptional changes. To validate our genomic findings, we aimed to identify genes of interest that were mutation and cell-type specific as well as concordant between the differential accessibility and expression analyses compared to the hTau^{WT} heterozygous control (**Figure 9A**).

We conducted sciATAC-seq for whole heads of 5 and 30-day old flies (mixed males and females) with the three clinically distinct FTD-associated

mutations, wildtype hTau^{WT}, and CS (**Figure 9A**; **Supplemental Figure 2**). We also included a dTau deletion (dTau^{del}) as a control for loss of dTau due to insertion of hTau (**Figure 9A**; **Supplemental Figure 1B-D**; **Supplemental Figure 2**). This dataset consists of 98,838 cells, which were clustered into broad cell classifications (**Figure 9B**). Cell typing was performed using a curated list of marker genes based on literature review and aggregating highly similar clusters into the broader cell type classes within the head: neurons, glia, fat body, muscle, hemocytes, and photoreceptors (**Table 2**; **Figure 9D, E**). We focused on 5-day old flies to assess changes between our FTD mutants and wildtype that occur early in disease progression, possibly contributing to pathology rather than being a consequence of the pathology. The 30-day old dataset was used to check if the changes found at 5 days of age persisted over time. We also focused our investigation on the heterozygous mutants as FTD patients are heterozygous for Tau mutations (Ghetti et al., 2015). Homozygous FTD hTau^{K369I} mutant flies were used to detect more subtle phenotypes that might not be detectable in the heterozygotes. For the single-nuclei RNA-seq, comprising of 36,798 nuclei, we focused on flies with the hTau^{K369I} mutation because only hTau^{K369I} heterozygous flies showed changes in HP1 α protein levels (**Supplemental Figure 1E, F**; **Figure 8D, E**). To map our sci-ATAC-seq cell-typing to the snRNA-seq, we employed unconstrained integration using ArchR, restricting our analysis to 5-days of age to avoid changes due to aging from confounding our cell type identification (**Supplemental Figure 1**; **Figure 9D, E**; Granja et al., 2021). Equivalent clusters were determined based on the integration confusion matrix and clusters were paired between ATAC and RNA

based on the highest fraction(s) of agreement (for all assigned ATAC clusters, >86% of each ATAC cluster was assigned to at most two RNA clusters; **Supplemental Figure 1A**; Granja et al., 2021). Integration was confirmed through known marker genes, which were consistent across equivalent clusters within the ATAC and RNA datasets (**Figure 9D, E, F**).

Due to the distinct clinical presentations in FTD patients, we speculated that there would be unique regions of chromatin disruption depending on the variant. We conducted a differential accessibility analysis between each mutant hTau and hTau^{WT} to identify putative sites of Tau-mediated chromatin disruption. Since hTau^{K369I} had the most prominent effects on HP1 α levels, we were particularly interested in regions specific to the hTau^{K369I} variant. In the 5-day old dataset, the fat body cell cluster had substantially more differentially accessible peaks across all chromosomes when comparing the mutants to hTau^{WT}, including interesting candidate regions that were specific to the hTau^{K369I} variant (**Figure 10A**; **Supplemental Figure 3**). This observation was consistent in the snRNA-seq dataset with the hTau^{K369I} mutant, which also had a high number of differentially expressed genes within the fat body cluster (**Figure 10B**). Based on this finding, we used the ArchR gene scores to look for genes that had changes in accessibility and gene expression in the hTau^{K369I}/CS mutant compared to hTau^{WT}/CS within the fat body cluster (Granja et al., 2021).

In the fat body cluster, we found that there were five genes that had significantly changed gene score accessibility (FDR \leq 0.05) and gene expression (p \leq 0.05) in 5-day old heads: *apolpp*, CG42329, *Fhos*, CG13704 and *Ten-a*

(Figure 10C). We utilized gene score in this comparison as this metric considers the differential accessibility in the distal regions and the gene body and thus, can be more readily compared to gene expression (Granja et al., 2021). *Apolpp* had decreased accessibility and gene expression in heterozygous hTau^{K369I} compared to heterozygous hTau^{WT} in 5-day old flies. *Apolpp* is a lipid carrier, which is assembled in the fat body and secreted to transport lipids to other tissues (Palm et al., 2012). It can also cross the blood brain barrier (Palm et al., 2012). In larvae, research has found that it accounts for 95% of the hemolymph lipids and knocking down *apolpp* in larva stages leads to impaired lipid transport as well as bigger neutral lipid droplets in the gut (Palm et al., 2012). This suggests that the hTau^{K369I} flies could have reduced hemolymph lipoprotein levels and potentially an increase in gut lipids due to insufficient mobilization. It is possible that the decrease in the expression of *apolpp* in the fat body in hTau^{K369I} could affect lipid transport into the brain and contribute to neurodegenerative phenotypes. Another gene that was differential changed in both ATAC and RNA was CG13704 (also known as hoka) and is known to act at the intestinal barrier, but there is no known human ortholog (Izumi et al., 2021). This hit was changed in the dTau^{del} and heterozygous hTau^{K369I} compared to heterozygous hTau^{WT} suggesting a loss of function mechanism and could be interesting for future work. *Ten-a* was also found in both the ATAC and RNA differential markers analysis for heterozygous hTau^{K369I}, CS and dTau^{del} compared to heterozygous hTau^{WT} and is known to be involved in synapse function (DePew et al., 2019). CG42329 is an acyltransferase that is expressed normally in the fat body as a cyclic transcript, which peaks in the late night and is

controlled by the local fat body clock (Xu et al., 2011 (Symbol Synonym - CG5156)). It was found to have decreased expression in CS, dTau^{del} and heterozygous hTau^{K369I} compared to heterozygous hTau^{WT}. This is an interesting gene for future work based on its relationship to the clock and the link between sleep disruption and dementia.

Within the fat body cluster, *Fhos*, *Formin homology 2 domain containing*, had increased chromatin accessibility and gene expression in heterozygous hTau^{K369I} (ATAC FDR=1.85E-05, FC=3.61; RNA Bonferroni adjusted p-value=9.81E-39, FC=1.17) and dTau^{del} (ATAC FDR=4.37E-09, FC=2.99; RNA Bonferroni adjusted p-value=9.25E-51, FC=1.02) compared to heterozygous hTau^{WT} in 5-day old flies (**Figure 11A-B**). This increase was also seen in the homozygous hTau^{K369I} mutant in our chromatin accessibility (ATAC FDR=1.48E-05, FC=4.43), but was not seen in either of the other FTD-associated variants, hTau^{P301L} or hTau^{V337M} within the fat body cluster in 5-day old flies (**Figure 11A**). Formins are known to facilitate actin nucleation and bundle actin, which has been shown *in vitro* with *Drosophila* Fhos (Patel et al., 2018). Also, actin dysregulation has been implicated in other tauopathy models and in aging. This positioned *Fhos* as an interesting candidate for further investigation (Bardai et al., 2018; Fulga et al., 2007; Schmid et al., 2023 preprint; Ordonez et al., 2018). The candidate accessibility peak in *Fhos* lies upstream from the 5'UTR for the shorter isoforms (chr3L:8766288-8766438; **Figure 11A**). This peak is also differentially accessible in the fat body cluster at 30-day old in the homozygous hTau^{K369I} (ATAC FDR=2.42E-08, FC=2.05) and dTau^{del} (ATAC FDR=2.88E-05, FC=2.13)

compared to heterozygous hTau^{WT} (**Supplemental Figure 4A**). In the neuronal cluster, there was also an increase in expression when comparing heterozygous hTau^{K369I} and dTau^{del} to the heterozygous hTau^{WT} control, but not as strong as the fat body cluster (**Figure 11B**). Our accessibility and expression datasets showed all strains had a strong signal in the glial cluster (**Figure 11A, B**). This finding suggests that *Fhos* may be an early modifier of Tau-related toxicity for the hTau^{K369I} variant, specifically in the fat body, which we aimed to validate by genetic interactions.

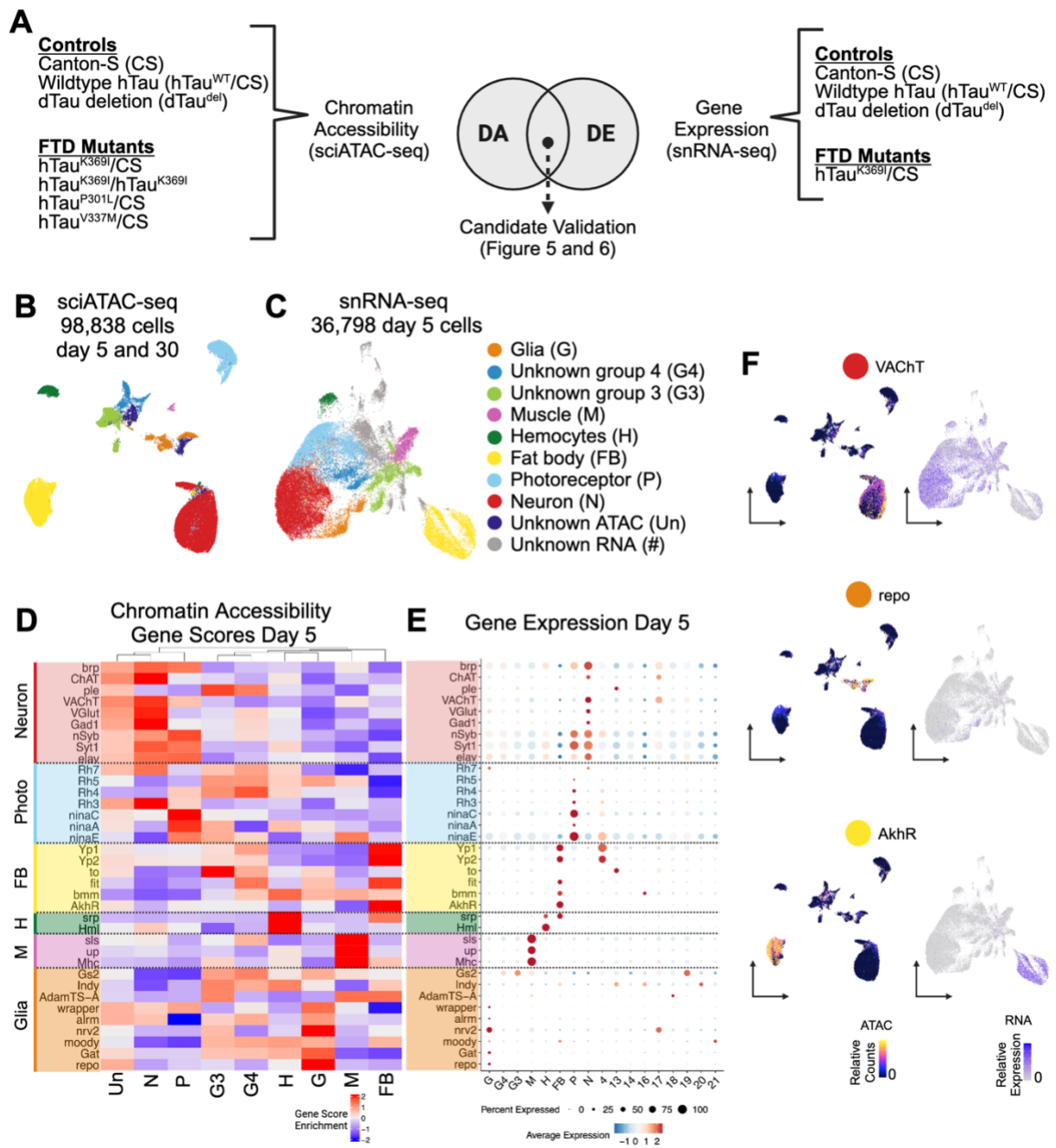


Figure 9: Cell-typing of single-cell genomics of FTD-associated mutants in *Drosophila* model.

(A) Overview of the single-cell genomics discovery of candidates of interest for behavioral validation. (B) UMAP of Single-Cell Combinatorial Indexing Assay for Transposase Accessible Chromatin (sciATAC-seq) of day 5 and day 30 of heterozygous hTau^{WT}, hTau^{V337M}, hTau^{P301L}, hTau^{K369I} (hetero- and homozygous), *Drosophila tau* deletion (dTau^{del}, homozygous) and Canton-S (CS). (C) UMAP of Single-nuclei RNA sequencing (snRNA-seq) of day 5 heterozygous hTau^{WT}, hTau^{K369I}, dTau^{del} (homozygous) and CS. Heterozygous flies were created by crossing the hTau line with CS. (D) Differential accessibility of curated list of marker

genes calculated by gene scores in ArchR (gene score calculation described in Granja et al., 2021). (E) Average expression of marker genes using Seurat (Hao et al., 2021). Dot size indicates the percent of cells that express the marker in the specified cluster. (F) Relative counts (ATAC) and expression (RNA) UMAPs of marker genes for the neuron (VACHT), glia (repo) and fat body (AkhR) cluster (ATAC - left column; RNA - right column).

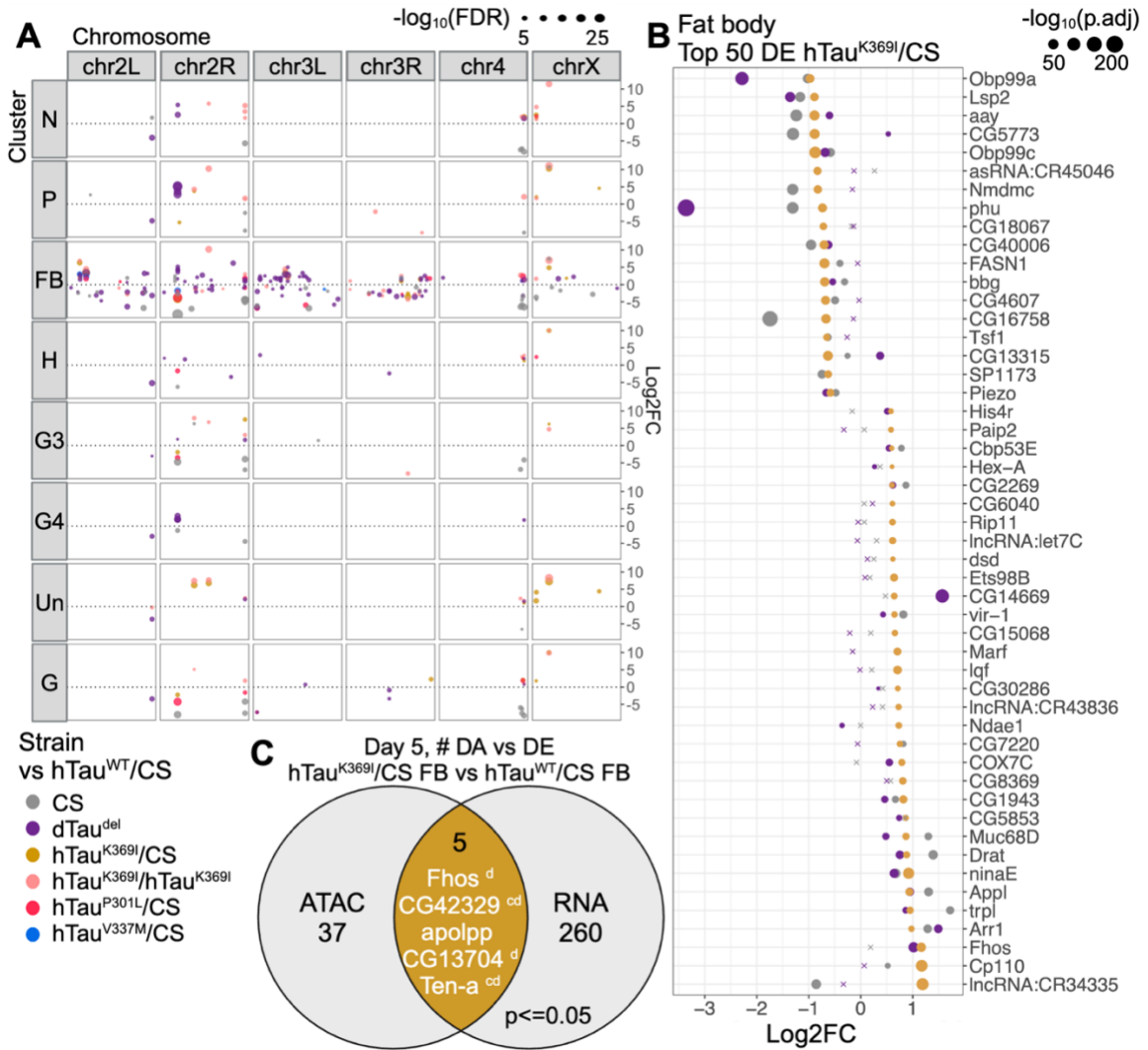


Figure 10: Differentially accessible peaks and gene expression in FTD-associated mutants compared to hTau^{WT} in day 5 shows changes within the fat body cluster.

(A) The fat body cluster showed high numbers of differential accessible peaks across all chromosomes at day 5 for each strain versus hTau^{WT}/CS (color corresponds to strain compared to hTau^{WT}/CS and size indicates the $-\log_{10}$ of the FDR with FDR filtered for ≤ 0.05 , Wilcoxon Rank Sum test). (B) Top 50 differentially expressed genes at day 5 in hTau^{K369I}/CS compared to hTau^{WT}/CS (filtered for $p < 0.01$ with Wilcoxon Rank Sum test and the Bonferroni adjustment and $\log_2\text{FC} > 0.25$, color corresponds to strain compared to hTau^{WT}/CS, X indicates that the gene is not differentially expressed in the strain compared to hTau^{WT}/CS and the size corresponds to the $-\log_{10}$ of adjusted p-value). (C) Intersection of significant differentially accessible (using ArchR gene score) and expressed genes within the fat body cluster in hTau^{K369I}/CS compared to hTau^{WT}/CS (d indicates that the gene is also significantly changed in the dTau^{del} compared to hTau^{WT}/CS; c indicates that the gene is also changed in CS compared to hTau^{WT}/CS,

suggesting a background effect). Filtered for FDR (ATAC) or Bonferroni adjusted p-value (RNA) \leq 0.05.

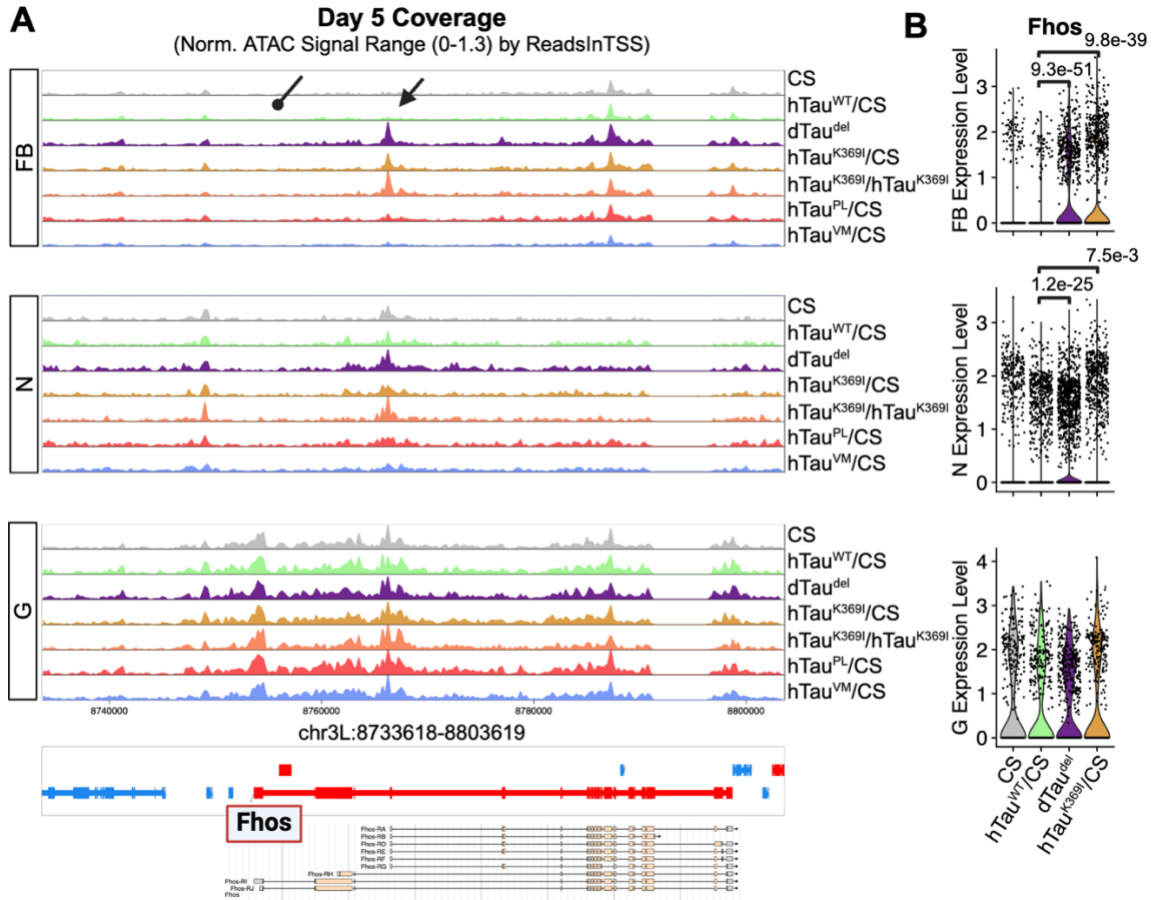


Figure 11: Early change in chromatin accessibility at day 5 within hTau^{K369I} in the Fhos gene translates to increased expression, specifically in the fat body and neuronal clusters.

(A) Coverage of chromatin accessibility in 5-day old heads normalized by reads in transcriptional start sites using ArchR (Granja et al., 2021). Increased accessibility is seen within the coding region of Fhos in the fat body (FB cluster) and neurons (N cluster) in hTau^{K369I} and dTau^{del}, which is not seen in the glial cluster (G cluster) (Arrow denotes peak of interest at TSS of shorter isoforms and line with dot shows TSS of longer isoforms). (B) Expression of Fhos in the fat body, neuron and glia clusters showing an increase of expression compared to hTau^{WT} in the fat body and neuron clusters for hTau^{K369I} and dTau^{del}. Bonferroni adjusted P-value. FlyBase *Drosophila melanogaster* (r6.56) JBrowse was used for the isoform schematic in A.

FTD mutant hTau^{K369I} has reduced locomotor drive in aged females

Changes in locomotion occur in a subset of patients with FTD. Previous work in the lab has shown that fast phototaxis is an effective read out for age-related decreases in locomotion in the hTau mutants (Cassar et al., 2020; Law et al, 2022). In this assay, the flies' innate response to light drives the fly forward in the counter-current apparatus. More active flies move towards the light, and thus have a higher percentage of "transition to light" as the flies get farther in the counter-current apparatus. To validate locomotion as a positive readout for FTD flies, the locomotion of hTau^{K369I} heterozygous flies was compared to CS and heterozygous hTau^{WT} controls at 14 and 30 days of age. We found that aged females (30 days) displayed decreased locomotor drive compared to both CS and heterozygous hTau^{WT} controls (**Supplemental Figure 5B**). We did not see any significant difference in 14-day old females or in males at either age (**Supplemental Figure 5A, C, D**). This demonstrated that we could use locomotion as a hTau^{K369I} age-related phenotype for genetic interaction experiments with our candidate gene, *Fhos*.

Fhos overexpression in the fat body induces decreased locomotor drive in aged flies

Prior to testing whether *Fhos* expression in the fat body impacted the Tau-associated locomotion phenotype, we needed to first understand the effect of *Fhos* expression manipulation alone in our control flies with dTau. To test whether *Fhos* overexpression in the fat body impairs locomotion, we utilized the UAS/GAL4

system with the AkhR promoter to induce overexpression (UAS-Fhos) or knockdown (UAS-Fhos-RNAi) of *Fhos* (**Figure 4B** shows the crossing schematic for this experiment). In 14-day old flies, *Fhos* overexpression decreased locomotor drive in females and males, compared to the driver (AkhR-GAL4) controls (**Figure 12A, C**). With aging (30 days), *Fhos* overexpression resulted in a significant decrease in locomotor drive compared to both the driver (AkhR-GAL4) and construct control (UAS) in females and males (**Figure 12B, D**). This confirms that an increase in *Fhos* levels in the fat body induces locomotion defects in aged flies in both sexes.

The knockdown of *Fhos* induced a significant decrease in locomotion in females at 14- and 30-days of age compared to the AkhR-GAL4 driver control (**Figure 12E, F**). However, the UAS-Fhos-RNAi construct control (without the driver) also displayed reduced locomotion compared to AkhR-GAL4 driver control in 14-day and 30-day old females (**Figure 12E, F**). This is likely due to leaky expression of the UAS-Fhos-RNAi gene construct in the absence of the GAL4 protein, which can occur with the UAS/GAL4 system. However, even taking this into account, the performance of the female *Fhos* knockdown at 30-days of age was worse than both controls, although it did not reach significance (**Figure 12F**). Based on the *Fhos* knockdown results, *Fhos* is likely important for locomotion in females. Overall, these experiments highlight that the level of *Fhos* expression in the fat body can impact locomotor drive, with increased *Fhos* expression being particularly detrimental.

***Fhos* manipulation in fat body alters locomotor drive in hTau flies**

Based on our sequencing experiments, we hypothesized that the increased *Fhos* expression in the hTau^{K369I} flies could be contributing to the behavioral phenotypes we see with aging. To validate *Fhos* as a potential modifier of *Tau* toxicity, we utilized the UAS/GAL4 system to genetically manipulate *Fhos* expression levels to see if this exacerbated or suppressed the phototaxis phenotype seen in aged hTau female flies (**Supplemental Figure 5B**). We overexpressed and knocked down *Fhos* in the fat body using the UAS/GAL4 system with the AkhR promoter, with co-expression of either hTau^{WT} or hTau^{K369I}. To create these lines, we utilized recombination on the third chromosome to create the AkhR-GAL4 hTau flies (**Figure 6**). These flies were then crossed with the UAS construct lines to create double mutants with either *Fhos* overexpression or knockdown with co-expression of hTau.

The experimental conditions are heterozygous for all exogenous constructs (AkhR-GAL4, UAS-*Fhos* and hTau). Therefore, for our hTau driver control, the AkhR-GAL4 hTau recombined lines were crossed with CS to create heterozygous hTau and AkhR-GAL4 flies (referred to here as hTau-AkhR). This allowed us to control for changes in behavior of the hTau flies due to the expression of AkhR-GAL4. In females, when compared to the AkhR-GAL4 control, hTau^{K369I}-AkhR had significantly lower locomotor drive at both ages while hTau^{WT}-AkhR had significantly reduced locomotion only in 14-day old flies (**Figure 12A**). However, with the AkhR construct, there was no significant decrease of locomotor drive at 30-days of age between hTau^{WT}-AkhR and hTau^{K369I}-AkhR. This is in contrast to

our results with hTau line without the recombination of AkhR (**Figure 12B**; **Supplemental Figure 5B**). However, the distribution of the data for hTau^{K369I}-AkhR females at 30-days of age is slightly more skewed towards less “transitions to light” compared to hTau^{WT}-AkhR, which supports our previous findings in hTau alone (mean % transition to light: AkhR-GAL4 - 55.8, hTau^{WT}-AkhR - 44.3, hTau^{K369I}-AkhR - 34.4; **Figure 12B**; **Supplemental Figure 5B**). These differences in behavior between hTau and hTau-AkhR flies are likely due to introduction of a different genetic background with the AkhR-GAL4 recombination. Within the recombined flies, we maintain the age-related decrease in locomotion in female flies from 14- to 30-days of age seen with just hTau (**Figure 12A, B**). Also, the hTau^{K369I}-AkhR females are significantly decreased when compared to the AkhR-GAL4/CS control at both ages (**Figure 12A, B**).

To see if *Fhos* overexpression or knockdown exacerbates or suppresses the hTau^{K369I} phenotype in locomotion, we crossed the hTau-AkhR flies to the *Fhos* overexpression and knockdown UAS-construct (for simplicity, we will refer to the hTau-AkhR as hTau for this paragraph). In 14-day old females, *Fhos* overexpression in hTau^{K369I} significantly reduced locomotor drive compared to both controls (**Figure 12A**). The hTau^{WT} *Fhos* overexpressing flies exhibited a slight decrease in locomotion compared to hTau^{WT} and was significantly reduced compared to the construct control (**Figure 12A**). In 30-day old females, we saw a similar decrease in both hTau^{K369I} and hTau^{WT} overexpressing *Fhos* compared to the respective controls without *Fhos* (**Figure 12B**). In 30-day old males, there was a significant decrease in locomotor drive in hTau^{K369I} *Fhos* overexpressing flies

and reduced locomotion in the hTau^{WT} *Fhos* overexpressing flies (**Figure 12D**). From these results, *Fhos* overexpression leads to decreased locomotion in all conditions, which supports that the increase in *Fhos* found in our sequencing experiments could be detrimental. The decrease in locomotion in young (14-day old) hTau^{K369I} *Fhos* overexpressing female flies suggests that *Fhos* overexpression is more detrimental in females than males (**Figure 12A, C**). While *Fhos* overexpression exacerbated hTau^{K369I} decreased locomotor drive, *Fhos* knockdown in hTau^{K369I} slightly increased median locomotion in 14-day old females (not reaching significance) and does not change locomotor drive in 30-day old females (**Figure 12E, F**). This is particularly interesting when compared to the hTau^{WT} flies, which have decreased locomotor drive in the *Fhos* knockdown in both sexes and ages, reaching significance at 14-day old females and 30-day old males (**Figure 12E, H**). Together, this further suggests that the increased levels of *Fhos* expression in the fat body could contribute to the toxicity of hTau^{K369I} because *Fhos* knockdown only improved locomotion in the hTau^{K369I} mutant.

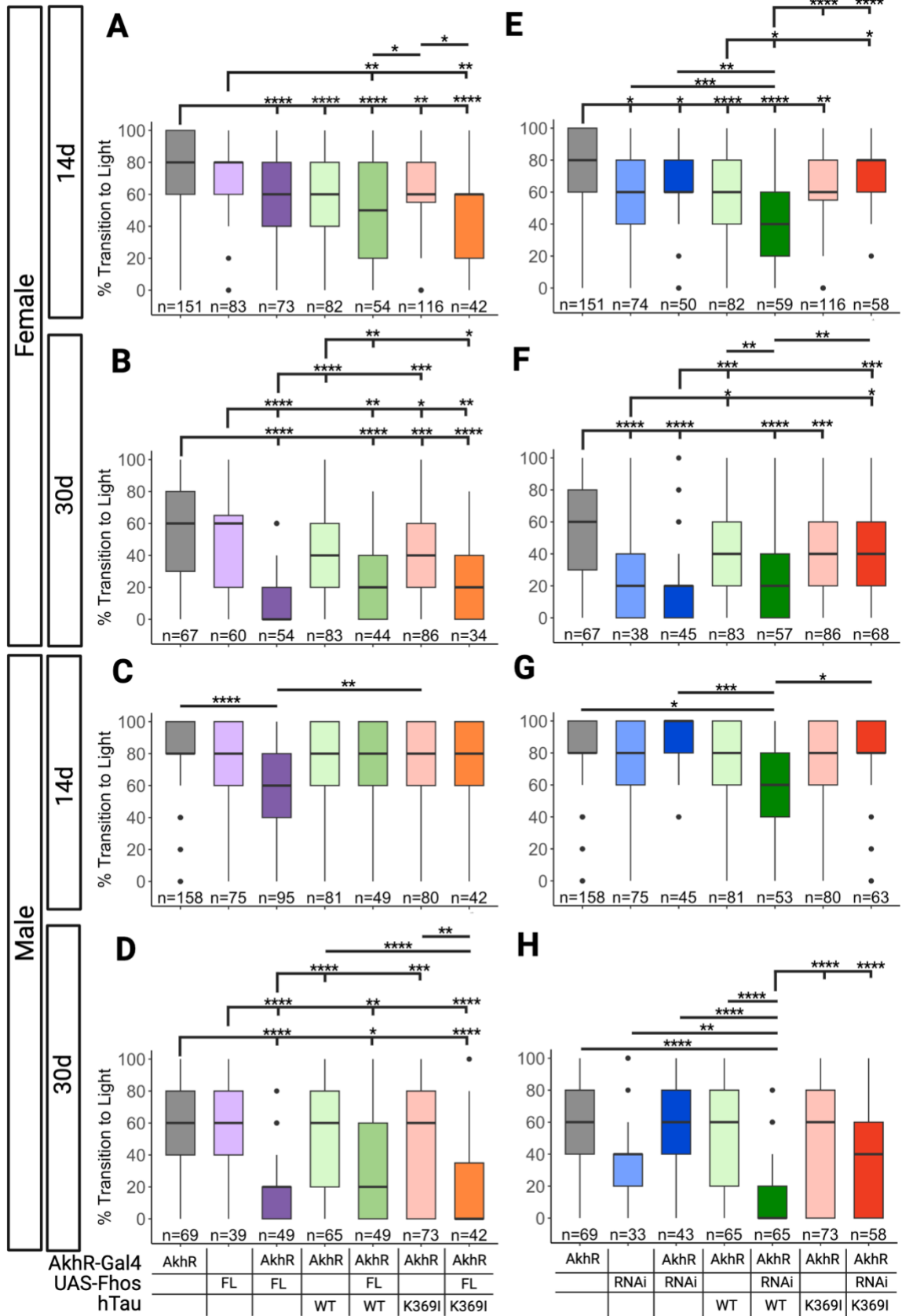


Figure 12: *Fhos* overexpression and knockdown alters locomotor drive in the fat body.

(A, B, C, D) *Fhos* overexpression in fat body decreases locomotor drive in all aged, 30-day old (30d) female and male flies. In contrast to other genotypes, *Fhos* overexpression also decreased locomotor drive in young, 14-day old (14d) female hTau^{K369I} flies. (E, F, G, H) *Fhos* knockdown in fat body has no effect on locomotor drive of hTau^{K369I} in both sexes or ages. Phototaxis counter-current apparatus was used to measure locomotor drive. Flies with the AkhR-GAL4 driver are labeled as AkhR (referred to as driver control). Flies with UAS-*Fhos* (FL, full length) have full length *Fhos* controlled by the UAS promoter (referred to as construct control). Flies with UAS-*Fhos*-RNAi (RNAi) have a dsRNA controlled by the UAS promoter to knockdown *Fhos* (referred to as construct control). Statistics were run across all conditions using Kruskal-Wallis with Dunn's multiple comparisons and Holm adjustment. Sample size is indicated on plots with whiskers indicating the 1.5xIQR (Interquartile range Q3 to Q1). *p<0.05, **p<0.01, ***p<0.001, ****p<0.0001.

Sleep fragmentation and decreased nighttime sleep in aged hTau^{K369I} flies

Frequent waking during sleep is a common symptom in dementia patients and is referred to as sleep fragmentation (McCarter et al., 2016). We can measure sleep fragmentation in *Drosophila* by comparing the average number of sleep bouts per day to the average bout length. If the bouts are increased and length is decreased compared to control, then the experimental condition is waking more. We previously showed that the hTau^{K369I} mutation enhanced age-related sleep fragmentation in males (Law et al, 2022). Due to the sex-specific phenotypes seen in our fast phototaxis assay, we wanted to determine if sleep is affected in our mutant hTau^{K369I} flies in a sex-specific manner. Analyzing the sleep pattern in 4-week-old flies (~30 days), we found that female flies with the hTau^{K369I} mutation have significant sleep fragmentation with more sleep bouts per day and shorter bout length compared to the CS control (**Supplemental Figure 5E, F**). The hTau^{WT} female flies show no difference in bout number per day but have a significant decrease in average bout length (**Supplemental Figure 5E, F**). We did not see a significant change in sleep bout number per day or length in males (**Supplemental Figure 5G, H**). This is in contrast to the previously published results showing sleep fragmentation in males (Law et al., 2022). Since the sleep phenotypes are relatively subtle, we postulate the differences between the results presented here and Law et al. (2022) could be due to the testing of slightly younger flies or lab-specific differences in fly care or data analysis (Law et al. (2022) experiments were performed at another institution). Although these phenotypes were subtle, we determined that sleep fragmentation was another behavioral assay to assess

genetic interaction between *Fhos* and our hTau model as sleep disturbances are a hallmark of FTD pathology.

Patients with dementia have also been found to have increased daytime napping and frequent nighttime sleep disruptions (McCarter et al., 2016). Therefore, we can also look at sleep quantity during the day and night to assess whether the mutant flies have disruptions in sleep. In the heterozygous hTau^{K369I} flies, we see a decrease in nighttime sleep in both females and males compared to both the CS and heterozygous hTau^{WT} controls (**Supplemental Figure 5I, J**). The sleep profile of hTau^{K369I}, hTau^{WT} and CS highlights that the changes in nighttime sleep are relatively minimal at 4-weeks of age (**Supplemental Figure 5K, L**). Next, we wanted to see whether *Fhos* overexpression and knockdown affected sleep quality.

***Fhos* manipulation modifies sleep fragmentation in hTau^{K369I}**

Before evaluating the genetic interaction of *Tau* and *Fhos*, we first tested whether *Fhos* manipulation alone altered sleep fragmentation by assessing the number of sleep bouts per day and the average duration of the sleep bouts in 4-week-old flies (~30 days old). In females, *Fhos* overexpression in the fat body resulted in significantly more sleep bouts per day compared to the driver control but not to the construct control (**Figure 13A**). The sleep bout length was not significantly different from controls (**Figure 13B**). In males, we did not detect significant differences in sleep bout number or length when *Fhos* was

overexpressed (**Figure 13C, D**). With *Fhos* knockdown, females had significantly fragmented sleep compared to the driver control but not compared to the construct control (**Figure 13E, F**). In males, none of the changes reached significance (**Figure 13G, H**). These results suggest that *Fhos* manipulation alone may have subtle effects on sleep fragmentation.

In sleep quantity, females with *Fhos* overexpression have significantly increased daytime sleep compared to the construct control and significantly decreased nighttime sleep compared to the driver control (**Supplemental Figure 6A, B**). Both of these changes are relatively small but align with what is seen in patients. In females with *Fhos* knockdown, we also see a decrease in nighttime sleep (**Supplemental Figure 6E**). Overall, the effects of *Fhos* on sleep quantity in females are subtle as we saw with hTau^{K369I}. Future work could test if these phenotypes worsen with age. Interestingly, males have a significant increase in daytime sleep and a decrease in nighttime sleep in both *Fhos* overexpression and knockdown when compared to both controls (**Supplemental Figure 7A, B, D, E**). For the most part, females have exhibited more severe phenotypes with *Fhos* changes. The sleep quantity changes in males further emphasizes the sexual dimorphic nature of *Fhos* in the fat body.

To test the genetic interaction of hTau and *Fhos*, we again used the recombined hTau-AkhR flies to overexpress or knockdown *Fhos* in the fat body. Similar to the phototaxis, with the AkhR-GAL4 addition, the subtle hTau^{K369I} phenotype of fragmented sleep seen in females was not detectable in hTau^{K369I}-AkhR flies (**Figure 13A, B**). Despite this, we chose to test for genetic interaction

due to our findings that altering *Fhos* levels differentially impacted the hTau^{WT}-AkhR and hTau^{K369I}-AkhR expressing flies in the phototaxis experiments (**Figure 12**; hTau-AkhR will be referred to as hTau below). In females, we found that hTau^{WT} with *Fhos* overexpressed does not significantly differ from hTau^{WT} alone (**Figure 13A, B**). In contrast, female hTau^{K369I} with *Fhos* overexpressed has significantly more bouts per day that are significantly shorter than the hTau^{K369I} driver control (**Figure 13A, B**). Again, this shows that hTau^{K369I} females are more susceptible to *Fhos* overexpression than hTau^{WT} females (**Figure 13A, B**). In males, we see no significant changes when overexpressing *Fhos* in hTau^{K369I} or hTau^{WT} (**Figure 13C, D**). This suggests that *Fhos* overexpression increases sleep fragmentation, specifically, in the hTau^{K369I} mutant females. This could be explained by hTau^{K369I} already having higher levels of *Fhos* expression. Thus, the *Fhos* overexpression exceeds the “threshold” for *Fhos* expression to impact sleep, which is not achieved in the hTau^{WT} flies.

The hTau^{WT} *Fhos* knockdown females had significant sleep fragmentation when compared to hTau^{WT} driver control (**Figure 13E, F**). In contrast, the *Fhos* knockdown in hTau^{K369I} females did not differ from hTau^{K369I} driver control (**Figure 13E, F**). In males, similar to the *Fhos* overexpression, knocking down *Fhos* in either hTau^{WT} or hTau^{K369I} had no significant effect on sleep fragmentation (**Figure 13G, H**). This suggests that knocking down *Fhos*, specifically in hTau^{K369I} females, protects sleep fragmentation while overexpression worsens sleep fragmentation.

For sleep quantity in female flies, there was a significant increase in daytime sleep in hTau^{WT} *Fhos* overexpression flies compared to both controls and no

change in the *Fhos* knockdown (**Supplemental Figure 6A**). The hTau^{K369I} *Fhos* overexpressing flies also had significantly increased daytime sleep compared to the construct control and also no change in the *Fhos* knockdown (**Supplemental Figure 6A**). hTau^{K369I} with *Fhos* knockdown had significantly decreased nighttime sleep compared to the hTau driver control (**Supplemental Figure 6E**). This suggests that *Fhos* can alter sleep quantity in hTau flies.

In males, we saw no change in sleep in the *Fhos* overexpression or knockdown with hTau^{WT} compared to the hTau driver control (**Supplemental Figure 7A-F**). hTau^{K369I} *Fhos* overexpression also did not have daytime changes compared to the hTau driver control (**Supplemental Figure 7A**). However, there was a significant decrease in nighttime sleep in the hTau^{K369I} *Fhos* overexpression compared to the hTau^{K369I} driver control (**Supplemental Figure 7B**). Interestingly, the hTau^{K369I} *Fhos* knockdown had increased daytime sleep and decreased nighttime sleep compared to both controls (**Supplemental Figure 7D, E**). These results demonstrate the complexity of sleep regulation. This also indicates that there is a sex specific mechanism for *Fhos* that is distinct for fragmentation and sleep quantity, as well as dependent on the hTau condition.

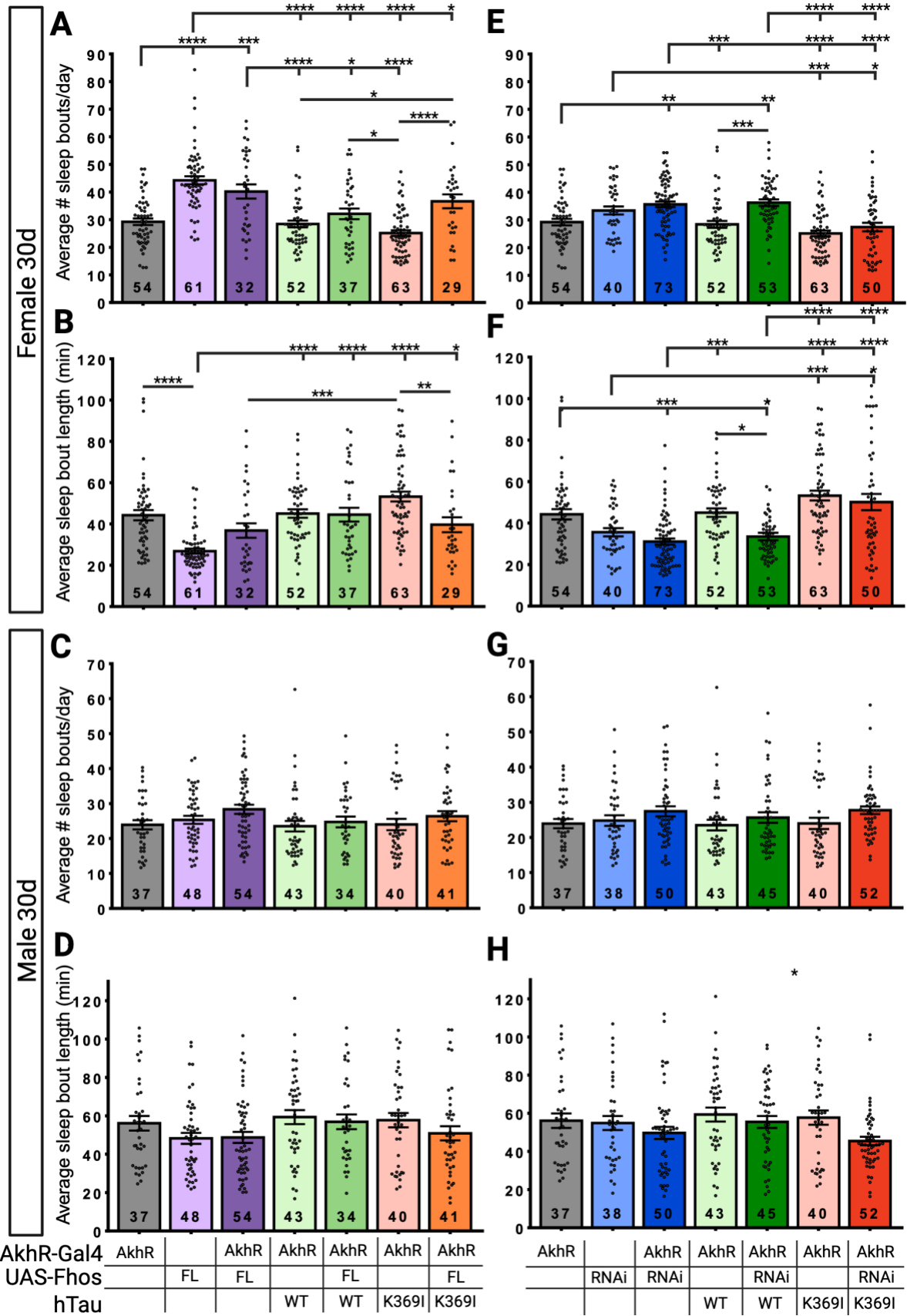


Figure 13: Overexpression and knockdown of *Fhos* results in changes in sleep fragmentation in aged female flies.

(A, B, C, D) *Fhos* overexpression in the fat body of hTau^{K369I} leads to sleep fragmentation with an increased number (A) and shorter length (B) of sleep bouts in aged (30d) female flies. There is no effect on sleep seen in male flies (C, D). (E, F, G, H) *Fhos* knockdown in the fat body has no effect on sleep bouts or length of hTau^{K369I} in females (E, F) or males (G, H). Female hTau^{WT} flies with *Fhos* knockdown trended towards sleep fragmentation with more bouts (E) that were shorter (F). Flies with the AkhR-GAL4 driver are labeled as AkhR. Flies with UAS-*Fhos* (FL) have full length *Fhos* controlled by the UAS promoter. Flies with UAS-*Fhos* RNAi (RNAi) have a dsRNA controlled by the UAS promoter (AkhR-GAL4 – driver control, UAS-*Fhos* FL or UAS-*Fhos*-RNAi – construct control). Statistics were run across all conditions using ANOVA with Bonferroni adjustment. Sample size is indicated on plots. * $p < 0.05$, ** $p < 0.01$, *** $p < 0.001$, **** $p < 0.0001$. Error bars indicate SEM.

Discussion

Mutations in Tau account for 5-20% of known genetic FTD cases (Sirakis et al., 2019). There is high heterogeneity of clinical presentation in FTD patients. Single-cell genomics has become a go-to method for understanding heterogeneous disease states, such as dissecting the relationship between tumors and the tumor microenvironment. To investigate cell-type specific mechanisms of tauopathy, we used our FTD hTau model to probe for changes in both the accessible chromatin regions and the transcriptome. Given that spatial memory and locomotion phenotypes begin in our model within two weeks of adulthood, we suspected that changes in gene regulation within the mutants would precede these phenotypes, so we focused on 5-day old flies for the chromatin accessibility and gene expression (Cassar et al., 2020; Law et al., 2022).

Our cell-type specific analysis of whole head nuclei highlighted the pericerebral fat body as a key cell-type of interest due to a high number of

differentially accessible and expressed genes. We narrowed our focus to identify key chromatin regions that were only altered in the hTau^{K369I} mutant as it also had significantly increased Heterochromatin Protein 1 suggesting possible changes in the epigenetic landscape. An actin nucleation gene, *Fhos*, was found as a potential candidate in both the chromatin accessibility and gene expression in the hTau^{K369I} mutant. It is known that actin dynamics are dysregulated in tauopathy both mechanistically in disease models and pathologically, as actin is found aggregated in patients within para-crystalline inclusions called Hirano bodies (Bardai et al., 2018; Fulga et al., 2007; Ordonez et al., 2018). In the fat body cluster at 5 days of age, we found increased accessibility near the transcriptional start site for the shorter isoforms of *Fhos* within the hTau^{K369I} hetero- and homozygous mutants, as well as the dTau^{del}. We confirmed that the hTau^{K369I} mutant had increased expression in 5-day old adults within the fat body cell cluster. Interestingly, we see the chromatin accessibility persisting in the 30-day old fat body cells but to a lesser extent and increased accessibility in all conditions. Previous work has shown that knocking down *Fhos* in neurons can increase lifespan and decrease age-related rise in actin filaments in *Drosophila* (Schmid et al., 2023 preprint). Another study addressing the mechanisms of toxicity of alpha-synuclein overexpression in *Drosophila*, a gene associated with Parkinson's, found that knocking down *Fhos* was protective for neuronal loss, climbing ability, and actin filament accumulation (Ordonez et al., 2018). In this work, *Fhos* was originally found in connection with retinal degenerative phenotypes in an unpublished screen. Specifically, *Fhos* knockout suppressed degeneration in the alpha-synuclein model of Parkinson's

(Ordonez et al., 2018). The established link of both *Fhos* and actin dynamics in age-related and disease phenotypes positioned *Fhos* as a top candidate for validation.

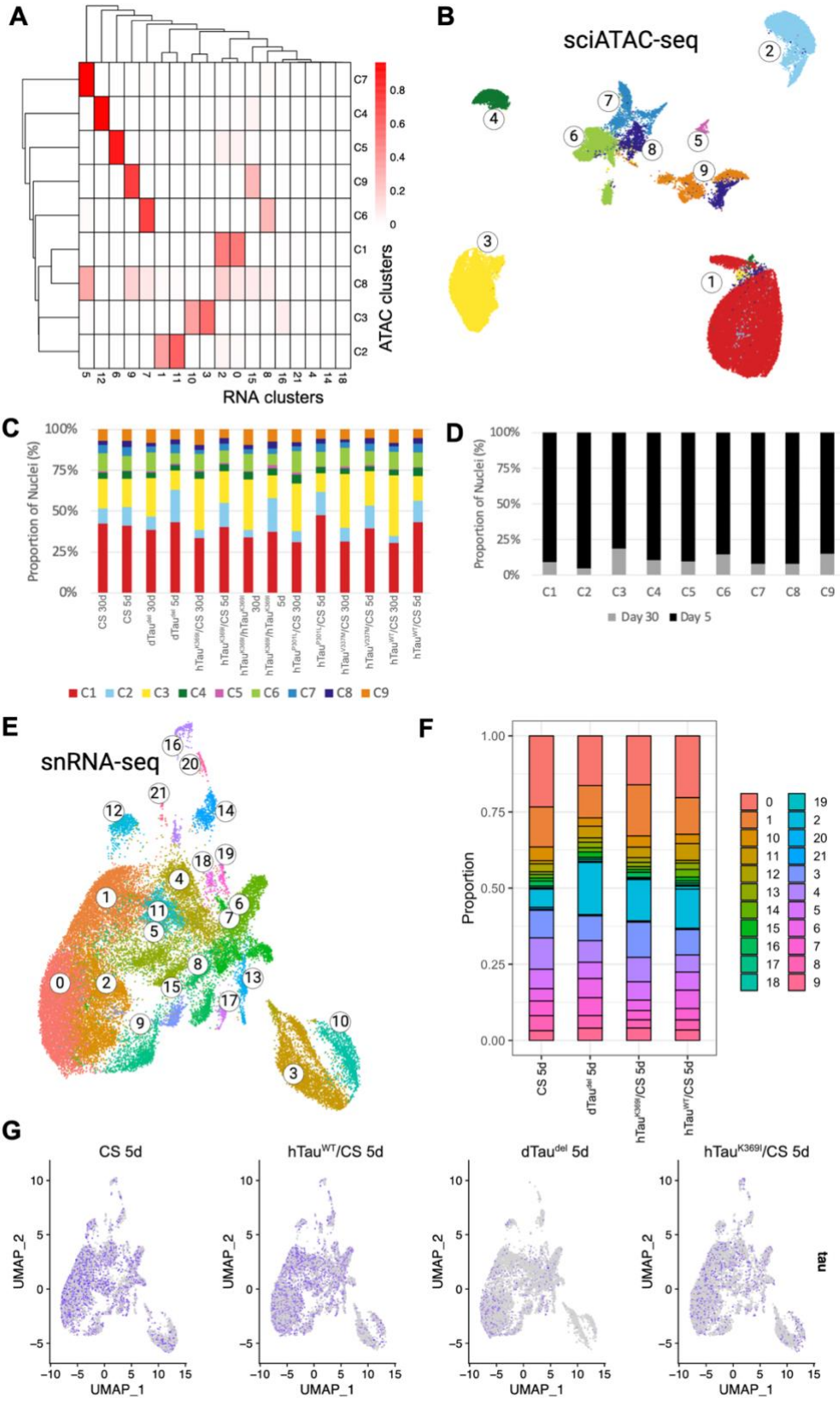
Formins are conserved across *Drosophila* and mammals. In mammals, there are two formins that are similar to the *Drosophila* Fhos: FHOD1 and FHOD3 (Lammel et al., 2014). Research in mammalian tissue has looked at FHOD1 and FHOD3 in its role at the nuclear membrane in the context of cardiomyopathy. FHOD interacts with the LINC complex, which spans the inner and outer nuclear membrane, to mechanically couple with Lamin at the nuclear periphery (Antoku et al., 2015; Antoku et al., 2019; Schwartz et al., 2017). FHOD3 variants have been found in hypertrophic cardiomyopathy patients and FHOD1 is thought to be primarily active in skeletal muscle (Antoku et al., 2023). Lamin has been implicated in aging diseases such as progeria (premature aging) and dementia. Past work in a *Drosophila* model of tauopathy has connected the LINC complex, Lamin and the actin network as a possible mechanism for changes in heterochromatin, as well as nuclear invaginations, which is seen in aging and dementia (Frost et al., 2016). Connecting these findings with our model will help us to understand whether Fhos could be regulating fat body function. Either through disruptions in the actin cytoskeleton influencing energy transport or perhaps causing changes in gene expression through LINC and Lamin. This could in turn influence metabolic output, or even result in changes in the immune response. Continuing these lines of inquiry in the fat body will allow for a greater understanding of the link between neuronal function and the fat body.

Our *Drosophila* FTD model allows for candidates of interest from our sequencing to be validated for behavioral phenotypes associated with FTD. Our behavioral validation with locomotion and sleep showed that knocking down *Fhos* in the fat body was protective but only in the context of the hTau^{K369I} mutant females. The behavioral phenotypes were more severe in the female flies, which could be due to differential energy storage demands between females and males that could impact locomotor activity and sleep (Parisi et al., 2011). However, the daytime and nighttime sleep changes were predominantly seen in the males, which is an interesting dichotomy. Overall, these findings suggest that the mechanism of actin toxicity with aging could extend beyond the central nervous system. Cortical actin dynamics have been implicated in fat body nutrient transport in larva (Ugrankar-Banerjee et al., 2023). Future work is needed to determine whether the behavioral changes could be due to malfunction of inter-organ nutrient transport.

Research has found that metabolism is dysregulated in dementia patients, including insulin resistance, APOB, and triglyceride levels (Garrett and Niccoli et al., 2022; Picard et al., 2022). Some patients with bvFTD have hyperphagia, increased caloric intake, and increased body mass index compared to other classifications of FTD and controls (Ahmed et al., 2014a; Ahmed et al., 2014b; Ahmed et al., 2016). The metabolism in the brain and body are interconnected with many systems maintaining metabolic homeostasis. When that equilibrium is disrupted, there can be global ramifications for the individual. The connection between the brain and the fat body in *Drosophila* is similar. The fat body can influence behavior such as sleep, feeding behavior and courtship (Lazareva et al.,

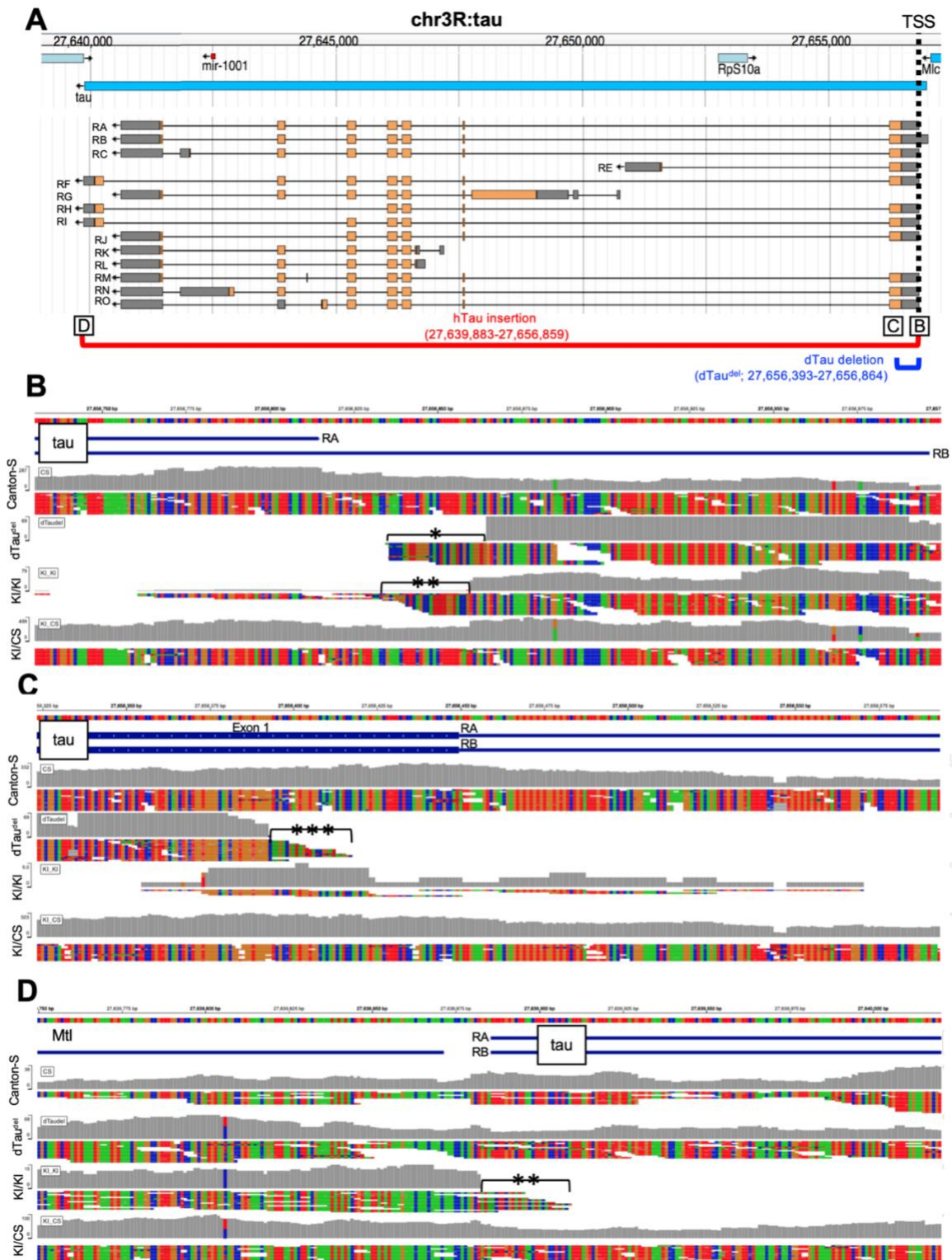
2007; Meschi and Delanoue, 2021; Yurgel et al., 2018). Recent work has connected the actin cytoskeleton within the fat body to behavior changes. A study focusing on cognition and obesity discovered Ezrin as a possible candidate within visceral adipose tissue in humans (Oliveras-Canellas et al., 2023). To validate this finding, the fly ortholog, *Moesin (Moe)*, was knocked down within the *Drosophila* fat body. The knockdown of *Moe* in the fat body led to decreases in learning using a courtship assay for short-term memory (Oliveras-Canellas et al., 2023). This study supports the importance of proper fat body function for neuronal function. Interestingly, Moesin, a member of the same protein family, was found upregulated through a network analysis of AD patient transcriptomes (Beckmann et al., 2023). This was validated in *Drosophila* and implicated in the neuronal actin dysregulation mechanism in a tauopathy model (Beckmann et al., 2023). It is important to not only study the brain in neurodegenerative diseases, but also the body systems that are important for proper neuronal function. With the expansion of single-cell technologies, it would be beneficial to investigate whether known neuronal mechanisms in dementia are altered in the metabolic tissues of patients or if there are novel mechanisms at play.

Supplemental



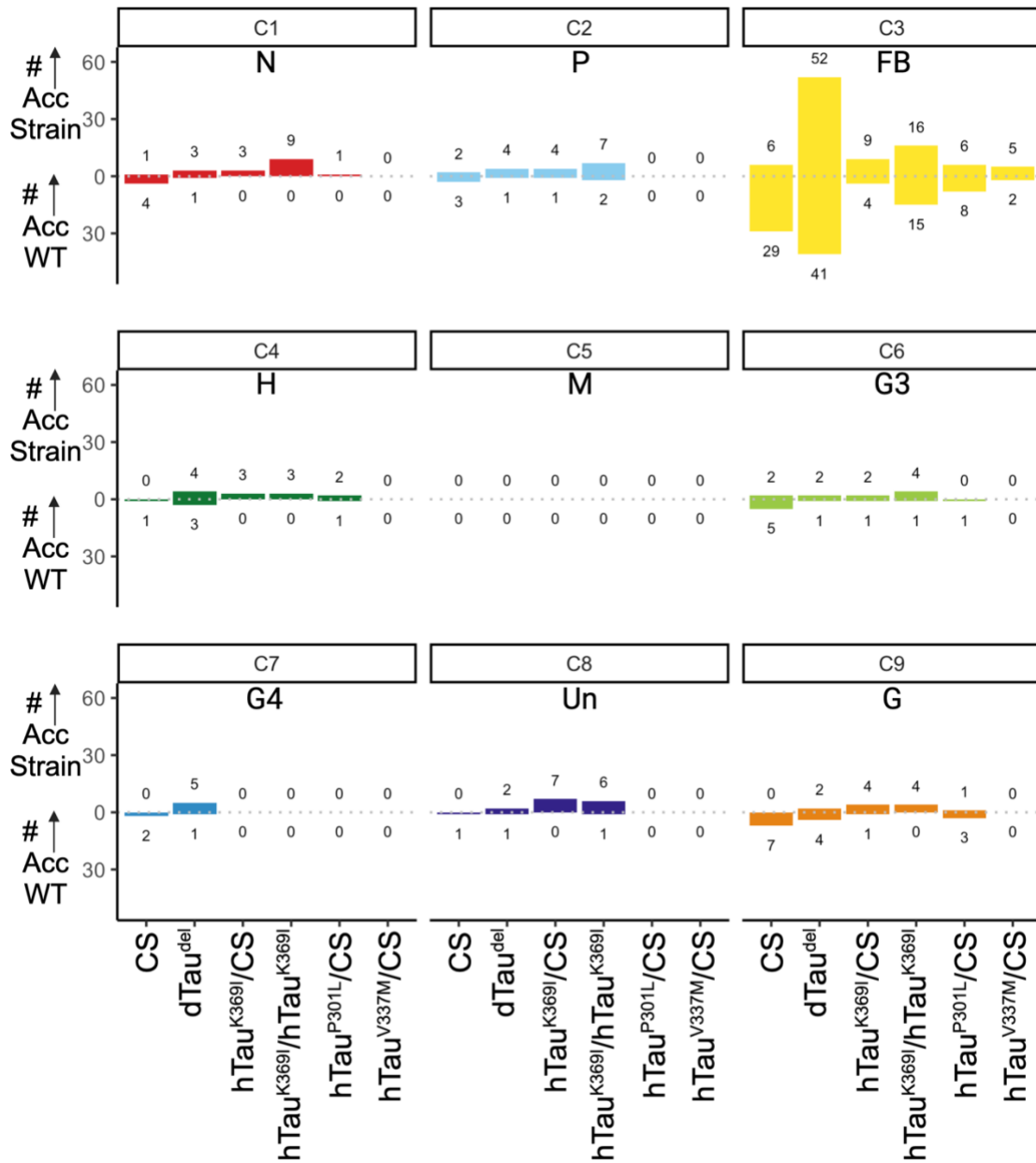
Supplemental Figure 1: Quality control metrics for sciATAC-seq and snRNA-seq experiments.

(A) The sciATAC-seq and snRNA-seq unconstrained integration confusion matrix was used to assign related clusters between modalities. The matrix represents the fraction of ATAC cells within the cluster that were predicted to be in the corresponding RNA cluster. (B) UMAP of sciATAC-seq with original cluster labeling, which corresponds to the matrix in A. (C) The proportion of nuclei for each age and strain across the sciATAC-seq clusters is roughly the same across conditions. (D) Proportion of 5- and 30-day old sciATAC-seq nuclei for each cluster. (E) UMAP of snATAC-seq with original cluster labeling, which corresponds to the matrix in A prior to merging of clusters for analysis. (F) The proportion of nuclei for each strain across the snRNA-seq clusters is approximately the same across conditions in 5-day old dataset. (G) UMAP of expression of dTau across strains in snRNA-seq.



Supplemental Figure 2: Coverage of sciATAC-seq reads within the dTau locus.

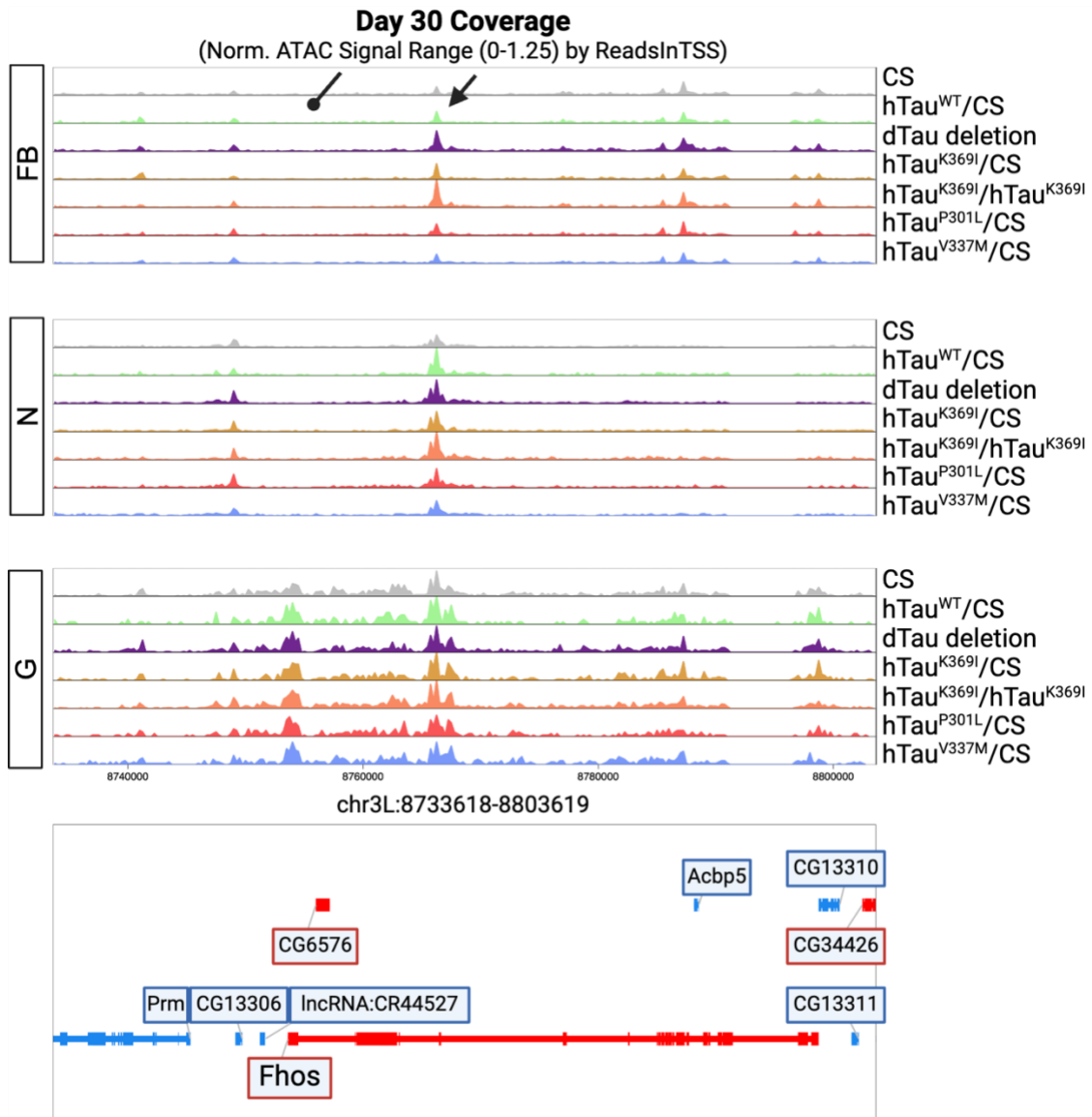
(A) FlyBase JBrowse *Drosophila melanogaster* (r6.56) was used for the isoform schematic of dTau with labels denoting the region of B-D are in the gene. (B) Raw sciATAC-seq reads for transcription start site (TSS) for longer isoforms. dTau^{del} (*) and hTau^{K369I} homozygous (**) flies have an absence of reads in the TSS region. (C) Beginning of exon 1 where reads for dTau^{del} are seen (***). (D) End of gene region showing reads in the hTau^{K369I} homozygous (**) flies. (KI – K369I)



Day 5 DA Strain vs hTau^{WT}/CS

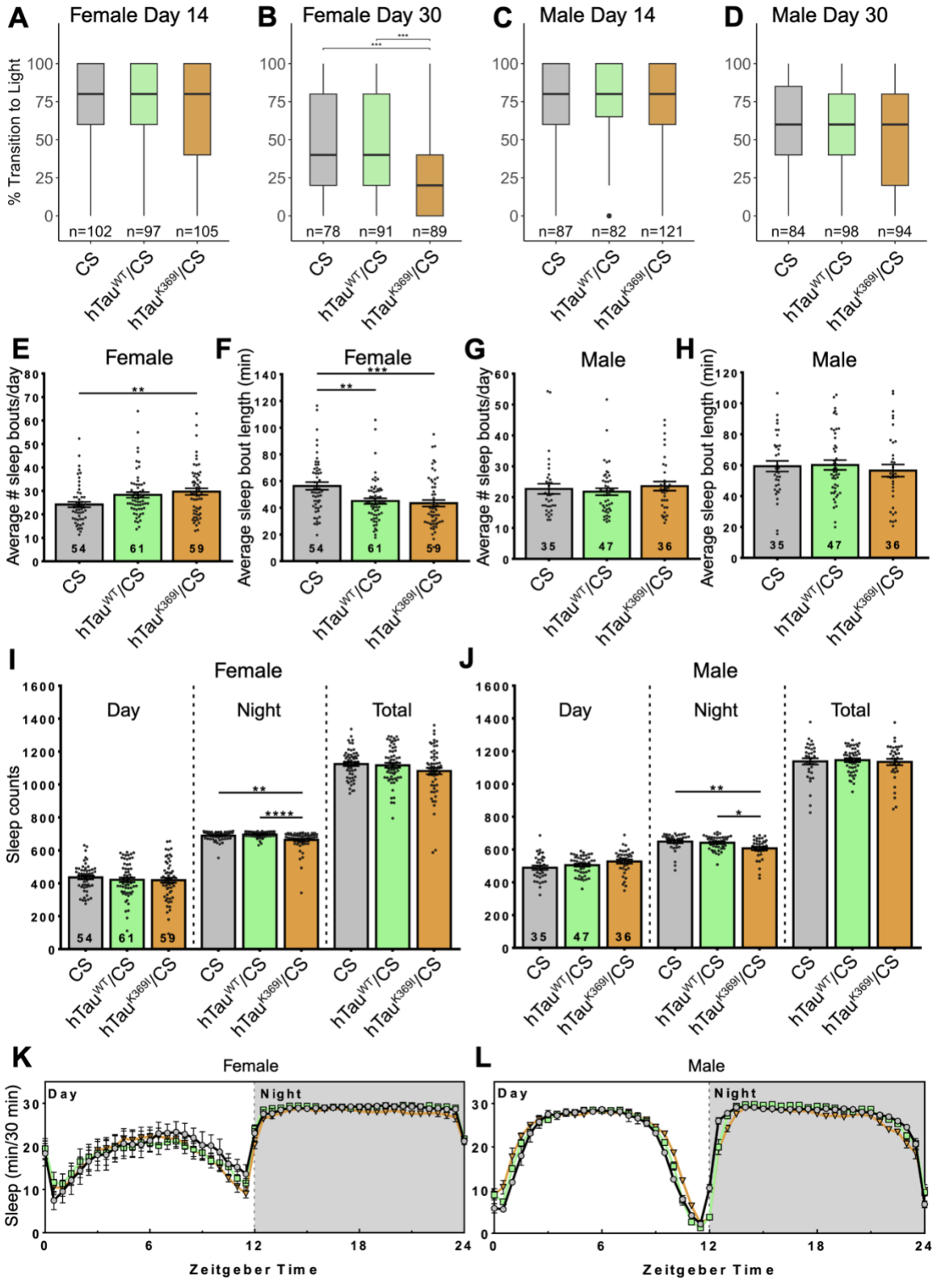
Supplemental Figure 3: Number of accessible peaks by cell type for each strain compared to hTau^{WT} heterozygous in 5-day old heads.

Above the zero line is the number of differential accessible (DA) peaks with increased accessibility in listed strain. Below the zero line is the number of DA that are increased in the hTau^{WT} heterozygote. (N neurons, P photoreceptors, FB fat body, H hemocytes, M muscle, G3 unknown group 3, G4 unknown group 4, Un unknown, G glia). Wilcoxon Rank Sum test, FDR ≤ 0.05 and Log2FC > 0. Acc – accessibility.



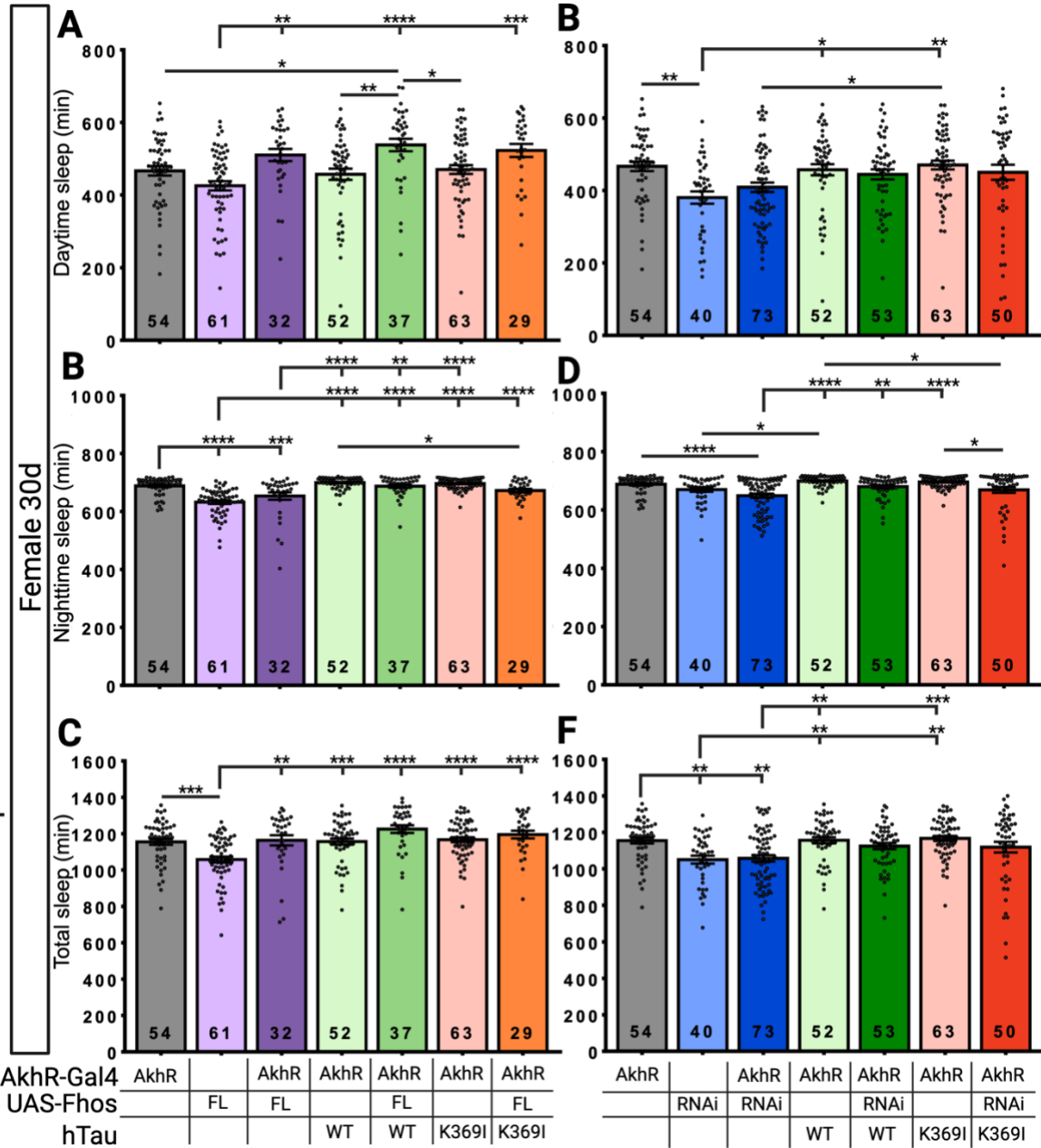
Supplemental Figure 4: Increased accessibility within *Fhos* gene in $hTau^{K369I}$ homozygous and dTaudel in fat body of aged flies.

ArchR coverage browser for chromatin accessibility of *Fhos* gene in 30-day old heads normalized by reads in transcriptional start sites (Granja et al., 2021). (A) Fat body, FB. (B) Neuron, N. (C) Glia, G.



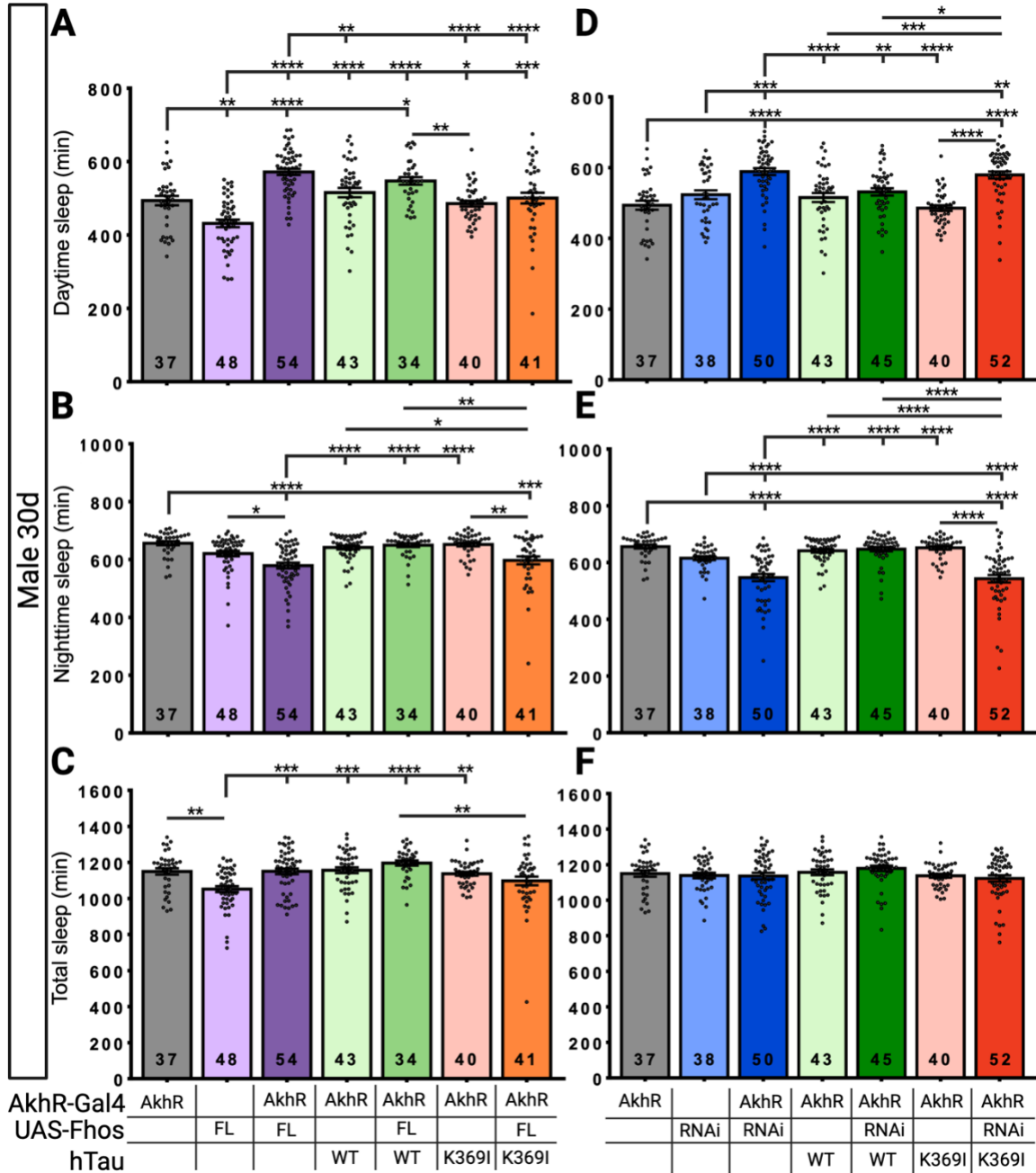
Supplemental Figure 5: Heterozygous hTau^{K369I} flies display decreased locomotor drive and fragmented sleep quality in aged females.

(A, B, C, D) hTau^{K369I} expression decreases locomotor drive in 30-day old female flies compared to controls. Statistics were run across all conditions using Kruskal-Wallis with Dunn's multiple comparisons and Holm adjustment. Sample size is indicated on plots with whiskers indicating the 1.5xIQR (Interquartile range Q3 to Q1). *p<0.05, **p<0.01, ***p<0.001, ****p<0.0001). (E, F, G, H) hTau^{K369I} expression results in sleep fragmentation with an increased average number (A) and shorter average length (B) of sleep bouts in 30-day old female flies compared to controls. (I, J) Female and male hTau^{K369I} expressing flies exhibit decreased nighttime sleep at 30-days of age. (K, L) Both female and male hTau^{K369I} flies have normal sleep profiles with increased activity in the early morning and late evening (Circle, CS; Square, hTau^{WT}/CS; Triangle, hTau^{K369I}/CS). Statistics were run across all conditions using ANOVA with Bonferroni adjustment. Sample size is indicated on plots. *p<0.05, **p<0.01, ***p<0.001, ****p<0.0001. Error bars indicate SEM.



Supplemental Figure 6: *Fhos* overexpression in the fat body increases daytime sleep in aged females.

(A) Flies with *Fhos* overexpression have significantly increased daytime sleep in 30-day old females. (B, C) *Fhos* overexpression in flies results in a slight but significant decrease in nighttime sleep and an increase in total sleep in 30-day old females. (E, D, F) *Fhos* knockdown slightly decreases daytime, nighttime, and total sleep in 30-day old females. Statistics were run across all conditions using ANOVA with Bonferroni adjustment. Sample size is indicated on plots. * $p < 0.05$, ** $p < 0.01$, *** $p < 0.001$, **** $p < 0.0001$. Error bars indicate SEM.



Supplemental Figure 7: *Fhos* knockdown in the fat body increases daytime and decreases nighttime sleep in hTau^{K369I} in aged males.

(A, B, E, F) *Fhos* overexpression and knockdown both result in increased daytime sleep and decreased nighttime sleep in 30-day old males. hTau flies with *Fhos* overexpression have minimal changes in daytime sleep. However, hTau^{K369I} males with *Fhos* overexpression have decreased nighttime sleep and with *Fhos* knockdown have increased daytime and decreased nighttime sleep. (C, F) *Fhos* overexpression cause small changes in total sleep. Statistics were run across all

conditions using ANOVA with Bonferroni adjustment. Sample size is indicated on plots. * $p < 0.05$, ** $p < 0.01$, *** $p < 0.001$, **** $p < 0.0001$. Error bars indicate SEM.

Chapter 4: Additional studies on candidate genes from single-cell genomics sequencing

Unpublished data

Funding: NIA F31AG076251

4.1 Validation of cell-type specific behavioral effects in *Tau* and *Fhos* genetic interaction

Experimental Rationale

In Chapter 3, we found that increasing *Fhos* expression in the fat body impacts both locomotion and sleep behavior (**Figure 12A-D**; **Figure 13A-B**; **Supplemental Figure 6A**; **Supplemental Figure 7A, B**). Knocking down *Fhos* in the fat body alleviated the behavioral phenotypes in the hTau^{K369I} mutant, but phenotypes were worsened in flies with homozygous dTau or heterozygous hTau^{WT} (**Figure 12E-H**; **Figure 13E, F**). This suggests that increased expression of *Fhos* could be contributing to the toxicity of the hTau^{K369I} mutant. The advantage of single-cell genomics is the resolution of cell-type specific changes. Thus, in Chapter 3, we wanted to validate our findings by specifically manipulating *Fhos* expression in the fat body by using cell-type specific GAL4 drivers (Chapter 3). We can also use the cell-type specific information to demonstrate that the protective effects of *Fhos* knockdown in hTau^{K369I} is specific to the fat body by manipulating *Fhos* in other cell types within our hTau model.

In the sequencing experiments (Chapter 3), we found that *Fhos* was highly accessible and expressed within the glia cluster across all strains (**Figure 11A, B**). Therefore, we hypothesized that manipulation of *Fhos* expression in glia will negatively impact behavior in all strains as it is likely necessary for proper cellular function. Similar to the fat body, the neuronal cluster also had increased expression of *Fhos* in the hTau^{K369I} mutant. Based on evidence that *Fhos* knockdown in neurons is beneficial for aging and disease phenotypes in

Drosophila, we hypothesized that increased expression of *Fhos* in the neuronal cluster would negatively affect behavior (Ordonez et al., 2018; Schmid et al., 2023 preprint). Here, we show that appropriate levels of *Fhos* in glia and neurons is required for normal behavior in all tau contexts (both dTau and hTau), which further supports the specificity of our phenotype within the fat body in Chapter 3.

Results and Discussion

Fhos manipulation in glial cells

In our initial experiments, we found that overexpression of *Fhos* in glia is developmentally lethal (at the larval and pupa stage) with few survivors. Therefore, we created a loco-GAL4 driver line, where expression of GAL4 is regulated by temperature using the GAL4/GAL80ts system. This expression system is described in **Figure 5** for reference. The strain genotypes, description and how the flies are referred to in the following text are outlined in **Table 1**. In this system, the binding of GAL4 to the UAS promoter is inhibited by the GAL80ts protein when the flies are grown at 18°C, but inhibition is lifted when the flies are kept at 29°C. This allows for restriction of *Fhos* overexpression to adulthood and resulted in viable adult flies. Therefore, all loco-GAL4 *Fhos* overexpression experiments were conducted at 18°C for development, and then adults were collected and moved to 29°C for aging. To create the double mutant with hTau and temperature controlled *Fhos* overexpression, we introduced hTau through recombination with the loco-GAL4 line, which is described in **Figure 6**. This line was then crossed into our GAL80ts line to create a stable line with UAS/GAL4/GAL80ts with hTau. The

GAL80ts expression was expressed ubiquitously through the tubulin promoter (**Figure 5**). The lifecycle and aging of the fly is influenced by temperature, with flies aging faster at higher temperatures. Therefore, instead of using 14 days old as our “young” timepoint, we tested flies at 10 days of age. Similarly for the aged flies, instead of 30-day old flies, we used 15 days of age as the “old” age timepoint. These testing days were used because we found a similar phenotype in the hTau^{K369I} flies compared to CS and hTau^{WT} when reared in the 18/29°C conditions compared to 25°C (**Supplemental Figure 5B, Figure 14B**).

Our sequencing experiments show that *Fhos* is highly expressed in glia, therefore, we expected that any manipulation of *Fhos* expression would negatively impact locomotion in the flies, regardless of which *Tau* is co-expressed. In young females, we found no significant locomotion differences between *Fhos* overexpression flies and the respective controls, except hTau^{WT} (**Figure 15A**). The hTau^{WT} *Fhos* overexpression flies had significantly decreased locomotor drive compared to the hTau^{WT} driver control (**Figure 15A**). In aged females, we found that both hTau^{WT} and hTau^{K369I} *Fhos* overexpression had significantly reduced locomotion compared to hTau driver controls (**Figure 15B**). In young males, there was a significant decrease of locomotor drive in hTau^{K369I} *Fhos* overexpression compared to the driver control (**Figure 15C**). In aged males, we see a decrease of both hTau^{WT} and hTau^{K369I} *Fhos* overexpression compared to the respective hTau driver controls (**Figure 15D**). The hTau^{K369I} *Fhos* overexpression flies were also significantly lower in locomotor drive than *Fhos* overexpression alone (**Figure 15D**). Overall, this data shows that *Fhos* overexpression is most detrimental in hTau^{K369I}.

However, it also negatively effects locomotion in *Fhos* overexpression alone and in the hTau^{WT} *Fhos* flies in both males and females. This is similar to the fat body *Fhos* overexpression locomotion phenotype (**Figure 12**).

We then tested whether the protective effects of *Fhos* knockdown in the hTau^{K369I} was specific to the fat body. The *Fhos* knockdown in glia was viable and thus we were able to use the UAS/GAL4 system with the loco-GAL4 driver at 25°C (**Figure 4D**). Again, we used recombination to create a line with loco-GAL4 and the hTau, which then could be combined with the UAS-*Fhos*-RNAi construct (**Figure 6**). In young females, knocking down *Fhos* in hTau^{WT} and hTau^{K369I} significantly decreased locomotion compared to *Fhos* knockdown alone (**Figure 15E**). hTau^{WT} *Fhos* knockdown was significantly decreased from the hTau^{WT} driver control as well (**Figure 15E**). In aged females, we also see a decrease in hTau^{K369I} *Fhos* knockdown compared to both the driver control and *Fhos* knockdown alone (**Figure 15F**). hTau^{WT} with *Fhos* knockdown was decreased but did not reach significance. This suggests that the protective effect of *Fhos* knockdown in hTau^{K369I} females may be fat body specific. In young males, hTau^{WT} was significantly decreased from the hTau^{WT} driver control as we saw in the females (**Figure 15G**). hTau^{K369I} *Fhos* knockdown was also decreased in young flies but was not significant (**Figure 15G**). In aged males, both *Fhos* knockdown, hTau^{WT} and hTau^{K369I} with *Fhos* knockdown were significantly worse than the respective driver controls (**Figure 15H**). This suggests that *Fhos* knockdown in glia hinders locomotion in aged male flies. It follows that endogenous levels of *Fhos* are important for glial function and that knockdown of *Fhos* does not protect hTau^{K369I}

as seen in females with fat body specific knockdown (**Figure 12**). The role of *Fhos* in glia has not been studied. Given that *Fhos* is involved in actin nucleation, it would be interesting if the mechanism of action was related to metabolic support of neurons since actin is important as an anchor for glycolysis machinery within the cell and can serve to activate or inactivate enzymatic function (DeWane et al., 2021). Glia is required for proper metabolic function in neurons and thus, proper neuronal signaling and behavior (McMullen et al., 2023). However, since actin is integral to numerous cellular pathways, there are many directions in which this work could go to determine the mechanism of action of *Fhos* in glia.

All sleep experiments had to be run in a 25°C incubator due to logistical issues (availability of incubator space). The temperature sensitive system is not as robust at 25°C and the flies were kept in the sleep incubator for 5 days (with one acclimation night). Therefore, any sleep phenotypes from *Fhos* overexpression would be due to overexpression prior to the sleep assay. Conversely, the lack of a phenotype could be due to the decrease in overexpression of *Fhos* at 25°C. These confounders should be taken into consideration when interpreting the glial *Fhos* overexpression experiments.

We looked at whether *Fhos* manipulation in glia influenced sleep fragmentation and quantity. As mentioned in the previous section, sleep fragmentation is a common issue in dementia patients (McCarter et al., 2016). We can measure sleep fragmentation by comparing the number of sleep bouts per day and the average length of the bouts. More bouts of a short length compared to the respective control is considered an increase in fragmented sleep. Flies were

tested at 2-weeks as they age faster in 29°C. Based on the expression of *Fhos* in glial cells and the role of the glia clock in sleep regulation, we expected that manipulation of *Fhos* expression could influence sleep fragmentation (Artiushin and Sehgal, 2020). In females, we see that the *Fhos* overexpression construct control has fragmented sleep compared with the driver control, but otherwise no significant changes (**Figure 16A, B**). Similarly in males, the *Fhos* overexpression construct control shows fragmented sleep compared to the driver control and the *Fhos* overexpression (**Figure 16C, D**). In contrast, *Fhos* overexpression in hTau^{WT} and hTau^{K369I} does not alter sleep fragmentation compared to the respective driver controls (**Figure 16C, D**). Repeating these sleep experiments at the correct temperature for *Fhos* overexpression (29°C) will be helpful in confirming these results and *Fhos*' role in sleep within glia cells.

Since the *Fhos* knockdown experiments were conducted with the UAS/GAL4 expression construct, the flies were grown and tested at 4-weeks of age at 25°C. In aged females, *Fhos* knockdown has significant fragmented sleep compared to the driver control but was similar to the construct control (**Figure 16E, F**). This is likely due to difference in genetic background and not a true phenotype. In males, we see significant increase of average bouts per day in hTau^{K369I} and hTau^{WT} with *Fhos* knockdown compared to both controls and a significant decrease in average length compared to the driver control (**Figure 16G, H**). This suggests that *Fhos* knockdown is harmful to sleep quality in the hTau^{K369I} males. We also see a trend towards increased fragmentation in the hTau^{WT} flies when *Fhos* is knocked down, and in *Fhos* knockdown alone but to a lesser extent (**Figure**

16G, H). Together, this shows that *Fhos* knockdown negatively impacts sleep quality in males and that the hTau^{K369I} are particularly susceptible.

In dementia patients, the ratio of daytime and nighttime sleep is shifted to more daytime and frequent waking at night (McCarter et al., 2016). Therefore, in addition to fragmentation of sleep, we assessed whether there are changes in sleep quantity in the day or nighttime. In females with *Fhos* overexpression, we found that there was an increase in daytime sleep compared to both controls in all conditions (**Figure 17A**). We see no changes from *Fhos* overexpression for nighttime sleep (**Figure 17B**). In total sleep, there were significant changes in the *Fhos* overexpression conditions compared to controls, which is driven by the changes in daytime sleep (**Figure 17C**). All aged female flies with *Fhos* knockdown exhibit a decrease in daytime and total sleep with *Fhos* alone and hTau^{K369I}, reaching significance compared to the respective driver controls (**Figure 17D, F**). There are minimal changes in nighttime sleep with *Fhos* knockdown (**Figure 17E**). This is interesting as *Fhos* overexpression is leading to increased daytime sleep and *Fhos* knockdown decreases daytime sleep in all flies with the *Fhos* construct (**Figure 17A, D**). This suggests that *Fhos* expression in glia can influence daytime sleep quantity. Repeating this experiment at 29°C will be important to see if this holds when *Fhos* is continuously overexpressed.

In males, we see a similar pattern with *Fhos* overexpression leading to increased daytime sleep as we saw in females (**Figure 18A**). *Fhos* overexpression alone and with hTau^{K369I} were both significantly increased compared to both controls, while hTau^{WT} was significantly increased compared to the construct

control (**Figure 18A**). As we saw in females, there are also slight increases in total sleep (**Figure 18C**). It is interesting to note that, although there is an increase in daytime sleep, the nighttime sleep did not reduce to compensate leading to greater total sleep quantity. In the *Fhos* knockdown in males, the opposite occurred. Daytime sleep is unaffected in all of the conditions except hTau^{WT} *Fhos* knockdown, which is decreased compared to the hTau driver control (**Figure 18D**). Nighttime sleep is decreased in hTau^{K369I} with *Fhos* knockdown compared to the driver control and hTau^{WT} *Fhos* knockdown compared to both controls (**Figure 18D, E**). These changes are subtle and only hTau^{WT} *Fhos* knockdown has significant decreases in total sleep compared to the hTau driver control (**Figure 18F**). Overall, these sleep experiments show that *Fhos* in glia is necessary for proper sleep quality and duration of sleep. The general trends of increased daytime sleep with *Fhos* overexpression and reduced nighttime sleep with *Fhos* knockdown is consistent with the effect of *Fhos* in the fat body. However, the changes in bouts per day are not consistent across glia and fat body. Lastly, unlike in the fat body, we did not see hTau^{K369I} specific “rescue” with *Fhos* knockdown. This suggests that proper *Fhos* levels are necessary for normal behaviors regardless of the Tau expressed.

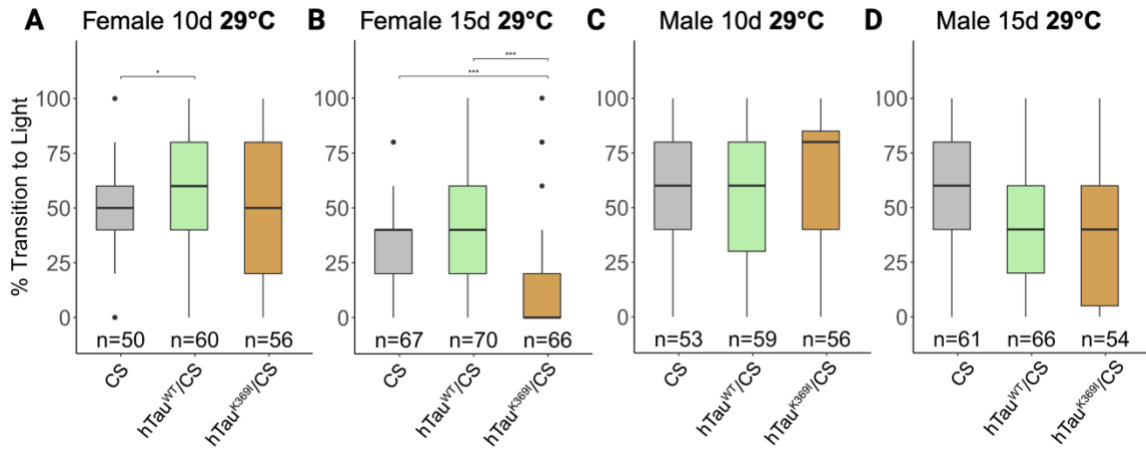


Figure 14: Heterozygous hTau^{K369I} females have reduced locomotor drive when aged at 29°C.

(A) Heterozygous hTau^{K369I} females have normal locomotor drive compared to controls at 10-days of age when raised at 29°C during adulthood. (B) Heterozygous hTau^{K369I} females display reduced locomotor drive compared to controls at 15-days of age when raised at 29°C during adulthood as seen in when aged at 25°C in **Supplemental Figure 5B**. (C, D) Male heterozygous hTau^{K369I} flies have no significant locomotor drive changes compared to controls at either age. Flies developed at 18°C and moved to 29°C during adulthood. 10d – 10-days old, 15d – 15-days old.

Figure 15: *Fhos* overexpression and knockdown in glia reduces locomotor drive in aged flies.

(A) *Fhos* overexpression does not significantly decrease locomotor drive in young female flies compared to the driver controls except in hTau^{WT}. (B, D) hTau^{WT} and hTau^{K369I} *Fhos* overexpression locomotor drive was significantly reduced locomotion compared to hTau driver controls in aged females (B) and males (D). (C) hTau^{K369I} *Fhos* overexpression had decreased locomotion compared to hTau driver control in young males. (E) In young female flies, *Fhos* knockdown decreased locomotor drive in the hTau flies but not in *Fhos* knockdown with homozygous dTau. (F) In aged females, *Fhos* knockdown in hTau^{K369I} flies significantly decreases locomotor drive compared to driver hTau control. (G) hTau^{WT} *Fhos* knockdown flies have significantly less locomotor drive in young males. (H) All aged males with *Fhos* knockdown have significantly decreased locomotion compared to driver controls. Statistics were run across all conditions using Kruskal-Wallis with Dunn's multiple comparisons and Holm adjustment. Sample size is indicated on plots with whiskers indicating the 1.5xIQR (Interquartile range Q3 to Q1). *p<0.05, **p<0.01, ***p<0.001, ****p<0.0001.

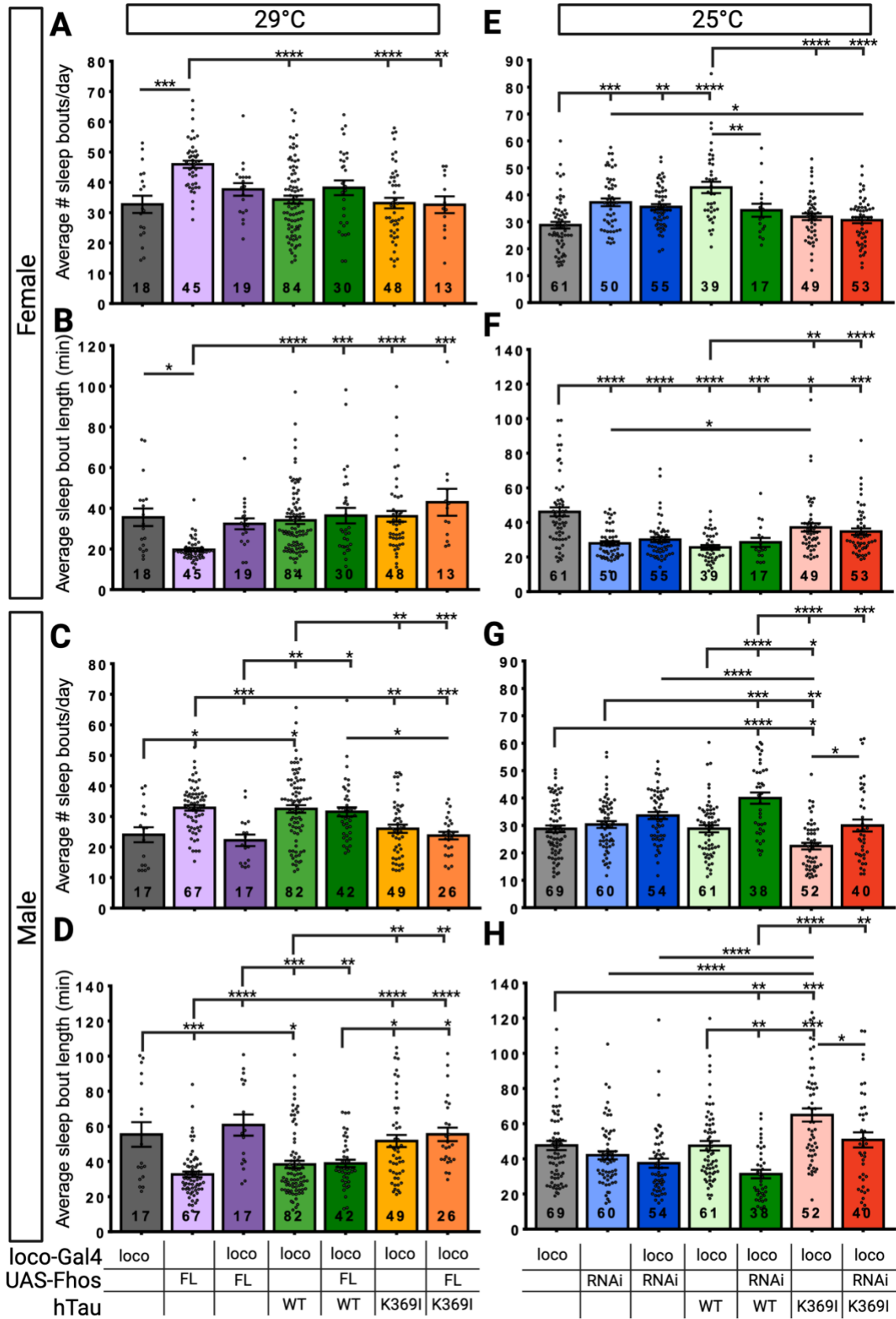


Figure 16: *Fhos* knockdown in glia leads to increased sleep fragmentation in hTau^{K369I} aged flies.

(A, B, C, D) *Fhos* overexpression does not significantly alter sleep fragmentation in aged females or males compared to respective driver controls. (E, F) *Fhos* knockdown in aged females have significant fragmented sleep compared to the driver control but is not different from the construct control. (G, H) In aged males, hTau^{K369I} and hTau^{WT} *Fhos* knockdown has significantly fragmented sleep compared to hTau driver control. Statistics were run across all conditions using ANOVA with Bonferroni adjustment. Sample size is indicated on plots. * $p < 0.05$, ** $p < 0.01$, *** $p < 0.001$, **** $p < 0.0001$. Error bars indicate SEM.

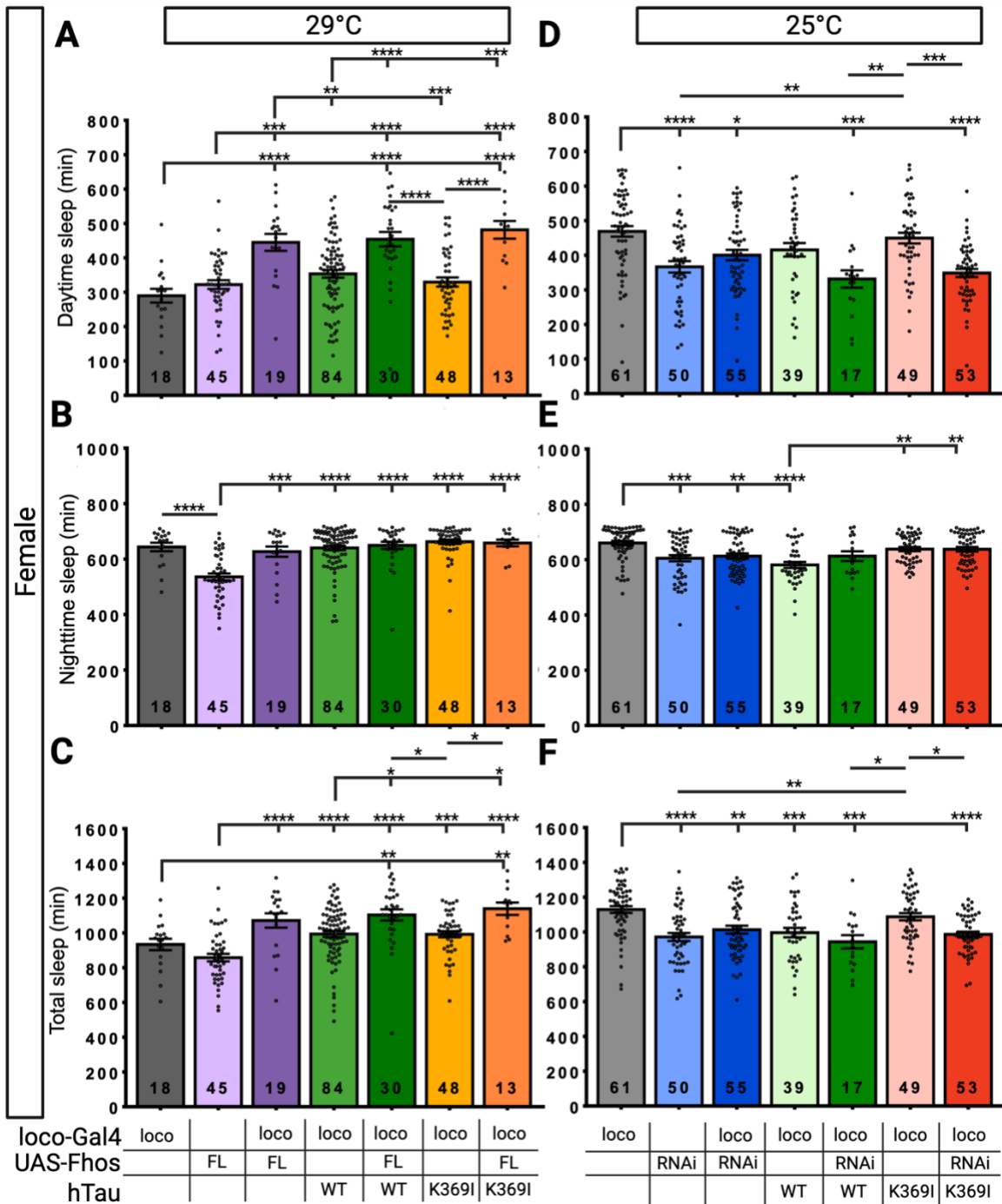


Figure 17: *Fhos* overexpression in glia increases daytime sleep in aged females.

(A, C) *Fhos* overexpression in all conditions resulted in increased daytime sleep compared to the respective construct and driver controls in aged females. These daytime sleep increases drive an increase in total sleep. (B) *Fhos* overexpression did not alter nighttime sleep in aged females. (D, F) *hTau*^{K369I} *Fhos* knockdown has

significantly decreased daytime and total sleep compared to hTau driver control in aged females. (E) *Fhos* knockdown has decreased nighttime sleep compared to driver control but not construct control. Statistics were run across all conditions using ANOVA with Bonferroni adjustment. Sample size is indicated on plots. * $p < 0.05$, ** $p < 0.01$, *** $p < 0.001$, **** $p < 0.0001$. Error bars indicate SEM.

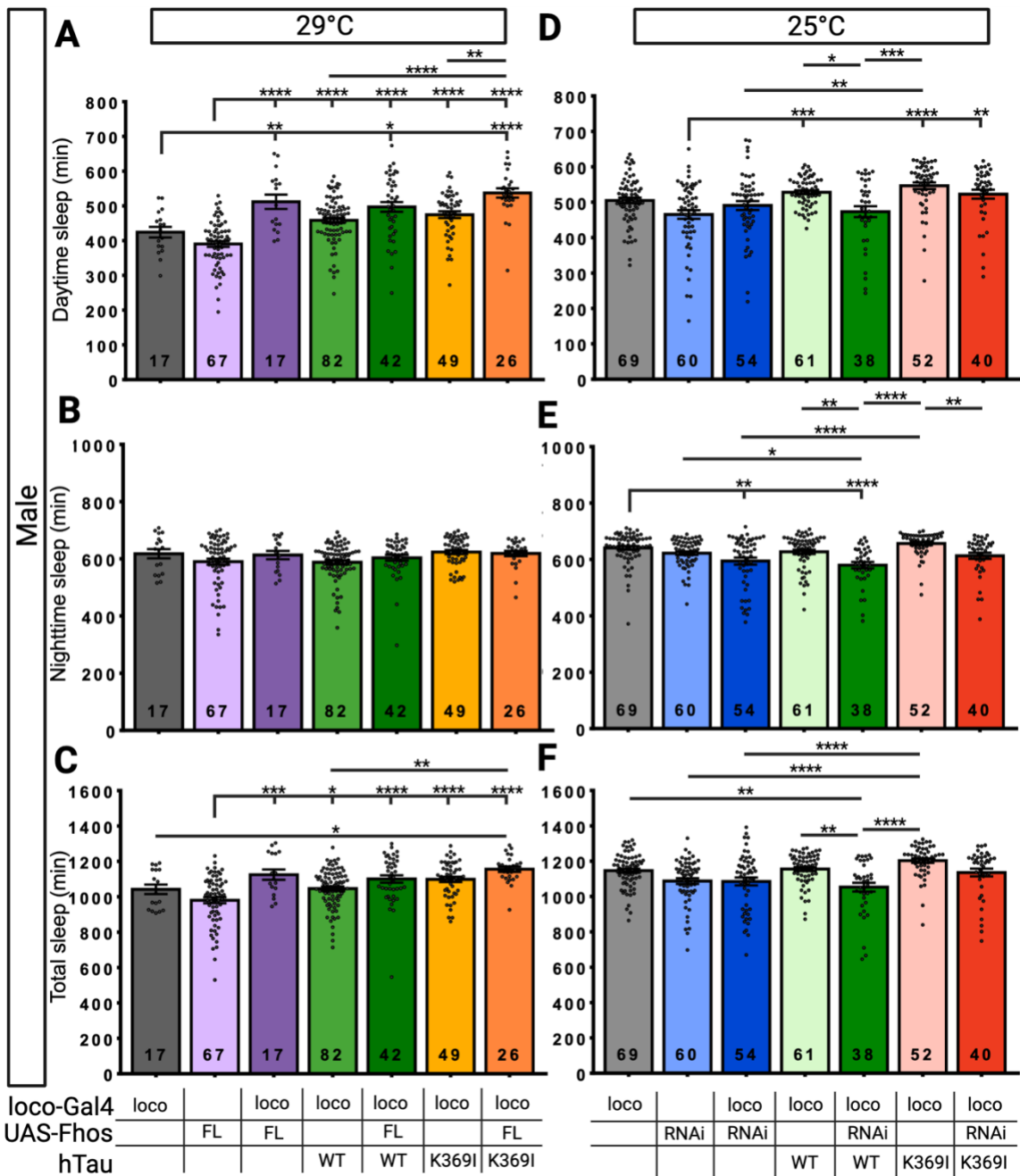


Figure 18: *Fhos* overexpression in glia increases daytime sleep and knockdown in glia decreases nighttime sleep in the hTau^{K369I} mutant males.

(A, C) *Fhos* overexpression leads to increased daytime and total sleep in 30-day old males. (B) *Fhos* overexpression does not alter nighttime sleep. (D, E) *Fhos* knockdown only impacts daytime sleep in hTau^{WT} but decreases nighttime sleep in *Fhos* alone, hTau^{K369I} and hTau^{WT} compared to respective driver controls. (F) *Fhos* knockdown in hTau^{WT} decreases total sleep which is driven by the reduction of nighttime sleep. Statistics were run across all conditions using ANOVA with

Bonferroni adjustment. Sample size is indicated on plots. * $p < 0.05$, ** $p < 0.01$, *** $p < 0.001$, **** $p < 0.0001$. Error bars indicate SEM.

***Fhos* manipulation in neurons**

For the neuronal genetic interaction experiments, we used the Appl-GAL4 driver to pan-neuronally express *Fhos* overexpression and knockdown constructs. This cross is outlined in **Figure 4C**. *Fhos* overexpression in neurons was developmentally lethal as we saw with *Fhos* overexpression in glia. However, it was only lethal in flies with homozygous dTau. We got viable offspring when *Fhos* was overexpressed with either heterozygous hTau^{WT} or hTau^{K369I}. This suggests that the presence of hTau is altering the toxicity of *Fhos* overexpression in the neurons. The mechanism behind this is unknown, but suggests that in neurons, *Fhos* could be specifically interacting with dTau, either directly or indirectly. It could be due to the dosage of dTau, since homozygous dTau flies died while heterozygous survived. Future experiments using either a deficiency line or crossing in the dTau deletion could help to answer this question.

Even though *Fhos* overexpression in neurons was lethal in the context of dTau, we decided to continue to test hTau with *Fhos* overexpression because the flies survived. Future work should repeat these experiments with another neuronal driver to see if this is an Appl-GAL4 specific finding. In addition, there were low numbers of offspring available for testing in the Appl-GAL4 crosses, which could point to the health of the Appl-GAL4 line. Therefore, repeating this experiment either with Appl-GAL4/GAL80ts system or with another neuronal driver will be necessary to confirm these findings and investigate *Fhos* overexpression phenotypes.

As with the fat body and glia validation, we conducted both locomotion (phototaxis) and sleep experiments to assess genetic interaction of *Fhos* and hTau within neurons. We utilized the UAS/GAL4 system for pan-neuronal expression (**Figure 4C**). Our preliminary results for phototaxis with *Fhos* overexpression in neurons showed no significant changes when compared to both controls in both sexes and ages (**Figure 19A-D**). However, this is likely due to our low sample number. Repeating this experiment to see if this pattern holds will be important to understanding the role of *Fhos* in neurons. It is also possible that we need to continue to age the neuronal *Fhos* overexpression to see a similar phenotype to the fat body and glia experiments.

Female 14-day old *Fhos* knockdown flies were not significantly different compared to controls, but the males were slightly decreased compared to the construct control (**Figure 19E, G**). Unfortunately, we had very few flies in the *Fhos* knockdown to test for locomotion phenotypes at 30 days of age. However, the majority of flies tested were only traveling through the first few vials in the counter-current apparatus (i.e., low transition to light; **Figure 19F, H**). In aged females, we see a decrease in locomotion in both of the hTau *Fhos* knockdown flies compared to the hTau driver controls, but only hTau^{WT} reached significance (**Figure 19F**). In aged males, we see a decrease in hTau^{WT} *Fhos* knockdown compared to the hTau^{WT} driver control, but it did not reach significance (**Figure 19H**). Although these decreases are not significant to both controls, this data suggests that knocking down *Fhos* in neurons could be impacting locomotion in both sexes, but to a greater extent in females. Based on the previous literature, we expected

knockdown of *Fhos* in neurons to be beneficial, as it has been shown to increase lifespan and improve negative geotaxis locomotion at 45-days of age when knocked down during adulthood (Schmid et al., 2023 preprint). Knockdown of *Fhos* has also been shown to suppress alpha-synuclein locomotion and neuronal death phenotypes in *Drosophila*, however, this was shown at a younger timepoint (20 days of age; Ordonez et al., 2018). The benefit of *Fhos* knockdown that other groups have seen could be due to the use of a different pan-neuronal GAL4 drivers (*elav*), restriction of knockdown to adulthood or use of a different behavioral assay (Ordonez et al., 2018; Schmid et al., 2023 preprint).

We again measured sleep fragmentation with *Fhos* overexpression and knockdown to see if there were similar effects in neurons as in glia and the fat body. Sleep fragmentation in *Fhos* overexpression hTau flies does not reach significance compared to both controls, which is likely due to the low sample number. If we observe the trends, we see a tendency for fragmented sleep in both the hTau^{WT} and hTau^{K369I} female flies with *Fhos* overexpression (more bouts per day of shorter length; **Figure 20A-B**). The males have no significant differences, similar to the fat body (**Figure 20C-D**).

When *Fhos* was knocked down in females, there was a tendency for fragmentation in all Tau conditions, but it did not reach significance when each were compared to both controls (**Figure 20E-F**). In males, the hTau^{WT} *Fhos* knockdown flies have significant fragmentation compared to both controls (**Figure 20G-H**). Interestingly, the hTau^{K369I} *Fhos* knockdown males are not significantly different from either control (**Figure 20G-H**). This could be due to the increase of

Fhos expression in the hTau^{K369I} mutant. Therefore, the knockdown could be lowering the levels of *Fhos* expression but not to the extent that causes a phenotype like we see with the hTau^{WT}. We saw a similar pattern in phototaxis – hTau^{WT} *Fhos* knockdown has a phenotype, while the hTau^{K369I} *Fhos* knockdown is similar to controls. These results again highlight the sex-specific differences when *Fhos* is manipulated, like we observed in the fat body.

Disruption of day and nighttime sleep is common in FTD patients (McCarter et al., 2016). We again wanted to determine the result of knocking down *Fhos* without hTau expression. Knockdown of *Fhos* in females has significantly less nighttime sleep compared to both controls (**Figure 21E**). Although not significant, the daytime and total are also slightly decreased in the *Fhos* knockdown, however, the sample size is low in these experiments (**Figure 21D, F**). This suggests again that proper *Fhos* levels are necessary for sleep quantity.

With *Fhos* overexpression and knockdown in hTau^{WT} females, we see a significant increase in daytime and total sleep compared to the hTau^{WT} driver control (**Figure 21A, C, D, F**). Hence, proper levels of *Fhos* in neurons are needed in hTau^{WT} for normal daytime sleep in females. There is no difference in sleep quantity in the *Fhos* overexpression or knockdown in hTau^{K369I}, although repeating this experiment will be necessary to increase sample size (**Figure 21A-F**). This could be due to the higher levels of *Fhos* expression, which is counteracted by the *Fhos* knockdown in hTau^{K369I} flies.

In males, there are no differences in sleep quantity from *Fhos* overexpression in any conditions (**Figure 22A-C**). In the *Fhos* knockdown, however, we see a slight increase in daytime sleep with knockdown alone and hTau^{WT} *Fhos* knockdown, both reaching significance compared to the respective driver control (**Figure 22D**). hTau^{WT} *Fhos* knockdown also shows a significant decrease in nighttime sleep compared to both controls and no change in total sleep (**Figure 22E, F**). In contrast, there are no significant changes in sleep quantity in the hTau^{K369I} *Fhos* knockdown flies from controls (**Figure 22E-F**). Repeating these behavioral experiments with restriction of *Fhos* overexpression to adulthood, either using temperature sensitive or drug inducible driver, will be necessary to understand the role of *Fhos* in neurons. Overall, this data supports that *Fhos* has a role in both locomotion and sleep control in neurons that is likely different than the fat body.

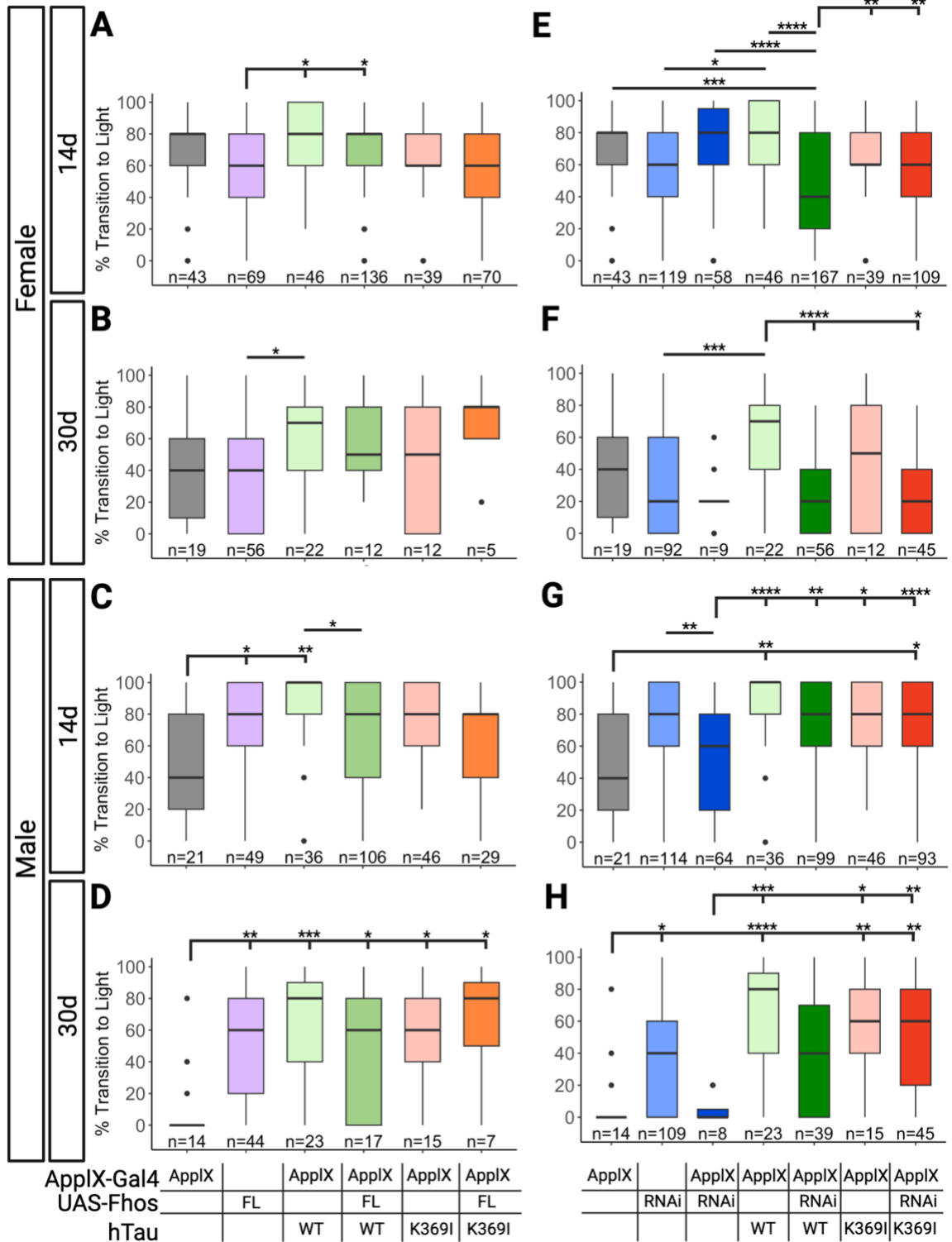


Figure 19: Knockdown of *Fhos* in neurons decreases locomotor drive in aged flies.

(A, B, C, D) *Fhos* overexpression in neurons has no significant effect on locomotor drive in females or males at either age. (E) *Fhos* knockdown in 14-day old females decreased locomotor drive in the hTau^{WT} compared to the hTau driver control. (F) In 30-day old females, hTau^{WT} was still significantly lower than the hTau driver control and hTau^{K369I} was reduced but did not reach significance. (G) There were no significant locomotor changes to controls in the 14-day old males (except *Fhos* knockdown was significantly lower than the construct control). (H) In 30-day old males, hTau^{K369I} *Fhos* knockdown was not significantly different from the hTau driver control. Statistics were run across all conditions using Kruskal-Wallis with Dunn's multiple comparisons and Holm adjustment. Sample size is indicated on plots with whiskers indicating the 1.5xIQR (Interquartile range Q3 to Q1). *p<0.05, **p<0.01, ***p<0.001, ****p<0.0001.

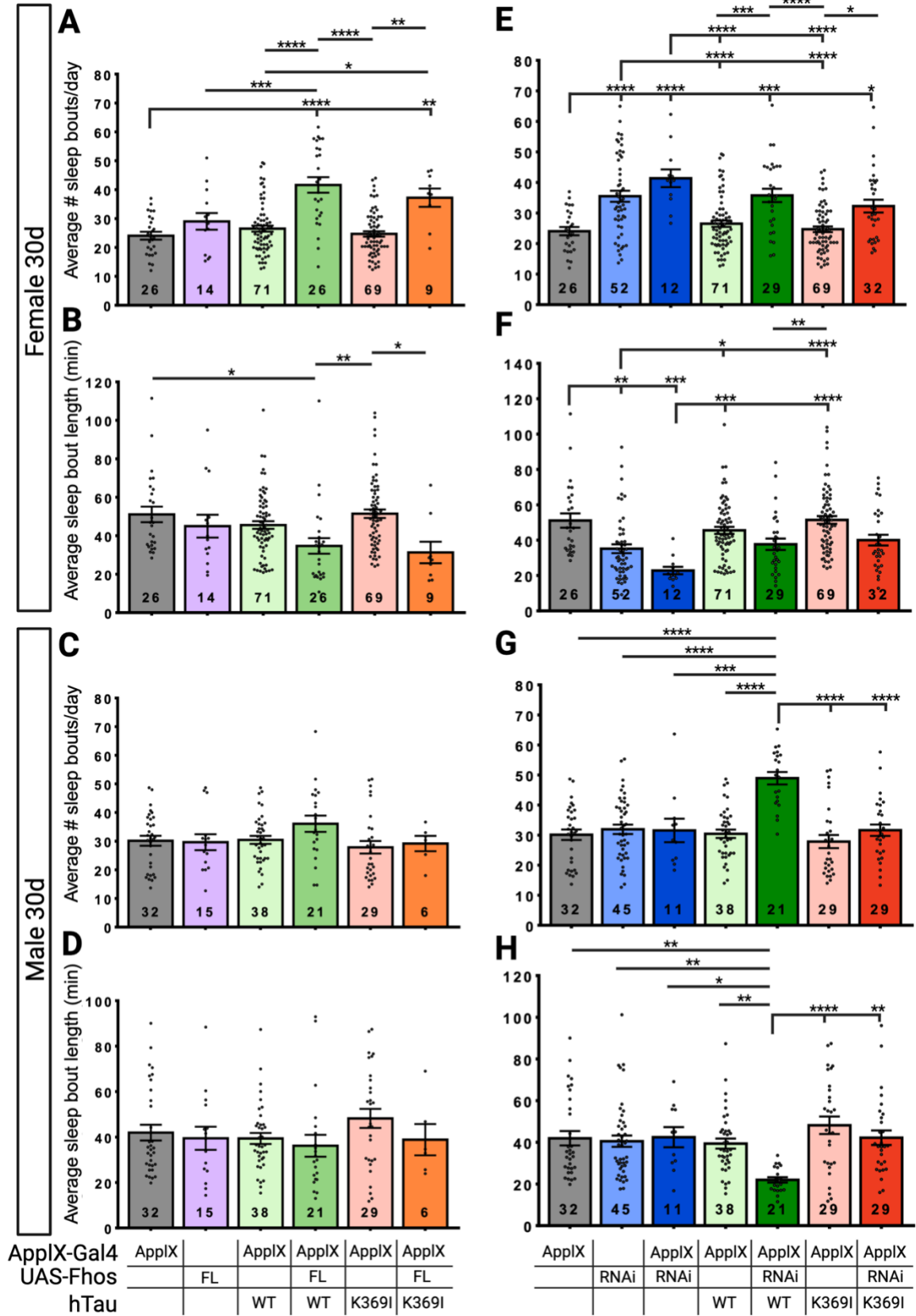


Figure 20: Overexpression and knockdown of *Fhos* in neurons worsens sleep fragmentation in females.

(A, B) *Fhos* overexpression significantly increased number of bouts per day (A) and decreased bout length compared to hTau driver controls in 30-day old females. (C, D) In 30-day old males, there were no significant changes in number of bouts (C) or length (D). (E, F) *Fhos* knockdown also significantly increased number of bouts per day (E) and decreased bout length (F) in 30-day old females. (G, H) hTau^{WT} *Fhos* knockdown reaches significance for both number of bouts (G) and length (H) compared to both controls. Statistics were run across all conditions using ANOVA with Bonferroni adjustment. Sample size is indicated on plots. * $p < 0.05$, ** $p < 0.01$, *** $p < 0.001$, **** $p < 0.0001$. Error bars indicate SEM.

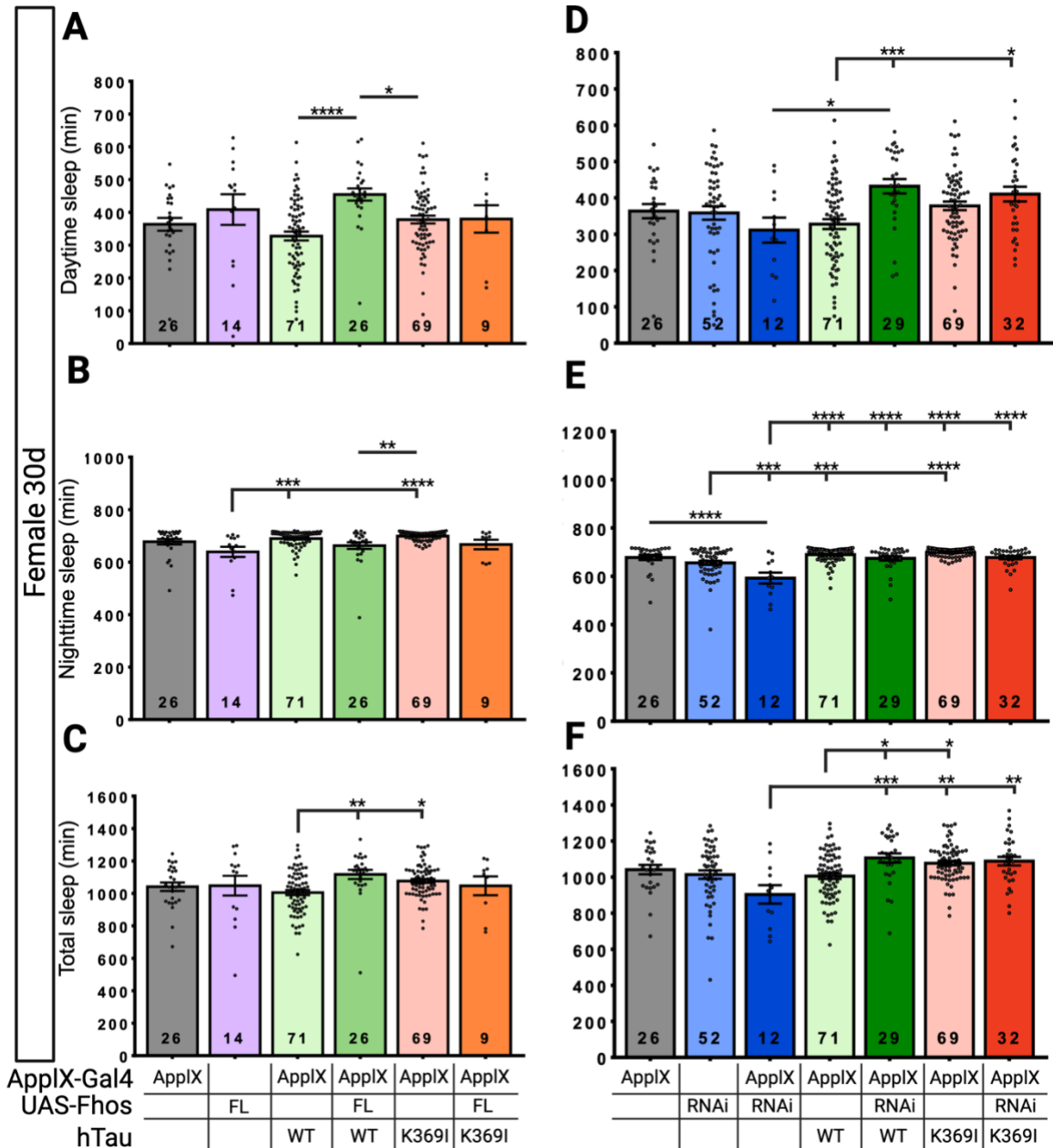


Figure 21: Duration of sleep is minimally impacted by *Fhos* overexpression and knockdown in neurons in aged females.

(A, C, D, F) hTau^{WT} *Fhos* overexpression and knockdown had increased daytime and total sleep compared to the hTau driver control but hTau^{K369I} was unchanged in 30-day old females. (B, E) *Fhos* overexpression and knockdown did not influence nighttime sleep in hTau flies. (E) *Fhos* knockdown significantly decreased nighttime sleep compared to both controls. Statistics were run across all conditions using ANOVA with Bonferroni adjustment. Sample size is indicated on plots. *p<0.05, **p<0.01, ***p<0.001, ****p<0.0001. Error bars indicate SEM.

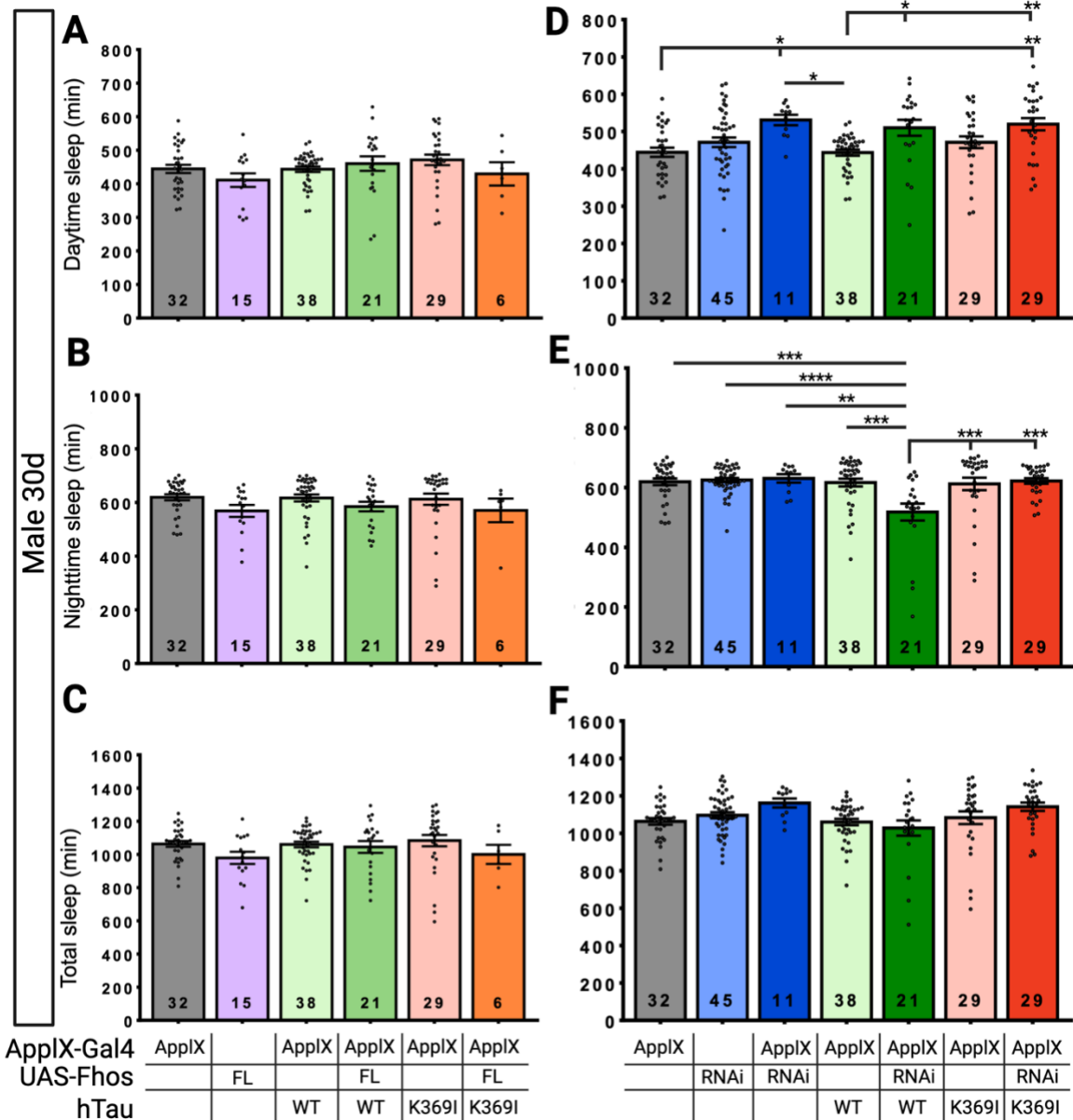


Figure 22: *Fhos* knockdown in neurons can impact nighttime sleep duration in aged *hTau*^{WT} males.

(A, B, C) *Fhos* overexpression had no effect on sleep quantity in 30-day old males. (D) *Fhos* knockdown increased daytime sleep with *hTau*^{WT} and homozygous *dTau* flies reaching significance. (E) *Fhos* knockdown decreases nighttime sleep in *hTau*^{WT} compared to controls but had no effect on *hTau*^{K369I}. (F) *Fhos* knockdown had no effect on total sleep for any conditions. Statistics were run across all conditions using ANOVA with Bonferroni adjustment. Sample size is indicated on plots. **p*<0.05, ***p*<0.01, ****p*<0.001, *****p*<0.0001. Error bars indicate SEM.

4.2 Patterns of Neurodegeneration in hTau^{K369I} FTD mutant

Experimental Rationale

Manipulation of *Fhos* expression in the fat body modulated both locomotion and sleep in hTau flies. We decided to assess if *Fhos* could also impact neurodegeneration in the context of hTau^{K369I}. There are a few ways to test for neuronal loss such as TUNEL (DNA fragmentation) or staining for apoptosis (caspase) and counting neuron numbers in a brain region. Another is to serially section the *Drosophila* brain and assess for neurodegenerative vacuoles. This allows for systemic evaluation of each brain. Vacuoles are dark, round holes that are visible in multiple sections and indicate cell or axon degradation. The neuropil of the *Drosophila* brain are the neuronal processes, and the cell bodies are within the cortex (**Figure 23**). In this dataset, we were limited by the number of brains and thus, we will discuss general observations that can be further classified in future work. We have previously seen neurodegenerative vacuoles at 60 days of age in the hTau^{V337M} FTD-associated mutant (Cassar et al., 2020). Due to low sample numbers with aging, we decided to use 45-day old female flies.

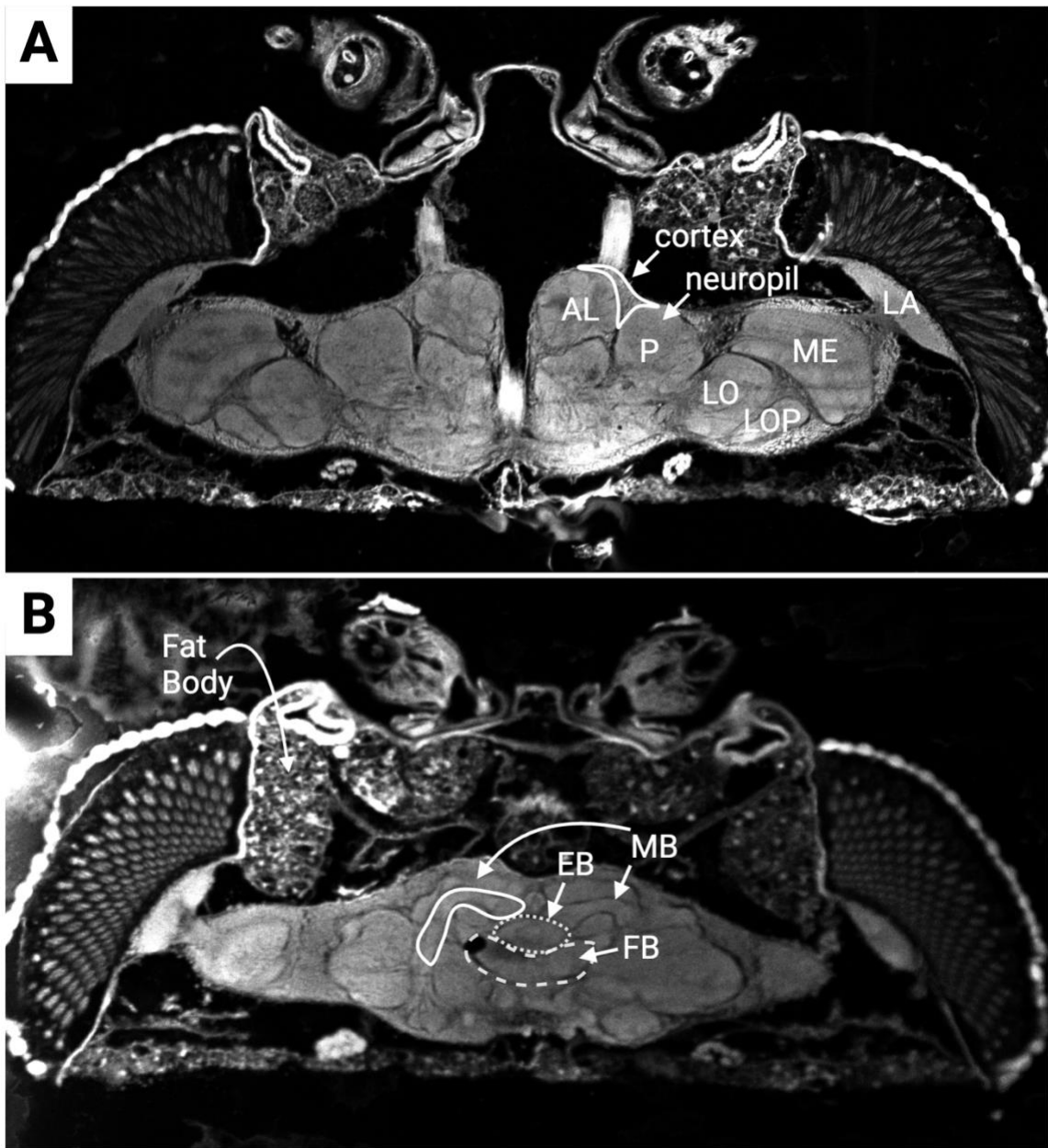


Figure 23: Neuroanatomical organization of *Drosophila* adult brain.

(A) AL antennal lobe, P protocerebrum. Optic Lobe: LO lobula, ME medulla, LA lamina. (B) EB ellipsoid body, FB fan-shaped body, MB mushroom body.

Results and Discussion

It is important to note that it is expected that hTau^{WT} flies will also have some neurodegeneration as vacuoles increase with age in normal flies (**Figure 24A**). Neurodegenerative vacuoles have been seen in brains as early as 30 days of age (Sunderhaus and Kretzschmar, 2016). The size of vacuoles in the brain can be highly variable ranging from a few microns to 40-micron large holes or larger (large holes pictured in **Figure 24C, F**). In future work, counting the number of holes and binning based on size may help to elucidate differences between FTD-associated mutants and wildtype. We saw general trends when images were classified by existence of small, medium, and large holes. There were more small and medium vacuoles in the hTau^{WT} and hTau^{K369I} alone as well as with hTau *Fhos* overexpression (**Figure 24A, D**). However, we had very low numbers for hTau^{K369I} so this would need to be confirmed with more samples. Interestingly, we saw many examples of large holes in the *Fhos* knockdown flies in both hTau^{WT} and hTau^{K369I} (**Figure 24C, F**). While the other conditions had more medium sized vacuoles (**Figure 24A, B, D, E**).

There has been extensive characterization of brain regions in the *Drosophila* and other insect systems (Ito, 1994; Ito et al., 2014). This allows us to generally classify regions where neurodegeneration is occurring. Neurodegenerative vacuoles are a late-stage phenotype in our model, which recapitulates the late-stage atrophy seen in FTD patients. Quantification of susceptible regions and determining whether *Fhos* manipulation alters accumulation of vacuoles will help to better understand the progression of disease

in the context of *Fhos*. It could also reveal where to focus future efforts for behavioral or cellular phenotypes. This pilot analysis showed potential susceptible regions when *Fhos* is manipulated in the fat body. In particular, there are a few large holes near the fan-shaped body and ellipsoid body in the hTau^{WT} *Fhos* knockdown (**Figure 24C**). The fan-shaped body and ellipsoid body are part of the central complex (**Figure 23**). There is research connecting these regions to homeostatic sleep and locomotor control (Donlea et al., 2018). Interestingly, the females with hTau^{WT} *Fhos* knockdown had decreased locomotion and increased fragmentation (**Figure 13**). This may be coincidental; however, it will be interesting if further sectioning of these flies shows these regions to be particularly susceptible and if holes in these regions are found in other conditions as well. In addition, repeating the experiment with males will be interesting since many of the behavioral phenotypes are sex specific.

In the hTau^{K369I} *Fhos* knockdown, the majority of the holes were in or near the antennal lobe (**Figure 24F**). This region is responsible for olfaction and interestingly, olfactory changes are one of the symptoms in FTD patients (Carnemolla et al., 2020; Rybak et al., 2016). We could test whether olfactory behavior is altered in the hTau^{K369I} mutant with aging and with *Fhos* manipulation in the fat body. Lastly, the hTau^{K369I} *Fhos* knockdown flies also had large vacuoles in the suboesophageal zone or the nearby cortex, which is the primary taste center (**Figure 24F**; Sterne et al., 2021). One could use a food choice assay to see if taste is altered in hTau^{K369I} flies. This is also an interesting region as FTD patients have changes in sucrose preference and increased caloric intake (Ahmed et al., 2016).

The pilot data for neurodegenerative vacuoles suggests that *Fhos* knockdown may cause the large neurodegenerative vacuoles, but this will need to be confirmed with *Fhos* knockdown alone. From this preliminary data, it appears that *Fhos* knockdown may be more prone to develop large neurodegenerative vacuoles compared to *Fhos* overexpression. However, this may be due to a selection of “healthier” *Fhos* overexpression flies as “sicker” flies could have already died by 45-days of age. Completing a lifespan assay of these flies will help determine whether 45-days of age is selecting for survivors in any of the genotypes. If this is the case, repeating this experiment in younger flies could help to see the overall variation in neurodegeneration before the majority of flies have died. Overall, this preliminary work shows potential for investigating regional neurodegeneration in the mutants.



Figure 24: Neurodegenerative vacuoles in hTau^{WT} and hTau^{K369I} *Fhos* flies.

(A) Cortex and antennal lobe holes in hTau^{WT}/CS. (B) hTau^{WT} *Fhos* overexpression brain with vacuole near suboesophageal zone in the cortex. (C) Large vacuole in hTau^{WT} *Fhos* knockdown in the ellipsoid body. (D) hTau^{K369I}/CS brain with vacuole in suboesophageal zone and cortex. (E) hTau^{K369I} *Fhos* overexpression brain with protocerebrum and cortex near antennal lobe. (F) hTau^{K369I} *Fhos* knockdown brain with large vacuole in suboesophageal zone. Total heads examined: A-9, B-16, C-6, D-3, E-7, and F-7. White arrows indicate vacuoles.

4.3 Screening differentially expressed candidate genes for genetic interaction with FTD-associated hTau^{V337M} mutant

Experimental Rationale

In Chapter 3, we found *Fhos* as a potential target for hTau^{K369I} toxicity. However, there were many interesting targets in the differential expression analysis that could give insight on the pathways that hTau^{K369I} could be modifying. Behavior is one way to screen for genetic interactions, however, this can be time intensive with a large number of candidates and requires aging. An alternative is to use the rough eye phenotype. This assay allows for quickly assessing whether there could be a genetic interaction between hTau and the candidate of interest. The highly ordered structure of the *Drosophila* eye makes it easy to determine if the structure of the ommatidia are altered. This manifests as a “roughness” that is visible under a light microscope. For this experiment, we utilize the UAS/GAL4 system to overexpress hTau^{V337M} in the developing eye (**Figure 25A**). We chose the V337M mutation because it is neurotoxic when overexpressed with the GMR-GAL4 driver, creates a rough eye phenotype, and was available as a stock (Fulga et al., 2007). This system also allows for the overexpression or knockdown of candidate genes in the eye with and without co-expression of hTau^{V337M} (**Figure 25B, C**). If the manipulation of the candidate gene alters the hTau mutant phenotype, then those are potentially interesting pathways to investigate further.

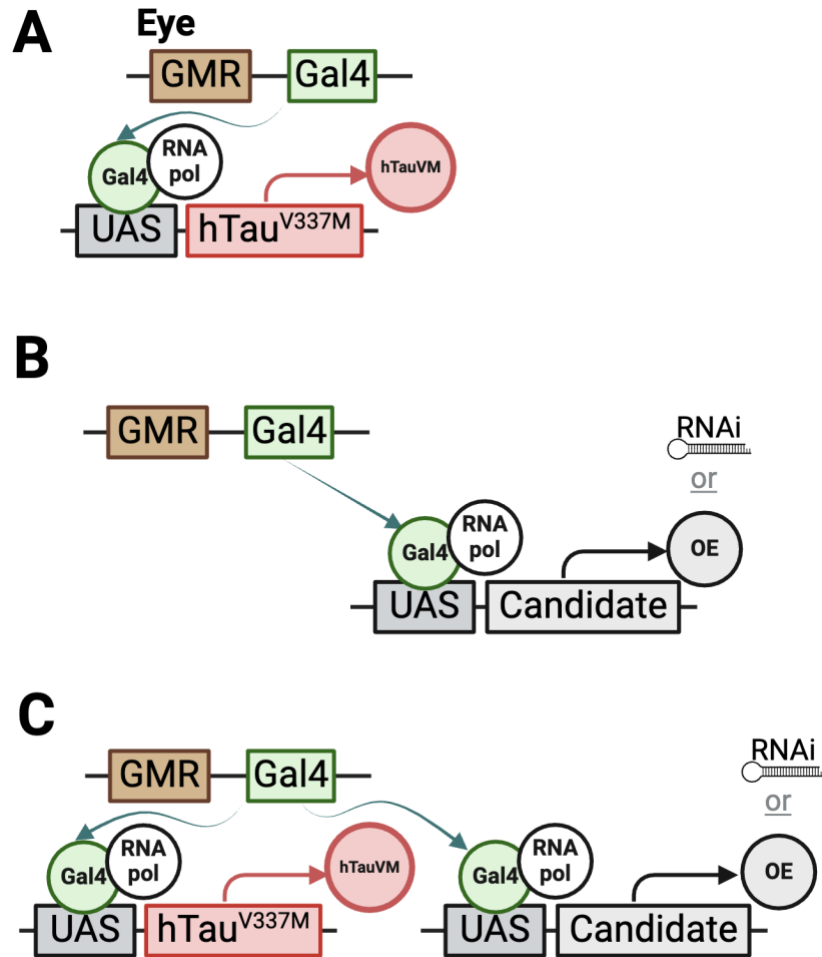


Figure 25: Schematic of expression system for rough eye screen.

(A) hTau^{V337M} overexpression with the UAS/GAL4 expression system in the eye (GMR promoter). (B) Expression of RNAi construct or gene construct of candidates of interest from the snRNA-seq experiment in Chapter 3. (C) Co-expression of hTau^{V337M} and candidate of interest construct in the eye.

One of the limitations of this assay is the gene must be expressed in the eye to see a result when using knockdown construct. Therefore, if there is no alteration to the hTau^{V337M} phenotype with co-expression of candidate gene knockdown, that does not mean that the candidate should be excluded from future investigation. Another limitation is the subjectivity of the roughness measure. As

we see in this experiment, “rough” can be overgrowth, necrosis, smaller eye, and abnormal shaping. Therefore, it was important to compare directly under the microscope to the hTau^{V337M} (note that we included multiple images of hTau^{V337M} (blue) based on the experiment date). For closer inspection of the rhabdomere structure, you can also section the head, similar to the neurodegeneration vacuole assay, but in the sagittal plane. Another option is to use electron microscopy to determine roughness. These are more time intensive but could be utilized to confirm our findings. Overall, this assay is beneficial for identifying promising candidates. These genes can then be validated by another behavioral or cellular assay relevant to dementia-related phenotypes and/or based on the function of the gene of interest.

Results and Discussion

We tested candidate genes from Chapter 3 differential expression in the fat body (**Figure 10**) that are involved in pathways associated with neurodegeneration: cytoskeleton, lipid dynamics, autophagy, insulin signaling, and mitochondrial function (**Table 3**). There were two formin genes (actin dynamics), *Fhos* and *Frl*, that were differentially expressed in the heterozygous hTau^{K369I} compared to heterozygous hTau^{WT} in the fat body. *Fhos* had increased expression while *Frl* had reduced expression (**Table 3**). We found that *Fhos* overexpression and *Frl* knockdown exacerbated the hTau^{V337M} phenotype with smaller and rougher eyes (**Figure 26B2, E2**). This suggests that the dysregulation of these transcripts in hTau^{K369I} could be detrimental, and this supports the previous work showing that

Fhos overexpression negatively impacted behavior. Knocking down *Fhos* did not change the hTau^{V337M} phenotype with either RNAi construct tested. Another cytoskeletal related gene was CLIP-190 but we found that neither knockdown nor overexpression altered the hTau^{V337M} phenotype (**Figure 32B2, C2**). However, this gene was also found in studies of Parkinson's and Tau and thus could be tested further (Kaltenbach et al., 2007; Feuillet et al., 2020).

Apolpp and *Apoltp* function in lipid transport between organ systems (Palm et al., 2012). We found that knocking down these genes in the eye did not alter the hTau^{V337M} phenotype (**Figure 27B2, D2**). An alternative experiment to test these targets could involve lipid droplet formation in the fat body. *Marf* has been linked to lipid droplet and mitochondria function (Bosch et al., 2020; Dorn et al., 2011; Liu et al., 2015; Yang et al., 2022). When *Marf* was knocked down in the hTau^{V337M} flies, we saw no effect on the roughness (**Figure 32J2**). Another candidate gene involved in lipid mobilization and ER stress was *Xbp1* (Zhao et al., 2021). *Xbp1* had reduced expression in hTau^{K369I} compared to hTau^{WT} in a subcluster of the fat body cluster, which we presume to be female due to the expression of female-specific transcripts (**Supplemental Figure 1E, Cluster 3 (C3)**). *Ire1* is upstream of *Xbp1* in the lipid mobilization pathway and *Ire1* also has significantly lower expression in the hTau^{K369I} mutant in the fat body cluster (Zhao et al., 2021). We tested *Xbp1* and found that overexpression with hTau^{V337M} did not alter the phenotype, but it would be interesting to test *Ire1* in the future (**Figure 32I2**). *Klar* is another exciting candidate as it is an ortholog of Nesprin (nuclear membrane protein in LINC complex) and has been shown to interact with lipid droplets

(Patterson et al., 2004; Girard et al., 2021). Expression of *klar* was reduced in the hTau^{K369I} fat body compared to hTau^{WT} (**Table 3**). Interestingly, overexpression of *klar* appears to exacerbate the hTau^{V337M} rough eye phenotype with smaller rougher eyes while knockdown did not alter the phenotype (**Figure 31B2, C2**). This could mean that reduced *klar* expression in the fat body could be beneficial for the hTau mutant. For now, this supports that one of the functions of *klar* may overlap with pathways that are impacted by hTau^{V337M}.

Another pathway that has been extensively studied in tauopathy models is autophagy. *Atg17* and *Atg13* are both involved in the initiation of autophagy (Kim et al., 2017). *Atg17* overexpression and *Atg13* knockdown in hTau^{V337M} flies appear to improve the hTau^{V337M} phenotype in terms of shape and roughness (**Figure 32G2, H2**). *Gyf* is also involved in autophagy and overexpression of *Gyf* rescues the hTau^{V337M} phenotype while knockdown does not alter the hTau^{V337M} phenotype (**Figure 29B2, D2**). In our differential expression analysis, *Gyf* had reduced expression in hTau^{K369I} compared to hTau^{WT} (**Table 3**). These results imply that the autophagy pathway could be a target for future work. In addition to autophagy, *Gyf* has also been linked to the insulin signaling pathway (Giovannone et al., 2003; Giovannone et al., 2009; Vinayagam et al., 2016).

In the differential expression analysis, we found many genes within the insulin signaling pathway (**Figure 33**). The insulin receptor *InR* had reduced expression in hTau^{K369I} compared to hTau^{WT} (**Table 3**). When we knocked down *InR* in the eye, we found that there was partial rescue of the rough eye phenotype in the hTau^{V337M} mutant (**Figure 28B2**). Notably, overexpressing *InR* alone lead to

a drastic overgrowth phenotype (**Figure 28D1**). This is pictured both in the sagittal view and front view to capture the overgrowth compared to control. When *InR* was co-expressed with hTau^{V337M}, we saw smaller, rough eyes that still appear to have an overgrowth compared to hTau^{V337M} alone (**Figure 28C2, D2**). In addition to *Gyf* and *InR*, *srl* and *Xrp1* are also associated with the insulin signaling pathway. *Srl* is known to couple mitochondrial activity to insulin signaling (Tiefenböck et al., 2010). Overexpression of *srl* rescued a *Drosophila* model of Parkinson's with increased dopamine neuron numbers, decreased mitochondrial size, and increased locomotion (Ng et al., 2017). In the rough eye screen, *srl* knockdown did not alter the hTau^{V337M} phenotype (**Figure 32E2**). Based on the previous literature, an overexpression of *srl* could potentially rescue the rough eye if tested. *Xrp1* has been linked to an ALS model in *Drosophila* and inter-organ growth coordination through *Drosophila insulin like peptide 8 (dilp8)*; Boulan et al., 2019; Mallik et al., 2018). *Xrp1* knockdown with hTau^{V337M} shows no change in phenotype from hTau^{V337M} alone (**Figure 30B2**). Interestingly, *Xrp1* overexpression shows severe cell death with a glossy appearance and smaller eye (**Figure 30C1**). When *Xrp1* is overexpressed with hTau^{V337M}, the eye is much smaller with a few necrotic areas (**Figure 30C2**). This suggests that *Xrp1* and hTau^{V337M} may act in similar pathways and that *Xrp1* is a promising candidate for future studies with both the hTau^{K369I} and hTau^{V337M} mutants. Overall, this screen yielded interesting targets, *InR*, *Gyf*, and *Xrp1* for future study and highlights the insulin pathway as a potential modifier of Tau toxicity.

Table 3: Rough eye phenotypes in differentially expressed genes in hTau^{K369I} from the fat body cluster.

Gene	Avg. Log2FC	Adj. P-value	Differential Expression in Fat Body Cluster (5-day old)	Func. (Ref)	RE	
					KD	OE
Fhos	1.17	9.81E-39	Up in hTau ^{K369I} and dTau ^{del}	Actin (Patel et al., 2018)	+/0,0	+/-
Frl	-0.26	6.27E-08	Down in hTau ^{K369I}	Actin (Dollar et al., 2016)	+/-	
apolpp	-0.28	5.12E-21	Down in hTau ^{K369I}	Lipid carrier (Palm et al., 2012)	+/0	
Apoltp	-0.43	4.25E-18	Down in hTau ^{K369I}	Lipid transfer (Palm et al., 2012)	+/0	
InR	-0.31	2.28E-07	Down in hTau ^{K369I}	Insulin receptor (Vinayagam et al., 2016)	+/+	-/-
Gyf	-0.27	1.70E-07	Down in hTau ^{K369I}	Autophagy, insulin (Kim et al., 2015; Giovannone et al., 2009)	+/0	+/+
Xrp1	-0.27	2.98E-07	Down in hTau ^{K369I} and dTau ^{del}	Transcription factor (Boulan et al., 2019)	+/0	-/-
klar	-0.27	1.56E-06	Down in hTau ^{K369I}	Nuclear, lipid droplets (Patterson et al., 2004; Girard et al., 2021)	+/0	+/-
CLIP-190	-0.40	3.72E-19	Down in hTau ^{K369I}	Cytoskeleton (Beaven et al., 2015)	+/0	+/0
lqf	0.71	4.07E-28	Up in hTau ^{K369I}	Autophagy (Csikós et al., 2009)	+/0	
srl	-0.28	1.49E-12	Down in hTau ^{K369I}	Insulin signaling, mitochondria (Tiefenböck et al., 2010)	+/0	
jing	-0.28	2.16E-14	Down in hTau ^{K369I}	CNS development (Sun et al., 2006)	+/0-	
Atg17	-0.29	1.76E-07	Down in hTau ^{K369I}	Autophagy (Cheong et al., 2005)		+/0+
Atg13	0.56	4.79E-03	Up in hTau ^{K369I}	Autophagy (Cheong et al., 2005)	+/0+	
Xbp1	-0.37	3.80E-12	Down in hTau ^{K369I}	ER stress, lipid mobilization (Zhao et al., 2021)		+/0
Marf	0.71	1.94E-20	Up in hTau ^{K369I}	Mitochondria (Dorn et al., 2011)	+/0	

Before (/) indicates the single mutant phenotype: + and - denote no phenotype or rough phenotype, respectively. After (/) indicated the double mutant phenotype with hTau^{V337M}: +, 0, and - denote suppression of hTau^{V337M}, no change from hTau^{V337M} and exacerbation of hTau^{V337M} phenotype, respectively. Multiple symbols used if the phenotype was questionable and would need follow up. Differential expression using Wilcoxon Rank Sum test with a Bonferroni adjustment. Asterisk indicates that the gene was not differential expressed in the entire fat body cluster but was significant in the presumed female fat body cluster (C3, classified by the expression of Yp1 and fit, which are female-specific).

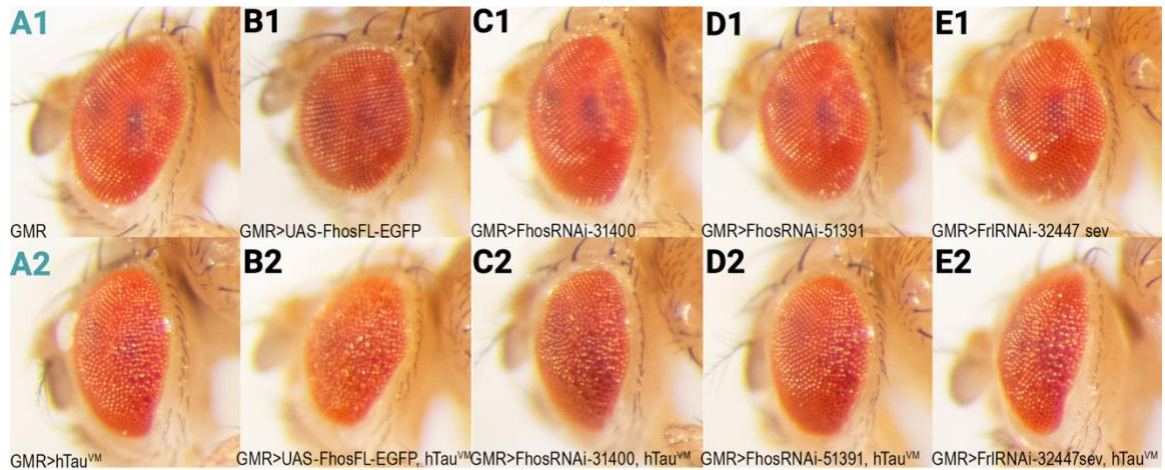


Figure 26: *Fhos* overexpression exacerbates hTau^{V337M} retina neurotoxicity.

- (A1) GMR-GAL4 control for B1, C1, D1, and E1.
- (A2) hTau^{V337M} rough eye control for B2, C2, D2, and E2.
- (B2) *Fhos* overexpression does not impact eye development.
- (B1) *Fhos* overexpression exacerbates hTau^{V337M} rough eye with smaller eyes and bubblier texture.
- (C1) *Fhos* knockdown (31400 stock) has no phenotype.
- (C2) *Fhos* knockdown (31400 stock) with hTau^{V337M} does not alter hTau^{V337M} phenotype.
- (D1) *Fhos* knockdown (51931 construct, used in Chapter 3 and 4) has no phenotype.
- (D2) *Fhos* knockdown (51931 construct, used in Chapter 3 and 4) with hTau^{V337M} does not alter hTau^{V337M} phenotype.
- (E1) *Frl* knockdown has no phenotype.
- (E2) *Frl* knockdown with hTau^{V337M} appears to worsen the size hTau^{V337M} phenotype.

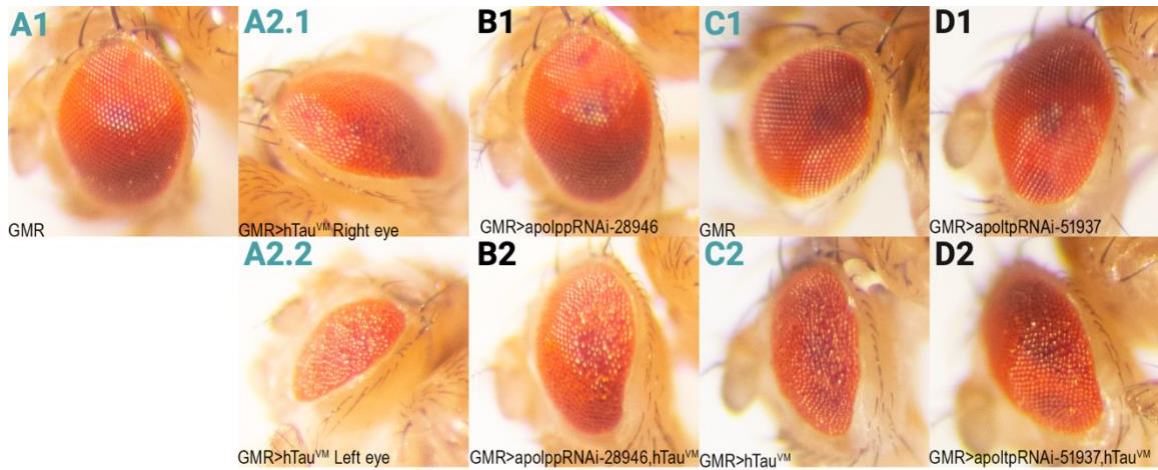


Figure 27: Apolipoproteins *apolpp* and *apoltp* do not alter hTau^{V337M} retina neurotoxicity.

- (A1) GMR-GAL4 control for B1.
- (A2.1, A2.2) hTau^{V337M} rough eye control for B2. These images highlight the variability in the rough eye phenotype within conditions (A2.1 right versus A2.2 left eye).
- (B1) *apolpp* knockdown does not change eye structure.
- (B2) *apolpp* knockdown with hTau^{V337M} does not alter hTau^{V337M} phenotype.
- (C1) GMR-GAL4 control for D1.
- (C2) hTau^{V337M} rough eye control for D2.
- (D1) *Apoltp* knockdown has no effect on normal eye development.
- (D2) *Apoltp* knockdown with hTau^{V337M} does not change hTau^{V337M} phenotype.

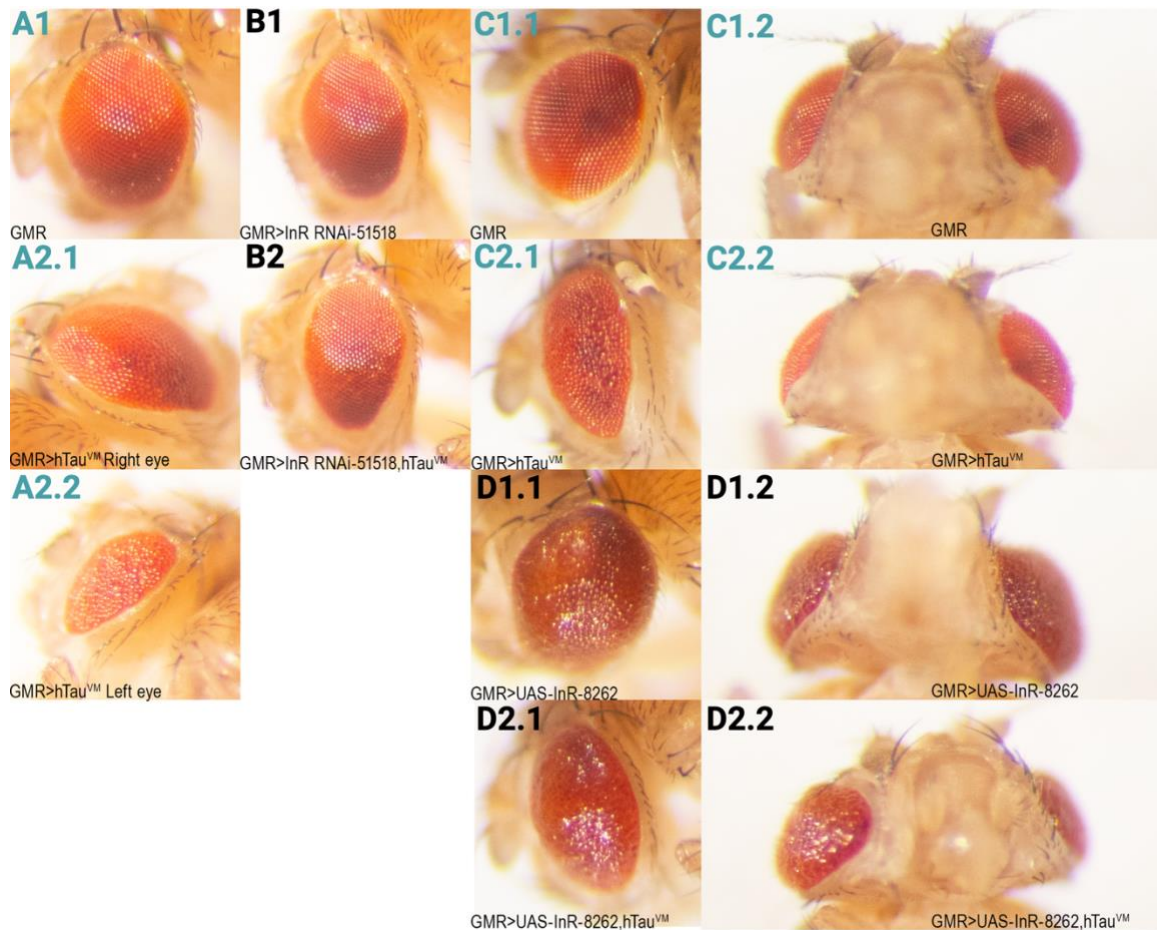


Figure 28: Insulin receptor *InR* modifies hTau^{V337M} retina neurotoxicity.

- (A1) GMR-GAL4 control for B1.
- (A2.1, A2.2) hTau^{V337M} rough eye control for B2. These images highlight the variability in the rough eye phenotype within conditions (A2.1 right versus A2.2 left eye).
- (B1) *InR* knockdown does not change eye structure.
- (B2) *InR* knockdown with hTau^{V337M} partially rescues the hTau^{V337M} phenotype.
- (C1.1, C1.2) GMR-GAL4 control for D1.1 and D1.2.
- (C2.1, C2.2) hTau^{V337M} rough eye control for D2.1 and D2.2. The front view (C2.2) highlights the smaller eyes compared to GMR-GAL4 (C1.2).
- (D1.1, D1.2) *InR* overexpression causes large, bulbous, and rough eyes.
- (D2.1, D2.2) *InR* overexpression with hTau^{V337M} worsens hTau^{V337M} phenotype and results in small, bulbous, and rough eyes.

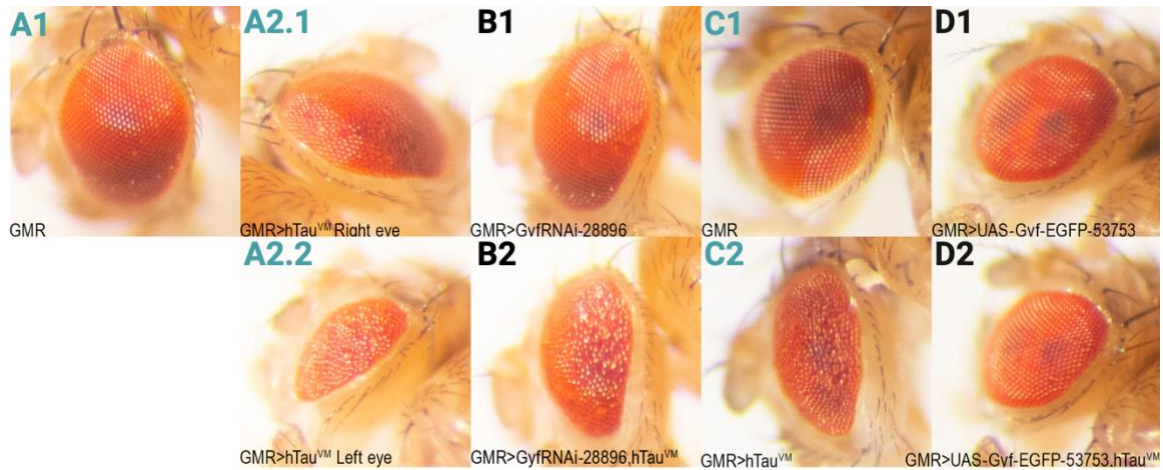


Figure 29: *Gyf* overexpression rescues hTau^{V337M} retina neurotoxicity.

(A1) GMR-GAL4 control for B1.

(A2.1, A2.2) hTau^{V337M} rough eye control for B2. These images highlight the variability in the rough eye phenotype within conditions (A2.1 right versus A2.2 left eye).

(B1) *Gyf* knockdown does not change eye structure.

(B2) *Gyf* knockdown with hTau^{V337M} does not alter the hTau^{V337M} phenotype.

(C1) GMR-GAL4 control for D1

(C2) hTau^{V337M} rough eye control for D2.

(D1) *Gyf* overexpression has no rough eye phenotype.

(D2) *Gyf* overexpression with hTau^{V337M} suppresses the hTau^{V337M} phenotype and results wildtype-like eyes.

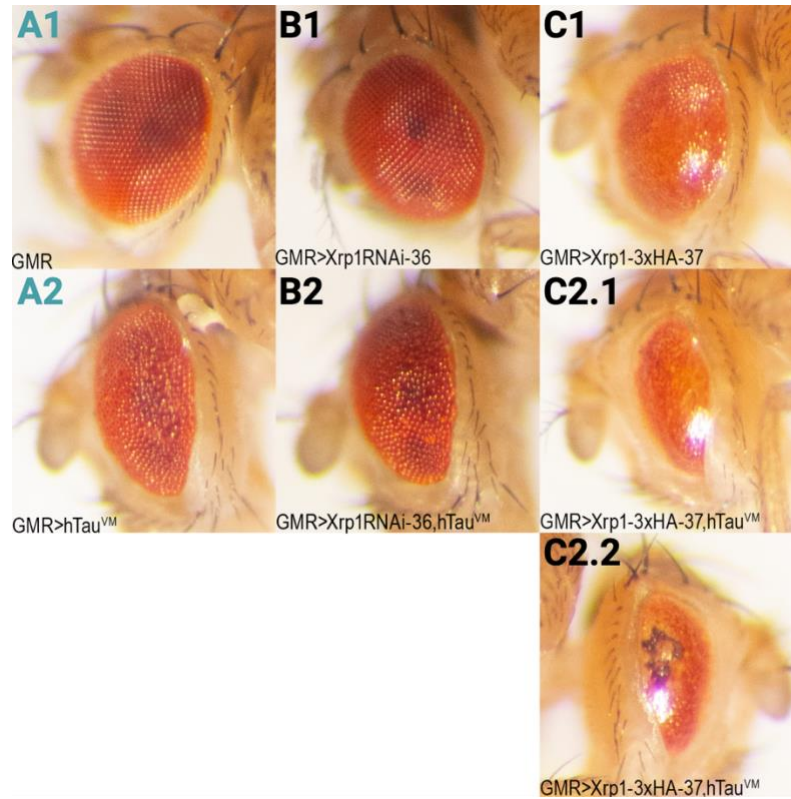


Figure 30: *Xrp1* overexpression results in glazed rough eye phenotype, which is worsened with hTau^{V337M} co-expression.

- (A1) GMR-GAL4 control for B1 and C1.
- (A2) hTau^{V337M} rough eye control for B2, C2.1 and C2.2.
- (B1) *Xrp1* knockdown does not change eye structure.
- (B2) *Xrp1* knockdown with hTau^{V337M} does not alter the hTau^{V337M} phenotype.
- (C1) *Xrp1* overexpression has a smaller size and glazed appearance suggesting cell death.
- (C2.1) *Xrp1* overexpression with hTau^{V337M} exacerbates both *Xrp1* overexpression and hTau^{V337M} phenotypes and results in smaller, glazed eyes (C2.1) and necrotic spots (C2.2).

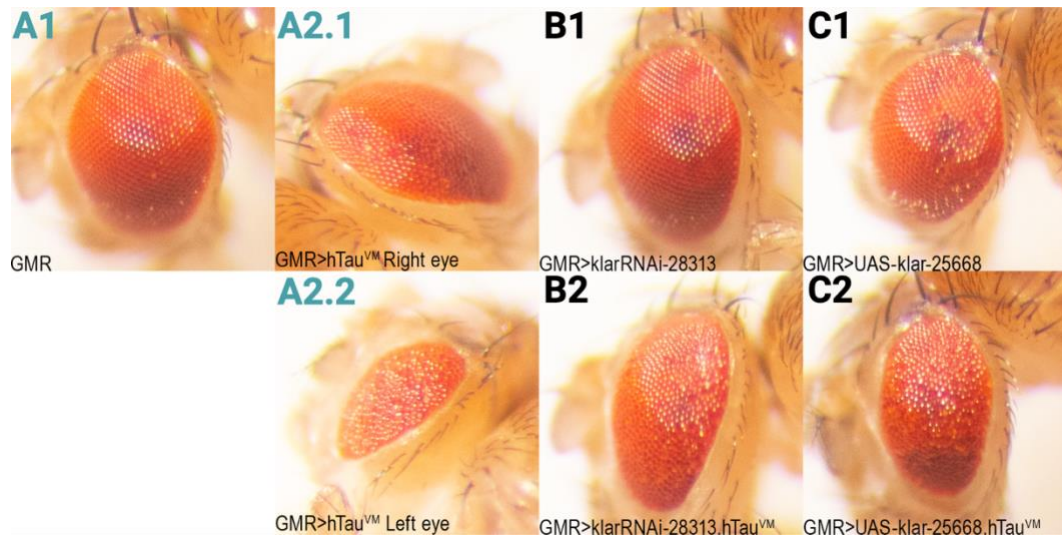


Figure 31: *klar* overexpression may increase rough eye phenotype in hTau^{V337M}.

(A1) GMR-GAL4 control for B1 and C1.

(A2.1, A2.2) hTau^{V337M} rough eye control for B2 and C2. These images highlight the variability in the rough eye phenotype within conditions (A2.1 right versus A2.2 left eye).

(B1) *klar* knockdown has no rough eye phenotype.

(B2) *klar* knockdown with hTau^{V337M} does not alter the hTau^{V337M} phenotype.

(C1) *klar* overexpression has no rough eye phenotype.

(C2) *klar* overexpression with hTau^{V337M} exacerbates the hTau^{V337M} phenotype and results slightly smaller and rougher eyes.

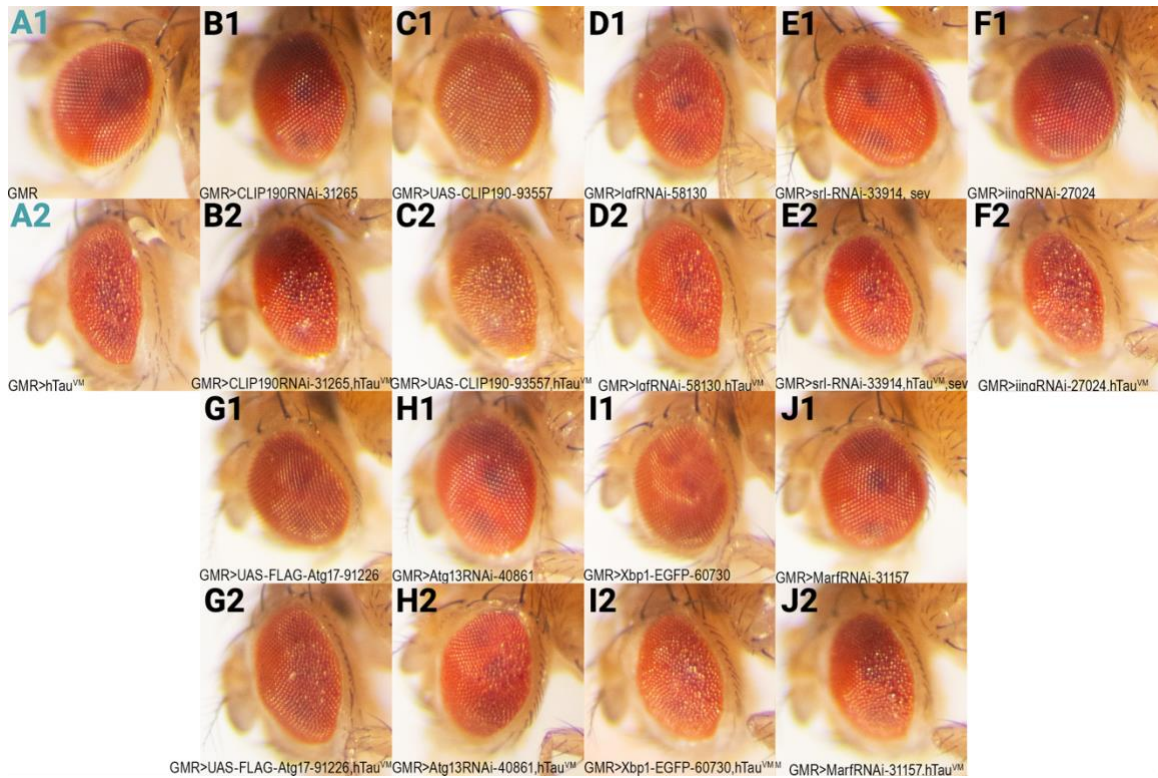


Figure 32: Candidate genes from differential expression analysis in the fat body cluster with subtle or no rough eye phenotype.

- (A1) GMR-GAL4 control for B1-J1.
 (A2) hTau^{V337M} rough eye control for B2-J2.
 (B1) *CLIP-190* knockdown does not change eye structure.
 (B2) *CLIP-190* knockdown with hTau^{V337M} does not alter the hTau^{V337M} phenotype.
 (C1) *CLIP-190* overexpression has no rough eye phenotype.
 (C2) *CLIP-190* overexpression with hTau^{V337M} does not change the hTau^{V337M} phenotype.
 (D1) *lqf* knockdown does not change eye structure.
 (D2) *lqf* knockdown with hTau^{V337M} does not alter the hTau^{V337M} phenotype.
 (E1) *srl* knockdown does not change eye structure.
 (E2) *srl* knockdown with hTau^{V337M} does not alter the hTau^{V337M} phenotype.
 (F1) *jing* knockdown does not change eye structure.
 (F2) *jing* knockdown with hTau^{V337M} slightly worsens the hTau^{V337M} phenotype.
 (G1) *Atg17* overexpression has no rough eye phenotype.
 (G2) *Atg17* overexpression with hTau^{V337M} partially rescues the hTau^{V337M} phenotype.
 (H1) *Atg13* knockdown does not change eye structure.
 (H2) *Atg13* knockdown with hTau^{V337M} slightly improves the hTau^{V337M} phenotype.
 (I1) *Xbp1* knockdown does not change eye structure.
 (I2) *Xbp1* knockdown with hTau^{V337M} does not alter the hTau^{V337M} phenotype.

(J1) *Marf* knockdown does not change eye structure.

(J2) *Marf* knockdown with hTau^{V337M} does not alter the hTau^{V337M} phenotype.

4.4 Model of Fat Body Metabolic Dysregulation in hTau^{K369I} FTD mutant

Experimental rationale

A benefit of single-cell genomics is the ability to perturb a system and observe the system wide changes. Differentially expressed genes between mutant and wildtype within specific cell types give insight into the pathways that are modulated by the presence of mutant *Tau*. In this section, we will briefly review the metabolic changes seen in the hTau^{K369I} mutant within the fat body. The brain is a metabolically demanding organ and the breakdown of metabolic function with aging and oxidative stress has been extensively linked to neurodegeneration (Butterfield et al., 2022). As the fat body serves as the liver, adipose tissue, and the immune system of *Drosophila*, any perturbations of metabolic output or storage could impact the function of the brain. We present a proposed metabolic map based on the differentially expressed genes within the fat body of heterozygous hTau^{K369I} compared to heterozygous hTau^{WT}. It is important to note that not all of these hits were specific to just hTau^{K369I}, some were also altered when comparing dTau^{del} or CS to hTau^{WT}. We chose to include these in the metabolic map to create a more complete picture of the pathways (**Figure 33**). However, if these hits were to be validated, it is important to know that the genes are also altered in the CS control compared to hTau^{WT} (DE both down or up: *aay*, *FASN1*, *Mondo*, *PyK*, *Rel*, *tobi*, *Treh*, and *Lsd-2*). Based on the findings in the metabolic map, we did a pilot experiment to assess body weight and look at lipid droplets in aged flies.

Results and Discussion

Glycolysis and Oxidative Phosphorylation

The fruit fly lab diet is high in carbohydrates, which the fat body can utilize as fuel through glycolysis. Trehalose is the major sugar in circulation in the *Drosophila* hemolymph (Tellis et al., 2023). In the fat body, glucose is converted to trehalose and transported to other tissues through Tret1-1, which is downregulated in hTau^{K369I} (**Figure 33**; Tellis et al., 2023). Trehalose can also be converted to glucose with Treh, which we see downregulated in hTau^{K369I} (Zappia et al., 2021). Glucose is broken down through glycolysis, and we find three of the glycolysis enzymes differentially expressed in hTau^{K369I} fat body cells. *Hex-A* and *Pfk* are upregulated while the rate limiting enzyme, *Pyk*, is downregulated. Whether these glycolysis enzymes are upregulated at the protein level will require further testing. In future work, we could also assess glycolytic output by measuring metabolite levels. Interestingly, complex IV oxidative phosphorylation genes were also upregulated (*COX8*, *COX7A*, *COX7C* and *Cyt-c-p*). Based on these findings and the dysregulation of lipogenesis and lipolysis (discussed later), it appears that the hTau^{K369I} fat body cells are relying on glycolysis and oxidative phosphorylation. Future experiments probing the metabolic state of these cells will be necessary to understand the entire picture (discussed in Conclusions).

Glutathione

Glutathione is important in the reduction of reactive oxygen species that can damage the cell. In hTau^{K369I}, *Cbs* is downregulated compared to hTau^{WT} (**Figure**

33). Cbs is an enzyme in the pathway to convert homocysteine to cysteine, which is upstream of glutathione synthesis (Sbodio et al., 2019). Hence, the levels of glutathione synthesis could be lower in hTau^{K369I} making the flies more susceptible to reactive oxygen species. The conversion of homocysteine to cysteine requires serine. Aay, a fly ortholog of an enzyme in the biosynthesis pathway of serine, is downregulated in hTau^{K369I} (Sonn et al., 2018). This further supports that glutathione could be lower in these flies and thus reactive oxygen species could be elevated. Homocysteine synthesis is also involved in the process where methyl groups are liberated, which can then be used to methylate DNA. Therefore, in addition to glutathione levels, there could be changes in epigenetic control due to change in methyl groups availability (Sbodio et al., 2019).

Lipogenesis, Lipolysis and Insulin Signaling

Both the lipolysis and lipogenesis pathways are downregulated in the hTau^{K369I} mutant (**Figure 33**). The lipolysis pathway is downregulated at both the transcription factor level (*Hnf4*, *Atf3*) and import into the mitochondria for fatty acid oxidation (*whd*). In addition, it appears that the insulin pathway could also be diminishing the transcription of lipolytic genes. The insulin signaling pathway inhibits Foxo, which controls expression of *bmm*, a lipase that converts TAGs to fatty acids and glycerol for oxidation (Heier et al., 2021). In hTau^{K369I}, the insulin receptor, *InR*, is downregulated, but downstream activator *Pdk1* is upregulated. *Pdk1* serves to activate Akt, which in turn inhibits the entry of Foxo into the nucleus through phosphorylation (Heier et al., 2021). In contrast, *Rel* is downregulated. *Rel*

is controlled by a different signaling pathway and serves to inhibit Foxo. In addition, in response to chronic starvation, endoplasmic reticulum protein, Ire1, activates splicing of Xbp1, which then translocates to the nucleus to inhibit Foxo and thus transcription of lipolysis genes (Zhao et al., 2021). Ire1 is downregulated in hTau^{K369I} in the fat body cluster and Xbp1 is downregulated in the putative female portion of the fat body cluster (**Supplemental Figure 1E**, Cluster 3 (C3)). Hence, the inhibition of Foxo could be decreased with starvation. This hints at the complexity of the system and poses the question of whether these opposing forces could be balancing out.

Lipogenesis is also downregulated with decreased expression of *Mondo*, a transcription factor that activates lipogenesis genes, and *FASN1*, an enzyme involved in the de novo synthesis of fatty acids (Heier et al., 2021). The decreased expression of *FASN1* in hTau^{K369I} should serve to lower the amount of triglyceride (TAG) storage in the fat body lipid droplets (Heier et al., 2021; Ugrankar et al., 2019). Similarly, downregulation of *apolpp* in hTau^{K369I} should have the same effect. Ugrankar et al. (2019) showed that knockdown of *FASN1* reduced lipid droplet in the cell interior while *apolpp* knockdown decreased the lipid droplets at the periphery. *Apoltp* is also reduced in the hTau^{K369I} mutant and is involved in the transport of lipids throughout the body (Heier et al., 2021). This could also impact the lipid droplets by either reducing transport from the gut or lowering the mobilization to other tissues.

The Akh hormone signaling pathway serves to upregulate lipolytic pathways upon starvation and inhibit lipogenesis. *Plc21C* and *Cam* are upregulated in

hTau^{K369I}. These proteins are activated by Akh signaling and involved in the inhibition of lipogenesis (Baumbach et al., 2014). This further supports that lipogenesis could be decreased in the hTau^{K369I} flies. Akh signaling also activates Lsd-1, which regulates lipid droplets in the interior of the cell by providing structural support and activating lipase, Bmm (Heier et al., 2021; Zheng et al., 2016). Lsd-2, in contrast, inhibits Bmm and associates with lipid droplets in the periphery (Zheng et al., 2016). *Lsd-1* is downregulated, and *Lsd-2* is upregulated in hTau^{K369I}. This suggests that Bmm is inhibited and thus there could be less lipolysis. Measuring the levels of triglycerides and diglycerides will be necessary to see if the lipid system is perturbed in the hTau^{K369I} flies.

Some FTD patients have increased cravings for carbohydrate rich foods based on caregiver questionnaires (Miller et al., 1995). In an ad libitum meal test, FTD patients preferred the high sucrose foods compared to controls and AD patients (Ahmed et al., 2016). Although this may not be tied to the changes seen in the lipid synthesis and mobilization in the fat body in our *Drosophila* model, it is something to consider. Future experiments could test dietary preference and food consumption in our *Drosophila* model to see if these expression changes are modifying behavior.

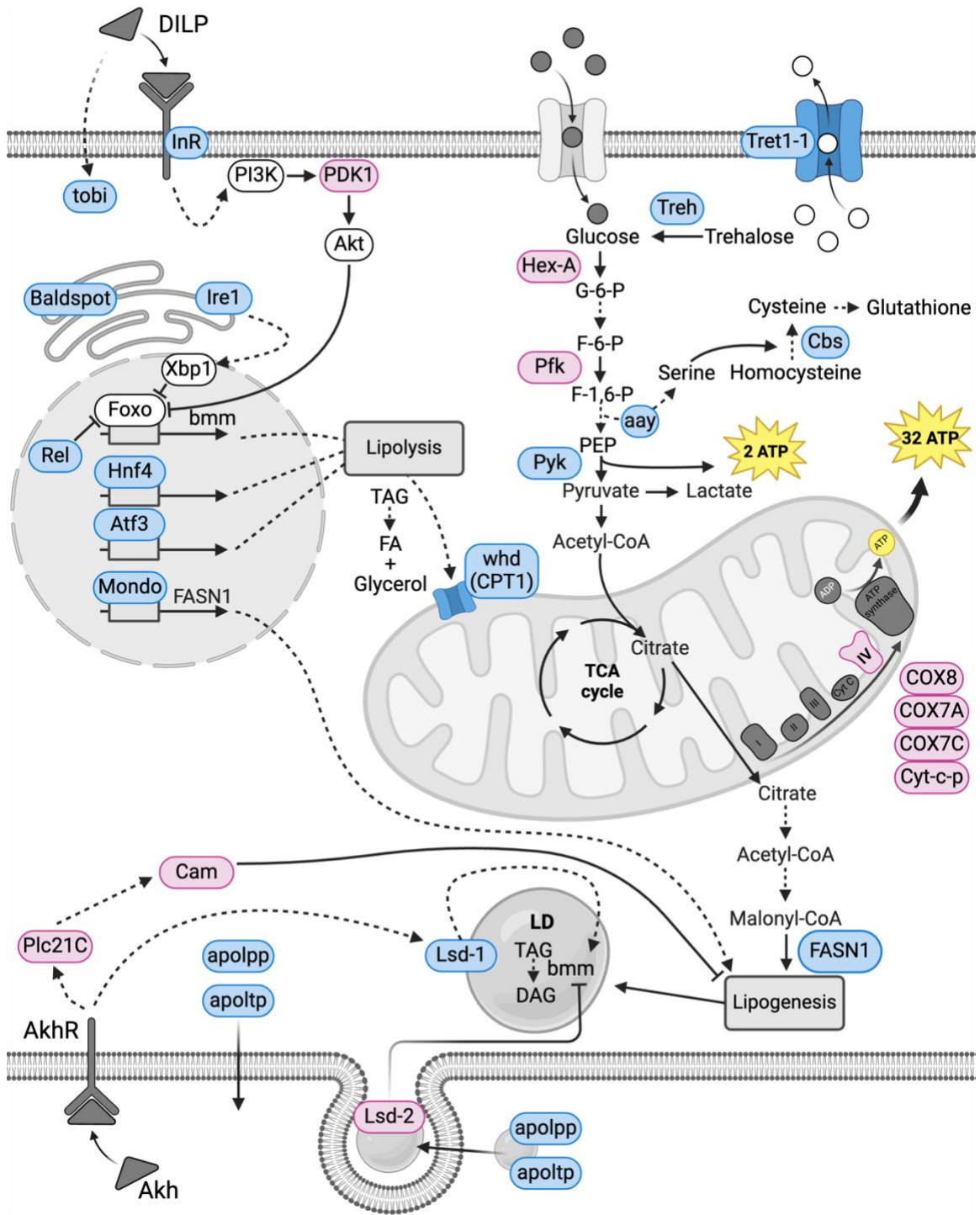


Figure 33: Metabolic map of differentially expressed genes in *hTau^{K369I}* fat body cells from 5-day old flies with genes involved in insulin signaling, lipid dynamics, glycolysis, and mitochondrial function.

The insulin signaling pathway is activated by *Drosophila*-like insulin peptides (DILP) through the insulin receptor (InR). Downstream through the PI3K/Akt pathway and others, the transcription factor Foxo, which controls lipolysis genes, is inhibited. Tobi is another gene involved with the insulin pathway, but its role has not been fully elucidated. In response to chronic starvation, the ER stress pathway of Ire1/Xbp1 can be activated to also inhibit Foxo. Lastly, immune response transcription factor Rel can also inhibit Foxo in a starvation dependent manner. Hnf4 and Atf3 are two other transcription factors that control expression of lipolysis genes. Lipogenesis transcription factor controls expression of lipogenic genes such as FASN1, which is involved in *de novo* lipid synthesis. Lipogenesis is inhibited by the Akh hormone pathway through Plc21C and cAMP/PKA. Lipid droplet stabilizing proteins, Lsd-1 and Lsd-2, associate with lipid droplets in the fat body and can inhibit or activate lipolysis proteins such as Bmm. Apolpp and Apoltp are involved in lipid transport across tissues. Lipolytic enzymes breakdown the triglycerides into free fatty acids and glycerol. The free fatty acids can then be broken down in the mitochondria through beta oxidation. Whd is responsible for the adding acyl carnitines to long-chain fatty acids to allow for transport into the mitochondrial matrix. Trehalose is the main sugar in the hemolymph of *Drosophila*, and it can be transported in and out of cells with Tret1-1. Treh is an enzyme that converts trehalose to glucose. Glucose can then be broken down for ATP and the resulting acetyl-CoA from glycolysis can be used by the citric acid cycle (TCA). The TCA cycle provides electron donors for oxidative phosphorylation and further ATP production. Oxidative phosphorylation generates reactive oxygen species, and these are scavenged by glutathione. Glutathione is produced through the cysteine synthesis pathway (Baumbach et al., 2014; Diaconeasa et al., 2013; Heier et al., 2021; Mattila et al., 2017; Molaei et al., 2019; Palanker et al., 2009; Palu and Chow, 2018; Ugrankar et al., 2019; Ugrankar-Banerjee et al., 2023; Zappia et al., 2021; Zhao et al., 2021; Zheng et al., 2016).

Alterations in body weight of hTau^{K369I} flies

Based on the metabolic map findings, we began pilot experiments to assess if the differentially expressed genes could impact body weight or lipid droplets within the fat body. We decided to measure body weight at two timepoints: young 11-day old and old 30-day old. The flies were crossed with the same numbers of females and males to control for density of offspring. We weighed males and females separately as *Drosophila* females are significantly larger than males. Due to the sensitivity of the scale, the flies had to be weighed in groups of 4-10 flies

and then we analyzed the per fly weight. Interestingly both the aged hTau^{K369I} females and males were significantly heavier than the hTau^{WT} (**Figure 34B, D**). Young males were also significantly heavier than the hTau^{WT} control (**Figure 34C**). Canton-S was also consistently heavier than all hTau flies (**Figure 34C**). This preliminary experiment suggests that the metabolic changes we see could be impacting both the hTau flies. Future experiments could utilize a high fat diet to see if there is a different outcome. The standard diet is high in carbohydrates, which could be helpful for the hTau^{K369I} fly based on the differentially decreased expression of lipid associated genes.

The following should be considered for future experiments evaluating body weight. First, multiple generations of parent flies should be grown with density control. The parent flies used for this experiment were taken from long term stocks and thus there could be more variation based on varying living conditions and how well the flies grow in the 18°C incubator (used for long-term stock maintenance). Second, it would be helpful to look at homozygous hTau flies to see if the difference in body weight between hTau^{WT} and hTau^{K369I} is greater than what we see with the heterozygotes (**Figure 34A-D**). Third, more timepoints throughout the lifespan of the fly would help to determine whether hTau^{K369I} is consistently larger throughout life. Fourth, due to time limitations, the body weight measure ranged from early morning to late afternoon. This could have influenced the body weight measure depending on egg production and food intake. Consistency of weighing time may help minimize the variability we see in weight measurements. Lastly due to low numbers, the weights were taken with 4-10 flies and then divided by the total

weighed. It would be helpful to consistently weigh the same number of flies to reduce variation and improve the accuracy of the weight measure.

Based on the increased body weight of the hTau^{K369I} flies and decrease in expression of both lipolysis and lipogenic pathways, we wanted to investigate lipid droplets within the fat body. This was a single experiment to see if there were any obvious changes in lipid droplets in the hTau^{K369I} flies and to troubleshoot the dissection and staining protocol. In this initial experiment, we did not see any qualitative changes in the hTau^{K369I} fat body lipid droplets compared to CS or hTau^{WT} (**Figure 34E**). Optimize this staining protocol to reduce the signal to noise ratio is necessary before we can determine whether the changes seen in the differential expression are translating to changes in lipid storage. It could be helpful to repeat this experiment at a younger timepoint. In addition, adding a plasma membrane and nuclear staining will allow for quantification of the periphery and interior lipid droplets in the fat body. Based on the decreased mRNA levels of *apolpp* and *FASN1* in our hTau^{K369I} mutant, we could expect to see both the peripheral and cell interior lipid droplet populations impacted. This experiment could also be expanded by starving the flies and then looking at the lipid droplets in the fat body once the system has been challenged. Inducing fasting conditions in the flies will test the metabolic flexibility of the hTau^{K369I} flies and will challenge energy mobilization. Starvation should result in decrease TAGs and thus decreased lipid droplet size in the fat body (Zhao et al., 2021). This could also be assayed by measuring levels of TAG in the fly in both the fed and starved state. These tests could also include starving the flies and measuring survival time by

counting the number of dead flies every 12 hours to see if the hTau^{K369I} flies are more susceptible. Based on the metabolic map, the hTau^{K369I} flies could struggle without carbohydrate food sources due to the decrease in expression of lipolytic transcription factors (Hnf4), fatty acid oxidation (whd) and lipid droplet stabilizing proteins (Lsd-1, Lsd-2).

To investigate whether *Fhos* manipulation impacts body weight, we conducted the body weight experiment for our double mutants with hTau and *Fhos*. We saw that AkhR hTau^{K369I} flies were not heavier than the AkhR hTau^{WT} flies (**Figure 35A, B, C, D**). This is similar to what we saw with the behavioral assays in Chapter 3. However, we do see that hTau flies with *Fhos* overexpression are consistently heavier than hTau alone with the greatest increase in aged females (**Figure 35B**). This suggests that *Fhos* could impact the metabolic state of the hTau^{K369I} mutant but a more sensitive assay like food consumption or TAG levels will be needed to better understand the function of *Fhos* in the fat body.

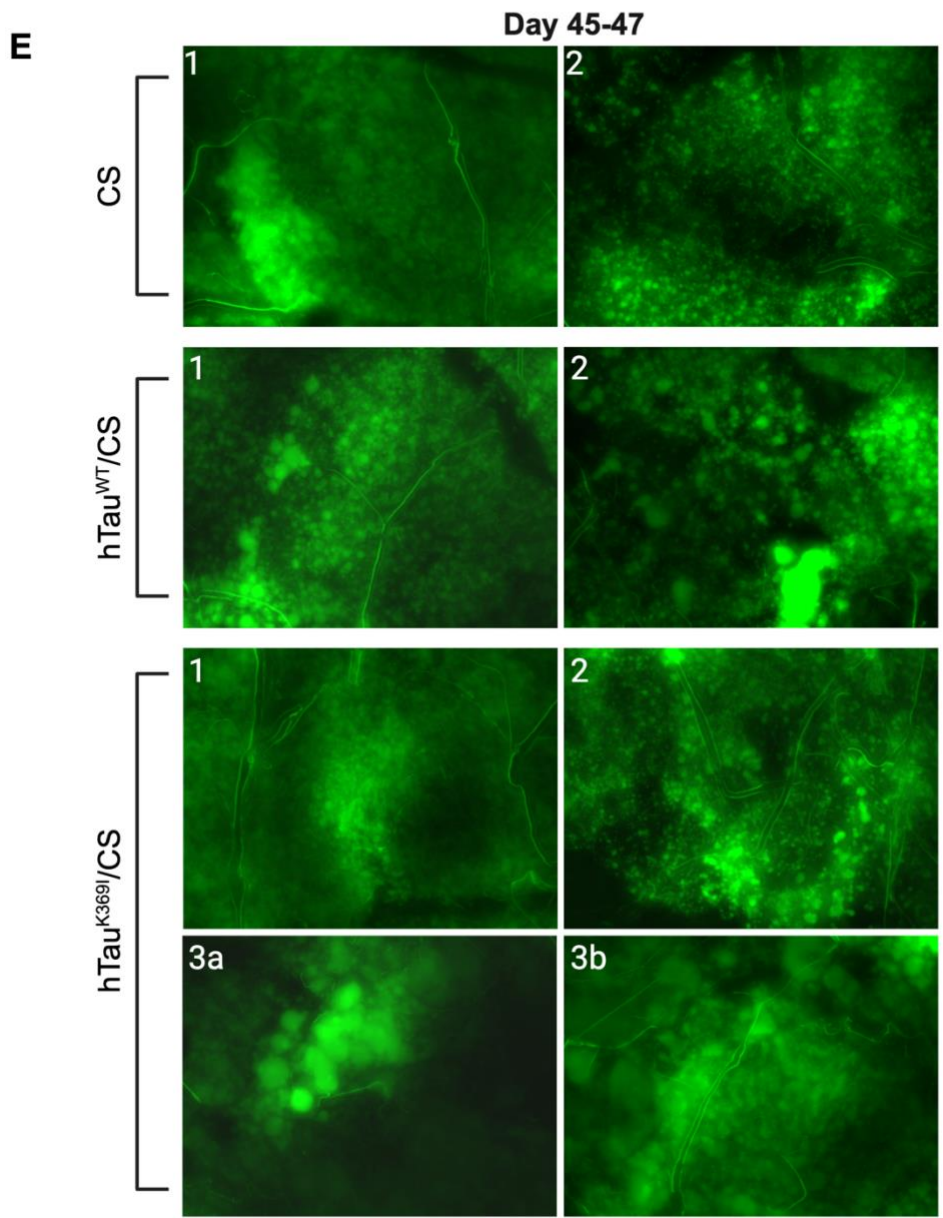
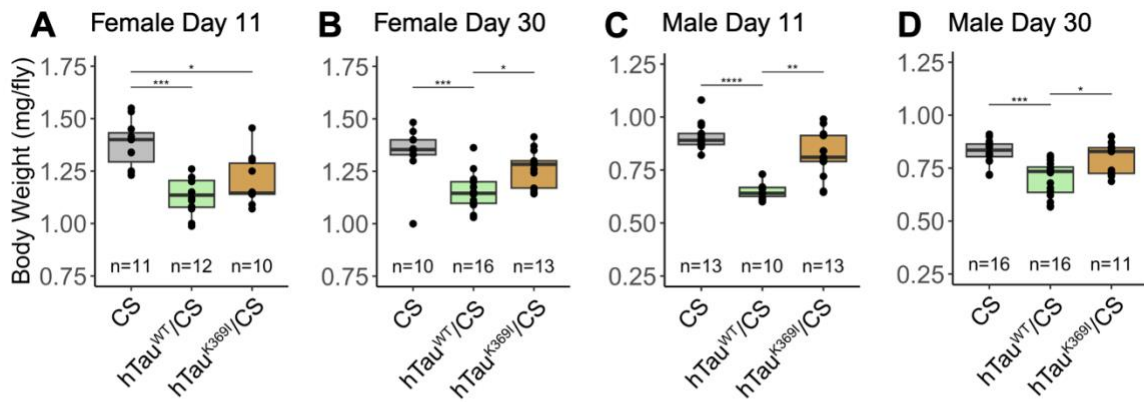


Figure 34: hTau^{K369I} mutation modifies body size in females and males.

(A, B, C, D) Heterozygous hTau^{K369I} mutants have increased body size compared to heterozygous hTau^{WT} across sex and age (11 and 30 days of age). (E) Example fat body preps showing variation in lipid droplets at 45 days of age. Numbers on images denote animal with letters indicating multiple images from one animal. Statistics were run across all conditions using Kruskal-Wallis with Dunn's multiple comparisons and Holm adjustment. Sample size is indicated on plots with whiskers indicating the 1.5xIQR (Interquartile range Q3 to Q1). *p<0.05, **p<0.01, ***p<0.001, ****p<0.0001.

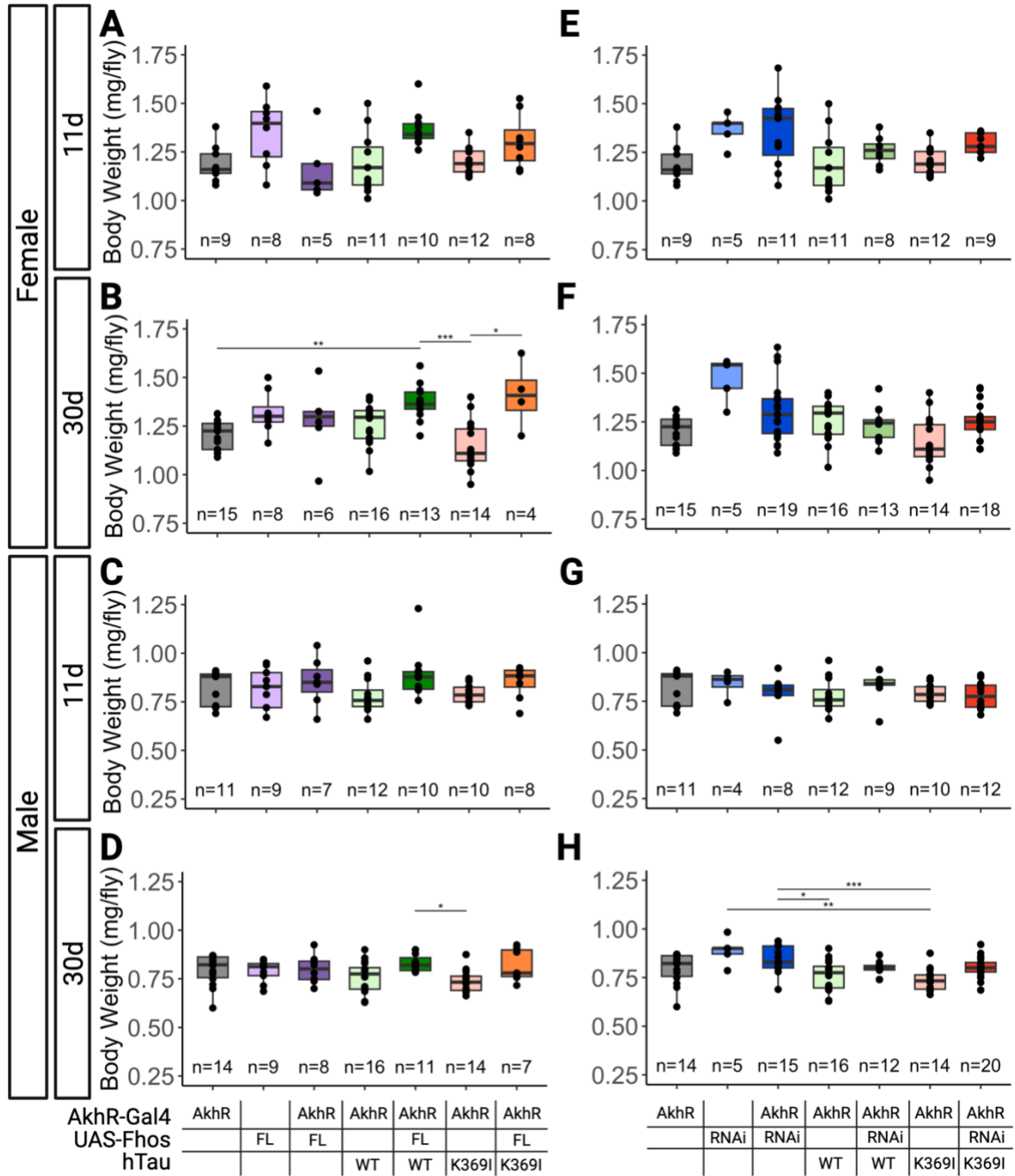


Figure 35: *Fhos* overexpression in the fat body increases body weight in aged female hTau^{K369I} mutant.

(B) *Fhos* overexpression increases body size at 30 days of age in hTau^{K369I} females compared to driver hTau control. (A, C, D) *Fhos* overexpression did not significantly change body weight in 11-day old females (A), 11-day old males (C) or 30-day old males (D). (E, F, G, H) *Fhos* knockdown did not significantly alter body weight. Statistics were run across all conditions using Kruskal-Wallis with

Dunn's multiple comparisons and Holm adjustment. Sample size is indicated on plots with whiskers indicating the 1.5xIQR (Interquartile range Q3 to Q1). * $p < 0.05$, ** $p < 0.01$, *** $p < 0.001$, **** $p < 0.0001$.

Conclusion

A deeper understanding of the physiological versus pathological functions across different cell types is needed to further elucidate how changes in Tau can lead to such varied disease phenotypes. The Tau 2022 global conference emphasized that Tau likely has varying functions across cell types, and that the initial discovery of Tau's role in MT stabilization has slowed discovery of its diverse functions (Sexton et al., 2024). Single-cell genomics allows for systems wide view. However, the biological effect size of a particular genomic change can be hard to determine. Validation of candidate hits using both molecular and behavioral techniques will be necessary to more fully understand the complicated onslaught of changes induced by the hTau^{K369I} mutation and beyond. However, determining how to validate can be difficult. In another study of the hTau^{R406W} mutation using single-cell transcriptomics, the authors found that the *NF-κB* (*Relish/Rel* in *Drosophila*) was perturbed both in a human dataset of AD and in the hTau^{R406W} model (Wu et al., 2023). From this analysis, they postulated that reducing levels of *Rel* could potentially rescue or slow neurodegenerative vacuole formation in hTau flies. However, there was no change in vacuole number with *Rel* knockdown. This highlights similar limitations to what we encountered in this dissertation. Phenotypes can be subtle, progress too quickly or can be difficult to quantify. In addition, it could be that the GAL4 drivers used for validation do not directly align with the cells that have changes within the single-cell assay. There are some efforts to utilize single-cell expression profiles to create GAL4 drivers for specific clusters. In the case of this dissertation, manipulating *Fhos* was lethal in neurons

and glia. It also led to a more subtle phenotype due to genetic background changes when adding the UAS/GAL4 constructs. That being said, the genetic tools in *Drosophila* are vast, and with time and troubleshooting, the ability to validate candidates from single-cell datasets will help to pinpoint potential modifiers for study in higher order systems.

Chapter 3: Summary and Future Directions

The evidence laid out in this dissertation points to the fat body as a cell type of interest for understanding the brain:body axis in tauopathies. This work also further supports *Fhos* as a gene of interest, but more effort is needed to parse the mechanism of *Fhos* within the fat body and how it could be modifying behavior. The early change in *Fhos* accessibility in the hTau^{K369I} and dTau^{del} in chromatin accessibility and gene expression positions *Fhos* as a potential driver of phenotypes related to fat body dysregulation. We originally focused on hTau^{K369I} due to the increased levels of HP1 α and the previous studies, which showed that heterochromatin structure is altered with aging and in tauopathy models (Frost et al., 2016; Haithcock et al., 2005; Scaffidi and Misteli, 2006). Locomotor defects and loss of heterochromatin in the *Drosophila* hTau^{R406W} model were rescued by knocking down histone demethylases in the CNS, which suggests that FTD phenotypes are linked to the heterochromatin state in Tau mutants. The fat body also has a breakdown of Lamin structural integrity with aging, which is thought to impact heterochromatin stability (Chen et al., 2016). Therefore, we propose assessing the nuclear architecture changes by mapping heterochromatin regions

in the hTau^{K369I} model. We could accomplish this by conducting single-cell CUT&Tag on hTau^{K369I} adult heads for 5-day and 30-day old flies for heterochromatin marks, H3K9me and HP1 α . Heads would include the CNS as well as the pericerebral fat body nuclei. This experiment would determine how the nuclear organization of heterochromatin changes between pre- and post-symptomatic ages. Additionally, it would show whether heterochromatin distribution is modified in our FTD mutant and if the regions of heterochromatin correspond to the differentially accessible and expressed regions found in Chapter 3. Further profiling the epigenetic changes will advance our understanding of the role of Tau in the nucleus and provide novel targets, which is key to developing targeted therapies to slow FTD progression.

Similarly, given the evidence of Lamin breakdown with aging and disease, we would like to look at both the brain (perhaps using the regions of interest from Chapter 4.3) and within the fat body to look for disruptions in Lamin in an aged timepoint. This could give us clues to whether the hTau^{K369I} mutant has similar mechanisms to the hTau^{R406W} mutant, and whether *Fhos* could be impacting Lamin (Frost et al., 2016). We could also use the antibody created in Schwartz et al. (2016) to stain for Fhos and a Lamin antibody to see if Fhos is co-localizing with the nuclear membrane or regions of blebbing/invaginations (Frost et al., 2016). As mentioned in the introduction, FHOD1 and Fhos are found in the perinuclear region (Anhezini et al., 2012; Ménard et al., 2006). Mammalian FHOD1 can interact with the LINC proteins in the nuclear membrane and associates with actin (Antoku et

al., 2015). Therefore, it is possible that *Drosophila* Fhos could have a similar function.

Fhos nucleates actin and can promote bundling (Patel et al., 2018). With aging, there is increased actin rod formations in the brain and knocking down *Fhos* ameliorates this phenotype (Schmid et al., 2023 preprint). Since *Fhos* is increased in fat body cells, it would be beneficial to assess whether there are increased actin bundles in the hTau^{K369I} fat body. For these experiments, it would be easiest to first check in the fat body located in the abdomen of the adult fly due to accessibility. However, one could also dissect or section for the pericerebral fat body. If actin bundling is altered, there are many further questions that could be asked in this system. First, we would want to know if changes in actin dynamics is impacting autophagy given that it has been linked to neurodegeneration (Kast and Dominguez, 2017). Second, we would also stain for actin and Lamin to see if there are actin foci associated with regions of nuclear disruption, which was found in the hTau^{R406W} *Drosophila* brains (Frost et al., 2016). If we find this in the hTau^{K369I} fat body, evaluating whether manipulation of *Fhos* expression could alter this phenotype would provide insight for the possible mechanism of *Fhos* within the hTau^{K369I} fat body.

It would be interesting to further characterize the FTD mutant behaviors such as learning/memory defects or depression, which are seen in patients. We would like to characterize these behaviors in the FTD mutants and then see how manipulation of *Fhos* in the fat body alters these phenotypes. Past work in the lab has looked at spatial memory but there are other learning and memory tests to use

in the *Drosophila* system (Law et al., 2022). One option is to use odor detection. One can use an aversive (electric shock) or appetitive (sucrose) stimulus associated with an odor then also introduce the flies to another odor without an external association. The flies are then given an odor choice in a T-maze (Mariano et al., 2020). If the flies formed a short-term memory, then the flies will avoid the adverse stimulus or prefer the appetitive stimulus. There are also ways to assess depression-like behavior such as inducing stress through vibration and then tasking wing-clipped flies with crossing an “insurmountable” gap (Pick and Strauss, 2005; Ries et al., 2017). Flies with increased depression-like behavior will have reduced crossing attempts. Additional characterization of the hTau mutant phenotypes will aid in the limitation discussed at the beginning of the chapter. For example, if a candidate gene is known to be involved in the mushroom body (the memory center of the *Drosophila* brain), then it would be beneficial to have behavioral validations to test if the candidate can alter the hTau memory phenotype.

In Chapter 3, we saw that the increased accessibility and gene expression of *Fhos* was specific to hTau^{K369I}, it would be interesting to know if this is the case for the behavioral experiments as well. Repeating the behavioral validation for the hTau^{V337M} and hTau^{P301L} would show if the recovery with *Fhos* knockdown is specific to hTau^{K369I}. hTau^{K369I} with *Fhos* knockdown had comparable locomotor drive and sleep fragmentation as hTau^{K369I} alone. Perhaps if the flies were aged longer, we could see more of a “rescue” in the *Fhos* knockdown hTau^{K369I} flies.

This would also indicate whether there is a specific window where the knockdown is helpful or if it is throughout aging.

Chapter 4: Summary and Future Directions

In Chapter 4.1, we presented *Fhos* manipulation in the hTau^{K369I} flies within glia and neurons to demonstrate that the *Fhos* fat body phenotype was cell-type specific. However, there were some limitations in these experiments that should be addressed. In Chapter 4.1, we utilized a temporal- and tissue-specific GAL4 to overexpress *Fhos* in glia due to lethality when using the tissue specific loco-GAL4. This meant that the flies developed at 18°C and were aged at 29°C to allow for overexpression of *Fhos* only in adulthood. For the sleep experiments, due to incubator availability, the flies were kept at 25°C. Temperature can influence activity rhythm in *Drosophila* (Majercak et al., 1999). At 29°C, flies have less activity in the late evening and more activity in the early night compared to flies at 25°C (Majercak et al., 1999). This would mean that flies will sleep more during the day and less at night when raised in 29°C. Although we do not see this in our flies aged at 29°C compared to the 25°C, the flies could be transitioning to the new temperature and have changes in sleep due to the temperature change. Although both controls and experimental conditions are undergoing the same temperature shift, it is possible that the control or experimental conditions could respond differently to the change in temperature. Therefore, to improve the validity of the interpretations, I would repeat this experiment maintaining the flies at 29°C to

ensure that the overexpression of *Fhos* is consistent. An alternative method would be to use the gene-switch system, which is a drug inducible system rather than temperature. Future work should assess the function of *Fhos* in glia because it is interesting that *Fhos* overexpression was lethal while *Fhos* knockdown was viable. This is likely a later developmental phenotype because there were necrotic larva and pupa. Glia at this stage of development are responsible for engulfing neurons undergoing programmed cell death (Freeman et al., 2015). It is possible that the disruption of *Fhos* could be impacting the phagocytic mechanisms.

For the neuronal validation, only *Fhos* overexpression in homozygous dTau flies died while hTau flies with *Fhos* overexpression survived. Figuring out this mechanism is another interesting side project to understand the function of *Fhos* in neurons. I suspect it could be due to the dosage of dTau in the flies. To test this, we could create a fly with a dTau homozygous deletion and *Fhos* overexpression. If these survived, then the lethality is likely due to the interaction between dTau and *Fhos*. I would also create a fly with heterozygous dTau deletion and *Fhos* overexpression. If this fly survives, then the viability of the hTau flies is likely due to the lower dosage of dTau. We could confirm the expression of dTau in both these flies using quantitative PCR. If the heterozygous dTau deletion was still lethal, then it is a gain of function of the hTau that leads to the viability in hTau flies. Again, the lethality seemed to occur later in development based on the necrotic larva, but you can use agar sucrose plates to count each stage of development and determine when the majority of the flies are no longer viable. It is important to understand this lethality paradigm because the hTau flies with *Fhos*

overexpression survive and have minimal behavioral phenotypes besides increased sleep fragmentation in females. Dissection of the lethality phenotypes will help to get a firmer picture of the interaction between *Fhos* and *Tau* across tissues.

Chapter 4.2 shows some potentially interesting patterns in neurodegeneration regions within the h*Tau Fhos* fat body knockdown. The *Fhos* overexpression h*Tau* flies appear to have less neurogenerative vacuoles but as stated in the chapter, it could be due to selection of more robust flies. Meaning that most of the flies have died before 45 days of age and thus we were analyzing the long-lived flies. This assertion is based on the numbers of flies that were available for behavioral experiments. Therefore, before repeating this experiment, a lifespan assay for the *Fhos* h*Tau* flies will help to determine a reasonable timepoint. Specifically, when there are disease phenotypes like locomotion but also high survival to allow for the assessment of progression rather than late-stage neurodegeneration. Also, repeating this experiment will be necessary to determine whether the seemingly vulnerable regions (ellipsoid body, fan-shaped body, and antennal lobe) in the *Fhos* h*Tau* knockdown flies are consistent across many samples.

For Chapter 4.3 and 4.4, I would like to repeat the single-cell gene expression experiment for an older timepoint to see if the metabolism pathways in the fat body that are changed at 5-days of age persist with age. Although, not discussed in this dissertation, there were also metabolic changes in neurons and glia and thus repeating the whole head will allow for comparison in all cell types.

This would also provide insight into whether there are more cytoskeleton genes altered with aging. Similarly, repeating the single-cell gene expression experiment with the hTau *Fhos* fat body knockdown flies could give insight into the mechanism of *Fhos* in the hTau^{K369I} mutant. The main candidates of interest from Chapter 4.3 were *InR*, *Xrp1*, and *Gyf* due to the modification of the hTau^{V337M} rough eye phenotype. All of these genes have been implicated in the insulin pathway and patients with neurodegenerative diseases can exhibit insulin resistance (Boulan et al., 2019; Giovannone et al., 2003; Giovannone et al., 2009; Kim and Arvanitakis, 2023; Vinayagam et al., 2016). This motivates evaluating whether the protein levels of *InR* are altered in the hTau^{K369I} mutant. It would also be interesting to look at the phosphorylation of Akt and nuclear localization of Foxo to assess whether the activation of the *InR* signaling pathway is altered (**Figure 33**).

To test if pathways in the Chapter 4.4 metabolic map are in fact altered in the hTau^{K369I} mutant, we could utilize the Agilent Seahorse XFp for dissected fat body tissue. This will allow for both the glycolytic rate and oxidative phosphorylation to be compared to wildtype (Fernandez-Acosta et al., 2022). It would also be beneficial to measure the ATP production in the hTau^{K369I} mutant and conduct a lipidomic analysis of the fat body (Fernandez-Acosta et al., 2022). One can also use microscopy to assess reactive oxygen species using Dihydroethidium (DHE; Fernandez-Acosta et al., 2022). These assays would complement morphological analysis of lipid droplets in the fat body. Based on preliminary lipid droplet staining, we would repeat the experiment in younger flies and also include a membrane staining to distinguish peripheral and interior lipid

droplets. Quantification of lipid droplet position within the cell would be particularly interesting due to the changes in mRNA levels of *apolpp* and *FASN1*, which have been shown to impact peripheral and interior droplets, respectively (Ugrankar et al., 2019). Also, introducing a starvation challenge will allow for the assessment of susceptibility of the flies and could indicate problems with lipid mobilization as discussed in Chapter 4.4. In addition to imaging lipid droplets, we could also measure the TAG and trehalose levels (Aditi et al., 2016; Wat et al., 2020). FTD patients have hyperphagia, increased caloric intake and higher BMI compared to controls and other neurodegenerative diseases (Ahmed et al., 2014a; Ahmed et al., 2014b; Ahmed et al., 2016). We observed that the hTau^{K369I} flies have higher body weight than the hTau^{WT} (**Figure 34**). To see if flies also have hyperphagia or preference for high sucrose foods, we could conduct feeding preference assay using the FLIC Fly Liquid-Food Interaction Counter, which allows for high-throughput testing and preference measures (Ro et al., 2014). All of these assays are well established in mouse models and thus in the future, it would be interesting to see how the different model systems coincide. This work could also be expanded to assess patients because, unlike the brain, the adipose tissue can be biopsied; however, there is risk of hemorrhage from this procedure (Kettwich et al., 2012). Alternatively, patients could be worked up with lipid panels and other metabolic tests that are commonly used in clinic for cardiovascular health assessment and metabolic disorders.

In sum

The *Drosophila* model system allows for a quicker assessment of disease phenotypes due to the low cost and quick lifespan. Based on these findings, there are many avenues to pursue in this model, which can then be further validated in a high order model organism, such as mice. This work also highlights why single-cell genomics is useful. Although previous research has linked FTD to metabolic dysregulation, we did not start this project wanting to investigate this particular aspect. However, given the number of changes in the fat body at an early age, we decided to characterize the changes within the fat body in the hTau^{K369I} mutant. The major questions from this dissertation are the following: (1) What is the function of *Fhos* in neuron and glia in development? (2) Could *Fhos* be interacting with the LINC complex and are actin dynamics changed in the hTau^{K369I} mutant? (3) How is h Tau^{K369I} changing heterochromatin distribution, and does it correspond to the changes in accessibility? (4) Do the metabolic gene expression changes in the fat body persist with aging? (5) Is the metabolic function altered in the hTau^{K369I} mutant and do we see similar changes in the other FTD-associated mutants? (6) Are there regions of susceptibility for neurodegeneration when *Fhos* is manipulated in the fat body and what could be the mechanistic basis for this susceptibility?

Throughout this work, I have come back to one of my favorite lines by Joni Mitchell: "I've looked at clouds from both sides now; From up and down and still somehow; It's cloud illusions I recall; I really don't know clouds at all." No matter how you look at the clouds of cells within a UMAP or any scientific question. There

will always be more to know, more to discover and more to show you how much we don't know. It was my goal with this dissertation to highlight some interesting tidbits from my studies of these clouds and I hope that one day the clouds will part, and we will have a more complete understanding.

References

- Abrahamsen, N., Martinez, A., Kjær, T., Søndergaard, L., Bownes, M., 1993. Cis-regulatory sequences leading to female-specific expression of yolk protein genes 1 and 2 in the fat body of *Drosophila melanogaster*. *Molec. Gen. Genet.* 237, 41–48. <https://doi.org/10.1007/BF00282782>
- Aditi, K., Shakarad, M.N., Agrawal, N., 2016. Altered lipid metabolism in *Drosophila* model of Huntington's disease. *Sci Rep* 6, 31411. <https://doi.org/10.1038/srep31411>
- Ahmed, R.M., Irish, M., Henning, E., Dermody, N., Bartley, L., Kiernan, M.C., Piguet, O., Farooqi, S., Hodges, J.R., 2016. Assessment of Eating Behavior Disturbance and Associated Neural Networks in Frontotemporal Dementia. *JAMA Neurol* 73, 282–290. <https://doi.org/10.1001/jamaneurol.2015.4478>
- Ahmed, R.M., Irish, M., Kam, J., van Keizerswaard, J., Bartley, L., Samaras, K., Hodges, J.R., Piguet, O., 2014b. Quantifying the Eating Abnormalities in Frontotemporal Dementia. *JAMA Neurology* 71, 1540–1546. <https://doi.org/10.1001/jamaneurol.2014.1931>
- Ahmed, R.M., Irish, M., van Eersel, J., Ittner, A., Ke, Y.D., Volkerling, A., van der Hoven, J., Tanaka, K., Karl, T., Kassiou, M., Kril, J.J., Piguet, O., Götz, J., Kiernan, M.C., Halliday, G.M., Hodges, J.R., Ittner, L.M., 2017. Mouse models of frontotemporal dementia: A comparison of phenotypes with clinical symptomatology. *Neuroscience & Biobehavioral Reviews* 74, 126–138. <https://doi.org/10.1016/j.neubiorev.2017.01.004>
- Ahmed, R.M., Mioshi, E., Caga, J., Shibata, M., Zoing, M., Bartley, L., Piguet, O., Hodges, J.R., Kiernan, M.C., 2014a. Body mass index delineates ALS from FTD: implications for metabolic health. *J Neurol* 261, 1774–1780. <https://doi.org/10.1007/s00415-014-7416-6>
- Anhezini, L., Saita, A.P., Costa, M.S.A., Ramos, R.G.P., Simon, C.R., 2012. Fhos encodes a *Drosophila* Formin-Like Protein participating in autophagic programmed cell death. *genesis* 50, 672–684. <https://doi.org/10.1002/dvg.22025>
- Antoku, S., Schwartz, T.U., Gundersen, G.G., 2023. FHODs: Nuclear tethered formins for nuclear mechanotransduction. *Front. Cell Dev. Biol.* 11. <https://doi.org/10.3389/fcell.2023.1160219>
- Antoku, S., Wu, W., Joseph, L.C., Morrow, J.P., Worman, H.J., Gundersen, G.G., 2019. ERK1/2 Phosphorylation of FHOD Connects Signaling and Nuclear Positioning Alternations in Cardiac Laminopathy. *Dev Cell* 51, 602-616.e12. <https://doi.org/10.1016/j.devcel.2019.10.023>
- Antoku, S., Zhu, R., Kutscheidt, S., Fackler, O.T., Gundersen, G.G., 2015. Reinforcing the LINC complex connection to actin filaments: the role of

- FHOD1 in TAN line formation and nuclear movement. *Cell Cycle* 14, 2200–2205. <https://doi.org/10.1080/15384101.2015.1053665>
- Artiushin, G., Sehgal, A., 2020. The Glial Perspective on Sleep and Circadian Rhythms. *Annu Rev Neurosci* 43, 119–140. <https://doi.org/10.1146/annurev-neuro-091819-094557>
- Bardai, F.H., Wang, L., Mutreja, Y., Yenjerla, M., Gamblin, T.C., Feany, M.B., 2018. A Conserved Cytoskeletal Signaling Cascade Mediates Neurotoxicity of FTDP-17 Tau Mutations In Vivo. *J Neurosci* 38, 108–119. <https://doi.org/10.1523/JNEUROSCI.1550-17.2017>
- Baumbach, J., Xu, Y., Hehlert, P., Kühnlein, R.P., 2014. *Gaq*, *Gγ1* and *Plc21C* Control *Drosophila* Body Fat Storage. *Journal of Genetics and Genomics, Lipid Metabolism and Lipidomics: An Emerging Frontier in Biology* 41, 283–292. <https://doi.org/10.1016/j.jgg.2014.03.005>
- Beaulieu-Bonneau, S., Hudon, C., 2009. Sleep disturbances in older adults with mild cognitive impairment. *Int Psychogeriatr* 21, 654–666. <https://doi.org/10.1017/S1041610209009120>
- Beaven, R., Dzhindzhev, N.S., Qu, Y., Hahn, I., Dajas-Bailador, F., Ohkura, H., Prokop, A., 2015. *Drosophila* CLIP-190 and mammalian CLIP-170 display reduced microtubule plus end association in the nervous system. *Mol Biol Cell* 26, 1491–1508. <https://doi.org/10.1091/mbc.E14-06-1083>
- Beckmann, A., Ramirez, P., Gamez, M., Gonzalez, E., Mange, J.D., Bieniek, K.F., Ray, W.J., Frost, B., 2023. Moesin is an effector of tau-induced actin overstabilization, cell cycle activation, and neurotoxicity in Alzheimer's disease. *iScience* 26. <https://doi.org/10.1016/j.isci.2023.106152>
- Benzer, S., 1967. BEHAVIORAL MUTANTS OF *Drosophila* ISOLATED BY COUNTERCURRENT DISTRIBUTION. *Proc Natl Acad Sci U S A* 58, 1112–1119.
- Bharucha, K.N., Tarr, P., Zipursky, S.L., 2008. A glucagon-like endocrine pathway in *Drosophila* modulates both lipid and carbohydrate homeostasis. *Journal of Experimental Biology* 211, 3103–3110. <https://doi.org/10.1242/jeb.016451>
- Booth, L.N., Brunet, A., 2016. The Aging Epigenome. *Molecular Cell* 62, 728–744. <https://doi.org/10.1016/j.molcel.2016.05.013>
- Boppana, S., Kendall, N., Akinrinsola, O., White, D., Patel, K., Lawal, H., 2017. Immunolocalization of the vesicular acetylcholine transporter in larval and adult *Drosophila* neurons. *Neurosci Lett* 643, 76–83. <https://doi.org/10.1016/j.neulet.2017.02.012>
- Bosch, M., Parton, R.G., Pol, A., 2020. Lipid droplets, bioenergetic fluxes, and metabolic flexibility. *Seminars in Cell & Developmental Biology*, The

- molecular cell biology, metabolism and physiological functions of lipid droplets 108, 33–46. <https://doi.org/10.1016/j.semcdb.2020.02.010>
- Boulan, L., Andersen, D., Colombani, J., Boone, E., Léopold, P., 2019. Inter-Organ Growth Coordination Is Mediated by the Xrp1-Dilp8 Axis in *Drosophila*. *Dev Cell* 49, 811-818.e4. <https://doi.org/10.1016/j.devcel.2019.03.016>
- Brand, A.H., Perrimon, N., 1993. Targeted gene expression as a means of altering cell fates and generating dominant phenotypes. *Development* 118, 401–415. <https://doi.org/10.1242/dev.118.2.401>
- Bukhari, H., Nithianandam, V., Battaglia, R.A., Cicalo, A., Sarkar, S., Comjean, A., Hu, Y., Leventhal, M.J., Dong, X., Feany, M.B., 2024. Transcriptional programs mediating neuronal toxicity and altered glial–neuronal signaling in a *Drosophila* knock-in tauopathy model. *Genome Res.* 34, 590–605. <https://doi.org/10.1101/gr.278576.123>
- Butterfield, D.A., Favia, M., Spera, I., Campanella, A., Lanza, M., Castegna, A., 2022. Metabolic Features of Brain Function with Relevance to Clinical Features of Alzheimer and Parkinson Diseases. *Molecules* 27, 951. <https://doi.org/10.3390/molecules27030951>
- Cardarelli, R., Kertesz, A., Knebl, J.A., 2010. Frontotemporal Dementia: A Review for Primary Care Physicians. *AFP* 82, 1372–1377.
- Carnemolla, S.E., Hsieh, J.W., Sipione, R., Landis, B.N., Kumfor, F., Piguet, O., Manuel, A.L., 2020. Olfactory dysfunction in frontotemporal dementia and psychiatric disorders: A systematic review. *Neuroscience & Biobehavioral Reviews* 118, 588–611. <https://doi.org/10.1016/j.neubiorev.2020.08.002>
- Cassar, M., Law, A.D., Chow, E.S., Giebultowicz, J.M., Kretschmar, D., 2020. Disease-Associated Mutant Tau Prevents Circadian Changes in the Cytoskeleton of Central Pacemaker Neurons. *Front. Neurosci.* 14. <https://doi.org/10.3389/fnins.2020.00232>
- Chen, H., Zheng, X., Xiao, D., Zheng, Y., 2016. Age-associated de-repression of retrotransposons in the *Drosophila* fat body, its potential cause and consequence. *Aging Cell* 15, 542–552. <https://doi.org/10.1111/accel.12465>
- Cheong, H., Yorimitsu, T., Reggiori, F., Legakis, J.E., Wang, C.-W., Klionsky, D.J., 2005. Atg17 Regulates the Magnitude of the Autophagic Response. *Mol Biol Cell* 16, 3438–3453. <https://doi.org/10.1091/mbc.E04-10-0894>
- Cornelison, G.L., Levy, S.A., Jenson, T., Frost, B., 2019. Tau-induced nuclear envelope invagination causes a toxic accumulation of mRNA in *Drosophila*. *Aging Cell* 18, e12847. <https://doi.org/10.1111/accel.12847>
- Coutinho-Budd, J.C., Sheehan, A.E., Freeman, M.R., 2017. The secreted neurotrophin Spätzle 3 promotes glial morphogenesis and supports neuronal

- survival and function. *Genes Dev.* 31, 2023–2038.
<https://doi.org/10.1101/gad.305888.117>
- Csikós, G., Lippai, M., Lukácsovich, T., Juhász, G., Henn, L., Erdélyi, M., Maróy, P., Sass, M., 2009. A novel role for the *Drosophila* epsin (Iqf): Involvement in autophagy. *Autophagy* 5, 636–648. <https://doi.org/10.4161/auto.5.5.8168>
- Cusanovich, D.A., Reddington, J.P., Garfield, D.A., Daza, R.M., Aghamirzaie, D., Marco-Ferreres, R., Pliner, H.A., Christiansen, L., Qiu, X., Steemers, F.J., Trapnell, C., Shendure, J., Furlong, E.E.M., 2018. The *cis*-regulatory dynamics of embryonic development at single-cell resolution. *Nature* 555, 538–542. <https://doi.org/10.1038/nature25981>
- Daniels, R.W., Collins, C.A., Chen, K., Gelfand, M.V., Featherstone, D.E., DiAntonio, A., 2006. A Single Vesicular Glutamate Transporter Is Sufficient to Fill a Synaptic Vesicle. *Neuron* 49, 11–16.
<https://doi.org/10.1016/j.neuron.2005.11.032>
- Dauwalder, B., Tsujimoto, S., Moss, J., Mattox, W., 2002. The *Drosophila takeout* gene is regulated by the somatic sex-determination pathway and affects male courtship behavior. *Genes Dev.* 16, 2879–2892.
<https://doi.org/10.1101/gad.1010302>
- Davie, K., Janssens, J., Koldere, D., De Waegeneer, M., Pech, U., Kreft, Ł., Aibar, S., Makhzami, S., Christiaens, V., Bravo González-Blas, C., Poovathingal, S., Hulselmans, G., Spanier, K.I., Moerman, T., Vanspauwen, B., Geurs, S., Voet, T., Lammertyn, J., Thienpont, B., Liu, S., Konstantinides, N., Fiers, M., Verstreken, P., Aerts, S., 2018. A Single-Cell Transcriptome Atlas of the Aging *Drosophila* Brain. *Cell* 174, 982-998.e20.
<https://doi.org/10.1016/j.cell.2018.05.057>
- DePew, A.T., Aimino, M.A., Mosca, T.J., 2019. The Tenets of Teneurin: Conserved Mechanisms Regulate Diverse Developmental Processes in the *Drosophila* Nervous System. *Front. Neurosci.* 13.
<https://doi.org/10.3389/fnins.2019.00027>
- DeSalvo, M.K., Hindle, S.J., Rusan, Z.M., Orng, S., Eddison, M., Halliwill, K., Bainton, R.J., 2014. The *Drosophila* surface glia transcriptome: evolutionary conserved blood-brain barrier processes. *Front Neurosci* 8, 346.
<https://doi.org/10.3389/fnins.2014.00346>
- DeWane, G., Salvi, A.M., DeMali, K.A., 2021. Fueling the cytoskeleton – links between cell metabolism and actin remodeling. *Journal of Cell Science* 134, jcs248385. <https://doi.org/10.1242/jcs.248385>
- Diaconeasa, B., Mazock, G.H., Mahowald, A.P., Dubreuil, R.R., 2013. Genetic Studies of Spectrin in the Larval Fat Body of *Drosophila melanogaster*: Evidence for a Novel Lipid Uptake Apparatus. *Genetics* 195, 871–881.
<https://doi.org/10.1534/genetics.113.155192>

- Dogterom, M., Koenderink, G.H., 2019. Actin–microtubule crosstalk in cell biology. *Nature Reviews Molecular Cell Biology* 20, 38–54.
<https://doi.org/10.1038/s41580-018-0067-1>
- Dollar, G., Gombos, R., Barnett, A.A., Sanchez Hernandez, D., Maung, S.M.T., Mihály, J., Jenny, A., 2016. Unique and Overlapping Functions of Formins Frl and DAAM During Ommatidial Rotation and Neuronal Development in *Drosophila*. *Genetics* 202, 1135–1151.
<https://doi.org/10.1534/genetics.115.181438>
- Domoto-Reilly, K., Davis, M.Y., Keene, C.D., Bird, T.D., 2017. Unusually long duration and delayed penetrance in a family with FTD and mutation in MAPT (V337M). *Am J Med Genet B Neuropsychiatr Genet* 174, 70–74.
<https://doi.org/10.1002/ajmg.b.32443>
- Donlea, J.M., Pimentel, D., Talbot, C.B., Kempf, A., Omoto, J.J., Hartenstein, V., Miesenböck, G., 2018. Recurrent Circuitry for Balancing Sleep Need and Sleep. *Neuron* 97, 378-389.e4. <https://doi.org/10.1016/j.neuron.2017.12.016>
- Dorn, G.W., Clark, C.F., Eschenbacher, W.H., Kang, M.-Y., Engelhard, J.T., Warner, S.J., Matkovich, S.J., Jowdy, C.C., 2011. MARF and Opa1 Control Mitochondrial and Cardiac Function in *Drosophila*. *Circulation Research* 108, 12–17. <https://doi.org/10.1161/CIRCRESAHA.110.236745>
- DuBoff, B., Götz, J., Feany, M.B., 2012. Tau promotes neurodegeneration via DRP1 mislocalization in vivo. *Neuron* 75, 618–632.
<https://doi.org/10.1016/j.neuron.2012.06.026>
- Dujardin, S., Colin, M., Buée, L., 2015. Invited review: Animal models of tauopathies and their implications for research/translation into the clinic. *Neuropathology and Applied Neurobiology* 41, 59–80.
<https://doi.org/10.1111/nan.12200>
- Elahi, F.M., Miller, B.L., 2017. A clinicopathological approach to the diagnosis of dementia. *Nature Reviews Neurology* 13, 457–476.
<https://doi.org/10.1038/nrneurol.2017.96>
- Enell, L., Hamasaka, Y., Kolodziejczyk, A., Nässel, D.R., 2007. γ -Aminobutyric acid (GABA) signaling components in *Drosophila*: Immunocytochemical localization of GABAB receptors in relation to the GABAA receptor subunit RDL and a vesicular GABA transporter. *Journal of Comparative Neurology* 505, 18–31. <https://doi.org/10.1002/cne.21472>
- Fenoglio, C., Scarpini, E., Serpente, M., Galimberti, D., 2018. Role of Genetics and Epigenetics in the Pathogenesis of Alzheimer’s Disease and Frontotemporal Dementia1. *J Alzheimers Dis* 62, 913–932.
<https://doi.org/10.3233/JAD-170702>
- Fernandez-Acosta, M., Romero, J.I., Bernabó, G., Velázquez-Campos, G.M., Gonzalez, N., Mares, M.L., Werbajh, S., Avendaño-Vázquez, L.A.,

- Rechberger, G.N., Kühnlein, R.P., Marino-Buslje, C., Cantera, R., Rezaval, C., Ceriani, M.F., 2022. orsai, the Drosophila homolog of human ETRF1, links lipid catabolism to growth control. *BMC Biol* 20, 233. <https://doi.org/10.1186/s12915-022-01417-w>
- Feuillette, S., Charbonnier, C., Frebourg, T., Champion, D., Lecourtois, M., 2020. A Connected Network of Interacting Proteins Is Involved in Human-Tau Toxicity in Drosophila. *Front. Neurosci.* 14. <https://doi.org/10.3389/fnins.2020.00068>
- Fong, H., Wang, C., Knoferle, J., Walker, D., Balestra, M.E., Tong, L.M., Leung, L., Ring, K.L., Seeley, W.W., Karydas, A., Kshirsagar, M.A., Boxer, A.L., Kosik, K.S., Miller, B.L., Huang, Y., 2013. Genetic Correction of Tauopathy Phenotypes in Neurons Derived from Human Induced Pluripotent Stem Cells. *Stem Cell Reports* 1, 226–234. <https://doi.org/10.1016/j.stemcr.2013.08.001>
- Freeman, M.R., 2015. Drosophila Central Nervous System Glia. *Cold Spring Harb Perspect Biol* 7, a020552. <https://doi.org/10.1101/cshperspect.a020552>
- Frost, B., 2023. Alzheimer's disease and related tauopathies: disorders of disrupted neuronal identity. *Trends in Neurosciences* 46, 797–813. <https://doi.org/10.1016/j.tins.2023.07.006>
- Frost, B., Bardai, F.H., Feany, M.B., 2016. Lamin Dysfunction Mediates Neurodegeneration in Tauopathies. *Curr. Biol.* 26, 129–136. <https://doi.org/10.1016/j.cub.2015.11.039>
- Frost, B., Hemberg, M., Lewis, J., Feany, M.B., 2014. Tau promotes neurodegeneration through global chromatin relaxation. *Nat Neurosci* 17, 357–366. <https://doi.org/10.1038/nn.3639>
- Fulga, T.A., Elson-Schwab, I., Khurana, V., Steinhilb, M.L., Spires, T.L., Hyman, B.T., Feany, M.B., 2007. Abnormal bundling and accumulation of F-actin mediates tau-induced neuronal degeneration in vivo. *Nat Cell Biol* 9, 139–148. <https://doi.org/10.1038/ncb1528>
- Garrett, L.R., Niccoli, T., 2022. Frontotemporal Dementia and Glucose Metabolism. *Front Neurosci* 16, 812222. <https://doi.org/10.3389/fnins.2022.812222>
- Ghetti, B., Oblak, A.L., Boeve, B.F., Johnson, K.A., Dickerson, B.C., Goedert, M., 2015. Invited review: Frontotemporal dementia caused by microtubule-associated protein tau gene (MAPT) mutations: a chameleon for neuropathology and neuroimaging. *Neuropathol. Appl. Neurobiol.* 41, 24–46. <https://doi.org/10.1111/nan.12213>
- Ghosh, S., Singh, A., Mandal, S., Mandal, L., 2015. Active Hematopoietic Hubs in Drosophila Adults Generate Hemocytes and Contribute to Immune

- Response. *Developmental Cell* 33, 478–488.
<https://doi.org/10.1016/j.devcel.2015.03.014>
- Giong, H.-K., Subramanian, M., Yu, K., Lee, J.-S., 2021. Non-Rodent Genetic Animal Models for Studying Tauopathy: Review of *Drosophila*, Zebrafish, and *C. elegans* Models. *Int J Mol Sci* 22, 8465.
<https://doi.org/10.3390/ijms22168465>
- Giovannone, B., Lee, E., Laviola, L., Giorgino, F., Cleveland, K.A., Smith, R.J., 2003. Two novel proteins that are linked to insulin-like growth factor (IGF-I) receptors by the Grb10 adapter and modulate IGF-I signaling. *J Biol Chem* 278, 31564–31573. <https://doi.org/10.1074/jbc.M211572200>
- Giovannone, B., Tsiaras, W.G., de la Monte, S., Klysik, J., Lautier, C., Karashchuk, G., Goldwurm, S., Smith, R.J., 2009. GIGYF2 gene disruption in mice results in neurodegeneration and altered insulin-like growth factor signaling. *Hum Mol Genet* 18, 4629–4639.
<https://doi.org/10.1093/hmg/ddp430>
- Girard, V., Jollivet, F., Knittelfelder, O., Celle, M., Arsac, J.-N., Chatelain, G., Van den Brink, D.M., Baron, T., Shevchenko, A., Kühnlein, R.P., Davoust, N., Mollereau, B., 2021. Abnormal accumulation of lipid droplets in neurons induces the conversion of alpha-Synuclein to proteolytic resistant forms in a *Drosophila* model of Parkinson's disease. *PLoS Genet* 17, e1009921.
<https://doi.org/10.1371/journal.pgen.1009921>
- Górska-Andrzejak, J., Salvaterra, P.M., Meinertzhagen, I.A., Krzeptowski, W., Görlich, A., Pyza, E., 2009. Cyclical expression of Na⁺/K⁺-ATPase in the visual system of *Drosophila melanogaster*. *J Insect Physiol* 55, 459–468.
<https://doi.org/10.1016/j.jinsphys.2009.02.003>
- Granja, J.M., Corces, M.R., Pierce, S.E., Bagdatli, S.T., Choudhry, H., Chang, H.Y., Greenleaf, W.J., 2021. ArchR is a scalable software package for integrative single-cell chromatin accessibility analysis. *Nature Genetics* 53, 403–411. <https://doi.org/10.1038/s41588-021-00790-6>
- Grönke, S., Mildner, A., Fellert, S., Tennagels, N., Petry, S., Müller, G., Jäckle, H., Kühnlein, R.P., 2005. Brummer lipase is an evolutionary conserved fat storage regulator in *Drosophila*. *Cell Metabolism* 1, 323–330.
<https://doi.org/10.1016/j.cmet.2005.04.003>
- Haithcock, E., Dayani, Y., Neufeld, E., Zahand, A.J., Feinstein, N., Mattout, A., Gruenbaum, Y., Liu, J., 2005. Age-related changes of nuclear architecture in *Caenorhabditis elegans*. *Proceedings of the National Academy of Sciences* 102, 16690–16695. <https://doi.org/10.1073/pnas.0506955102>
- Hao, Y., Hao, S., Andersen-Nissen, E., Mauck, W.M., Zheng, S., Butler, A., Lee, M.J., Wilk, A.J., Darby, C., Zager, M., Hoffman, P., Stoeckius, M., Papalexi, E., Mimitou, E.P., Jain, J., Srivastava, A., Stuart, T., Fleming, L.M., Yeung, B., Rogers, A.J., McElrath, J.M., Blish, C.A., Gottardo, R., Smibert, P.,

- Satija, R., 2021. Integrated analysis of multimodal single-cell data. *Cell* 184, 3573-3587.e29. <https://doi.org/10.1016/j.cell.2021.04.048>
- Heier, C., Klishch, S., Stilbytska, O., Semaniuk, U., Lushchak, O., 2021. The *Drosophila* model to interrogate triacylglycerol biology. *Biochimica et Biophysica Acta (BBA) - Molecular and Cell Biology of Lipids* 1866, 158924. <https://doi.org/10.1016/j.bbalip.2021.158924>
- Hendricks, J.C., Sehgal, A., 2004. Why a Fly? Using *Drosophila* to Understand the Genetics of Circadian Rhythms and Sleep. *Sleep* 27, 334–342. <https://doi.org/10.1093/sleep/27.2.334>
- Hu, Y., Comjean, A., Attrill, H., Antonazzo, G., Thurmond, J., Chen, W., Li, F., Chao, T., Mohr, S.E., Brown, N.H., Perrimon, N., 2023. PANGEA: a new gene set enrichment tool for *Drosophila* and common research organisms. *Nucleic Acids Res* 51, W419–W426. <https://doi.org/10.1093/nar/gkad331>
- Illescas, M., Peñas, A., Arenas, J., Martín, M.A., Ugalde, C., 2021. Regulation of Mitochondrial Function by the Actin Cytoskeleton. *Front Cell Dev Biol* 9, 795838. <https://doi.org/10.3389/fcell.2021.795838>
- Ito, K., 1994. Concise Atlas of A Fly Brain [WWW Document]. URL https://jfly.uni-koeln.de/html/figures/Brain_K_Ito/brain_k_ito.html (accessed 6.25.24).
- Ito, K., Shinomiya, K., Ito, M., Armstrong, J.D., Boyan, G., Hartenstein, V., Harzsch, S., Heisenberg, M., Homberg, U., Jenett, A., Keshishian, H., Restifo, L.L., Rössler, W., Simpson, J.H., Strausfeld, N.J., Strauss, R., Vosshall, L.B., Insect Brain Name Working Group, 2014. A systematic nomenclature for the insect brain. *Neuron* 81, 755–765. <https://doi.org/10.1016/j.neuron.2013.12.017>
- Izumi, Y., Furuse, K., Furuse, M., 2021. The novel membrane protein Hoka regulates septate junction organization and stem cell homeostasis in the *Drosophila* gut. *Journal of Cell Science* 134, jcs257022. <https://doi.org/10.1242/jcs.257022>
- Janssens, J., Mangeol, P., Hecker, N., Partel, G., Spanier, K., Ismail, J., Hulselmans, G., Aerts, S., Schnorrer, F., 2024. Spatial transcriptomics in adult *Drosophila* reveals new cell types in the brain and identifies subcellular mRNA patterns in muscles. *eLife* 13. <https://doi.org/10.7554/eLife.92618.1>
- Kaltenbach, L.S., Romero, E., Becklin, R.R., Chettier, R., Bell, R., Phansalkar, A., Strand, A., Torcassi, C., Savage, J., Hurlburt, A., Cha, G.-H., Ukani, L., Chepanoske, C.L., Zhen, Y., Sahasrabudhe, S., Olson, J., Kurschner, C., Ellerby, L.M., Peltier, J.M., Botas, J., Hughes, R.E., 2007. Huntingtin Interacting Proteins Are Genetic Modifiers of Neurodegeneration. *PLoS Genet* 3, e82. <https://doi.org/10.1371/journal.pgen.0030082>
- Kang, J.-E., Lim, M.M., Bateman, R.J., Lee, J.J., Smyth, L.P., Cirrito, J.R., Fujiki, N., Nishino, S., Holtzman, D.M., 2009. Amyloid- β Dynamics Are Regulated

- by Orexin and the Sleep-Wake Cycle. *Science* 326, 1005–1007.
<https://doi.org/10.1126/science.1180962>
- Kast, D.J., Dominguez, R., 2017. The Cytoskeleton–Autophagy Connection. *Current Biology* 27, R318–R326. <https://doi.org/10.1016/j.cub.2017.02.061>
- Kato, K., Orihara-Ono, M., Awasaki, T., 2020. Multiple lineages enable robust development of the neuropil-glia architecture in adult *Drosophila*. *Development* 147, dev184085. <https://doi.org/10.1242/dev.184085>
- Kettwich, L.G., Sibbitt, W.L., Emil, N.S., Ashraf, U., Sanchez-Goettler, L., Thariani, Y., Bankhurst, A.D., 2012. New Device Technologies for Subcutaneous Fat Biopsy. *Amyloid* 19, 66–73.
<https://doi.org/10.3109/13506129.2012.666508>
- Kim, A.B., Arvanitakis, Z., 2023. Insulin resistance, cognition, and Alzheimer disease. *Obesity* 31, 1486–1498. <https://doi.org/10.1002/oby.23761>
- Kim, M., Ho, A., Lee, J.H., 2017. Autophagy and Human Neurodegenerative Diseases-A Fly’s Perspective. *Int J Mol Sci* 18, 1596.
<https://doi.org/10.3390/ijms18071596>
- Kim, M., Semple, I., Kim, B., Kiers, A., Nam, S., Park, H.-W., Park, H., Ro, S.-H., Kim, J.-S., Juhász, G., Lee, J.H., 2015. *Drosophila* Gyf/GRB10 interacting GYF protein is an autophagy regulator that controls neuron and muscle homeostasis. *Autophagy* 11, 1358–1372.
<https://doi.org/10.1080/15548627.2015.1063766>
- Lai, W.-F., Wong, W.-T., 2020. Roles of the actin cytoskeleton in aging and age-associated diseases. *Ageing Res Rev* 58, 101021.
<https://doi.org/10.1016/j.arr.2020.101021>
- Lammel, U., Bechtold, M., Risse, B., Berh, D., Fleige, A., Bunse, I., Jiang, X., Klämbt, C., Bogdan, S., 2014. The *Drosophila* FHOD1-like formin Knittrig acts through Rok to promote stress fiber formation and directed macrophage migration during the cellular immune response. *Development* 141, 1366–1380. <https://doi.org/10.1242/dev.101352>
- Larson, K., Yan, S.-J., Tsurumi, A., Liu, J., Zhou, J., Gaur, K., Guo, D., Eickbush, T.H., Li, W.X., 2012. Heterochromatin Formation Promotes Longevity and Represses Ribosomal RNA Synthesis. *PLOS Genetics* 8, e1002473.
<https://doi.org/10.1371/journal.pgen.1002473>
- Law, A.D., Cassar, M., Long, D.M., Chow, E.S., Giebultowicz, J.M., Venkataramanan, A., Strauss, R., Kretschmar, D., 2022. FTD-associated mutations in Tau result in a combination of dominant and recessive phenotypes. *Neurobiol Dis* 170, 105770.
<https://doi.org/10.1016/j.nbd.2022.105770>

- Lazareva, A.A., Roman, G., Mattox, W., Hardin, P.E., Dauwalder, B., 2007. A Role for the Adult Fat Body in Drosophila Male Courtship Behavior. *PLoS Genet* 3, e16. <https://doi.org/10.1371/journal.pgen.0030016>
- Lee, M.Y., Lee, J., Hyeon, S.J., Cho, H., Hwang, Y.J., Shin, J.-Y., McKee, A.C., Kowall, N.W., Kim, J.-I., Stein, T.D., Hwang, D., Ryu, H., 2020. Epigenome signatures landscaped by histone H3K9me3 are associated with the synaptic dysfunction in Alzheimer's disease. *Aging Cell* n/a, e13153. <https://doi.org/10.1111/acer.13153>
- Lee, S., Huang, E.J., 2017. Modeling ALS and FTD with iPSC-derived neurons. *Brain Research, Modeling neurological diseases with patient-derived neurons* 1656, 88–97. <https://doi.org/10.1016/j.brainres.2015.10.003>
- Liu, F., Gong, C.-X., 2008. Tau exon 10 alternative splicing and tauopathies. *Mol Neurodegener* 3, 8. <https://doi.org/10.1186/1750-1326-3-8>
- Liu, L., Zhang, K., Sandoval, H., Yamamoto, S., Jaiswal, M., Sanz, E., Li, Z., Hui, J., Graham, B.H., Quintana, A., Bellen, H.J., 2015. Glial Lipid Droplets and ROS Induced by Mitochondrial Defects Promote Neurodegeneration. *Cell* 160, 177–190. <https://doi.org/10.1016/j.cell.2014.12.019>
- Liu, X., Jiao, B., Shen, L., 2018. The Epigenetics of Alzheimer's Disease: Factors and Therapeutic Implications. *Front. Genet.* 9. <https://doi.org/10.3389/fgene.2018.00579>
- Lu, T.-C., Brbić, M., Park, Y.-J., Jackson, T., Chen, J., Kolluru, S.S., Qi, Y., Katheder, N.S., Cai, X.T., Lee, S., Chen, Y.-C., Auld, N., Liang, C.-Y., Ding, S.H., Welsch, D., D'Souza, S., Pisco, A.O., Jones, R.C., Leskovec, J., Lai, E.C., Bellen, H.J., Luo, L., Jasper, H., Quake, S.R., Li, H., 2023. Aging Fly Cell Atlas identifies exhaustive aging features at cellular resolution. *Science* 380, eadg0934. <https://doi.org/10.1126/science.adg0934>
- Luquez, T., Gaur, P., Kosater, I.M., Lam, M., Lee, D.I., Mares, J., Paryani, F., Yadav, A., Menon, V., 2022. Cell type-specific changes identified by single-cell transcriptomics in Alzheimer's disease. *Genome Med* 14, 136. <https://doi.org/10.1186/s13073-022-01136-5>
- Maciver, S.K., Harrington, C.R., 1995. Two actin binding proteins, actin depolymerizing factor and cofilin, are associated with Hirano bodies. *Neuroreport* 6, 1985–1988. <https://doi.org/10.1097/00001756-199510010-00008>
- Maina, M.B., Bailey, L.J., Wagih, S., Biasetti, L., Pollack, S.J., Quinn, J.P., Thorpe, J.R., Doherty, A.J., Serpell, L.C., 2018. The involvement of tau in nucleolar transcription and the stress response. *Acta Neuropathologica Communications* 6, 70. <https://doi.org/10.1186/s40478-018-0565-6>

- Majercak, J., Sidote, D., Hardin, P.E., Edery, I., 1999. How a Circadian Clock Adapts to Seasonal Decreases in Temperature and Day Length. *Neuron* 24, 219–230. [https://doi.org/10.1016/S0896-6273\(00\)80834-X](https://doi.org/10.1016/S0896-6273(00)80834-X)
- Mallik, M., Catinozzi, M., Hug, C.B., Zhang, L., Wagner, M., Bussmann, J., Bittern, J., Mersmann, S., Klämbt, C., Drexler, H.C.A., Huynen, M.A., Vaquerizas, J.M., Storkebaum, E., 2018. Xrp1 genetically interacts with the ALS-associated FUS orthologue caz and mediates its toxicity. *Journal of Cell Biology* 217, 3947–3964. <https://doi.org/10.1083/jcb.201802151>
- Maloney, B., Lahiri, D.K., 2016. Epigenetics of dementia: understanding the disease as a transformation rather than a state. *The Lancet Neurology* 15, 760–774. [https://doi.org/10.1016/S1474-4422\(16\)00065-X](https://doi.org/10.1016/S1474-4422(16)00065-X)
- Mangleburg, C.G., Wu, T., Yalamanchili, H.K., Guo, C., Hsieh, Y.-C., Duong, D.M., Dammer, E.B., De Jager, P.L., Seyfried, N.T., Liu, Z., Shulman, J.M., 2020. Integrated analysis of the aging brain transcriptome and proteome in tauopathy. *Mol Neurodegener* 15, 56. <https://doi.org/10.1186/s13024-020-00405-4>
- Mansuroglu, Z., Benhelli-Mokrani, H., Marcato, V., Sultan, A., Violet, M., Chauderlier, A., Delattre, L., Loyens, A., Talahari, S., Bégard, S., Nessler, F., Colin, M., Souès, S., Lefebvre, B., Buée, L., Galas, M.-C., Bonnefoy, E., 2016. Loss of Tau protein affects the structure, transcription and repair of neuronal pericentromeric heterochromatin. *Scientific Reports* 6, 1–16. <https://doi.org/10.1038/srep33047>
- Mariano, V., Achsel, T., Bagni, C., Kanellopoulos, A.K., 2020. Modelling Learning and Memory in *Drosophila* to Understand Intellectual Disabilities. *Neuroscience, Animal Models of Neurodevelopmental Disorders* 445, 12–30. <https://doi.org/10.1016/j.neuroscience.2020.07.034>
- Mattila, J., Hietakangas, V., 2017. Regulation of Carbohydrate Energy Metabolism in *Drosophila melanogaster*. *Genetics* 207, 1231–1253. <https://doi.org/10.1534/genetics.117.199885>
- McCarter, S.J., St Louis, E.K., Boeve, B.F., 2016. Sleep Disturbances in Frontotemporal Dementia. *Curr Neurol Neurosci Rep* 16, 85. <https://doi.org/10.1007/s11910-016-0680-3>
- McMullen, E., Hertenstein, H., Strassburger, K., Deharde, L., Brankatschk, M., Schirmeier, S., 2023. Glycolytically impaired *Drosophila* glial cells fuel neural metabolism via β -oxidation. *Nat Commun* 14, 2996. <https://doi.org/10.1038/s41467-023-38813-x>
- Ménard, I., Gervais, F.G., Nicholson, D.W., Roy, S., 2006. Caspase-3 cleaves the formin-homology-domain-containing protein FHOD1 during apoptosis to generate a C-terminal fragment that is targeted to the nucleolus. *Apoptosis* 11, 1863–1876. <https://doi.org/10.1007/s10495-006-0087-8>

- Meschi, E., Delanoue, R., 2021. Adipokine and fat body in flies: Connecting organs. *Molecular and Cellular Endocrinology* 533, 111339. <https://doi.org/10.1016/j.mce.2021.111339>
- Miki, T., Yokota, O., Takenoshita, S., Mori, Y., Yamazaki, K., Ozaki, Y., Ueno, S., Haraguchi, T., Ishizu, H., Kuroda, S., Terada, S., Yamada, N., 2018. Frontotemporal lobar degeneration due to P301L tau mutation showing apathy and severe frontal atrophy but lacking other behavioral changes: A case report and literature review. *Neuropathology* 38, 268–280. <https://doi.org/10.1111/neup.12441>
- Miller, B.L., Darby, A.L., Swartz, J.R., Yener, G.G., Mena, I., 1995. Dietary changes, compulsions and sexual behavior in frontotemporal degeneration. *Dementia* 6, 195–199. <https://doi.org/10.1159/000106946>
- Molaei, M., Vandehoef, C., Karpac, J., 2019. NF- κ B Shapes Metabolic Adaptation by Attenuating Foxo-Mediated Lipolysis in *Drosophila*. *Developmental Cell* 49, 802-810.e6. <https://doi.org/10.1016/j.devcel.2019.04.009>
- Moore, K.M., Nicholas, J., Grossman, M., McMillan, C.T., Irwin, D.J., Massimo, L., Van Deerlin, V.M., Warren, J.D., Fox, N.C., Rossor, M.N., Mead, S., Bocchetta, M., Boeve, B.F., Knopman, D.S., Graff-Radford, N.R., Forsberg, L.K., Rademakers, R., Wszolek, Z.K., van Swieten, J.C., Jiskoot, L.C., Meeter, L.H., Dopper, E.G., Papma, J.M., Snowden, J.S., Saxon, J., Jones, M., Pickering-Brown, S., Le Ber, I., Camuzat, A., Brice, A., Caroppo, P., Ghidoni, R., Pievani, M., Benussi, L., Binetti, G., Dickerson, B.C., Lucente, D., Krivensky, S., Graff, C., Öijerstedt, L., Fallström, M., Thonberg, H., Ghoshal, N., Morris, J.C., Borroni, B., Benussi, A., Padovani, A., Galimberti, D., Scarpini, E., Fumagalli, G.G., Mackenzie, I.R., Hsiung, G.-Y.R., Sengdy, P., Boxer, A.L., Rosen, H., Taylor, J.B., Synofzik, M., Wilke, C., Sulzer, P., Hodges, J.R., Halliday, G., Kwok, J., Sanchez-Valle, R., Lladó, A., Borrego-Ecija, S., Santana, I., Almeida, M.R., Tábuas-Pereira, M., Moreno, F., Barandiaran, M., Indakoetxea, B., Levin, J., Danek, A., Rowe, J.B., Cope, T.E., Otto, M., Anderl-Straub, S., de Mendonça, A., Maruta, C., Masellis, M., Black, S.E., Couratier, P., Lautrette, G., Huey, E.D., Sorbi, S., Nacmias, B., Laforce, R., Tremblay, M.-P.L., Vandenberghe, R., Damme, P.V., Rogalski, E.J., Weintraub, S., Gerhard, A., Onyike, C.U., Ducharme, S., Papageorgiou, S.G., Ng, A.S.L., Brodtmann, A., Finger, E., Guerreiro, R., Bras, J., Rohrer, J.D., FTD Prevention Initiative, 2020. Age at symptom onset and death and disease duration in genetic frontotemporal dementia: an international retrospective cohort study. *Lancet Neurol* 19, 145–156. [https://doi.org/10.1016/S1474-4422\(19\)30394-1](https://doi.org/10.1016/S1474-4422(19)30394-1)
- Nässel, D.R., Enell, L.E., Santos, J.G., Wegener, C., Johard, H.A., 2008. A large population of diverse neurons in the *Drosophila* central nervous system expresses short neuropeptide F, suggesting multiple distributed peptide functions. *BMC Neuroscience* 9, 90. <https://doi.org/10.1186/1471-2202-9-90>

- Neumann, M., Schulz-Schaeffer, W., Crowther, R.A., Smith, M.J., Spillantini, M.G., Goedert, M., Kretzschmar, H.A., 2001. Pick's disease associated with the novel Tau gene mutation K369I. *Ann Neurol* 50, 503–513.
<https://doi.org/10.1002/ana.1223>
- Ng, C.-H., Basil, A.H., Hang, L., Tan, R., Goh, K.-L., O'Neill, S., Zhang, X., Yu, F., Lim, K.-L., 2017. Genetic or pharmacological activation of the *Drosophila* PGC-1 α ortholog *spargel* rescues the disease phenotypes of genetic models of Parkinson's disease. *Neurobiology of Aging* 55, 33–37.
<https://doi.org/10.1016/j.neurobiolaging.2017.03.017>
- Oliveras-Cañellas, N., Castells-Nobau, A., de la Vega-Correa, L., Latorre-Luque, J., Motger-Albertí, A., Arnoriaga-Rodriguez, M., Garre-Olmo, J., Zapata-Tona, C., Coll-Martínez, C., Ramió-Torrentà, L., Moreno-Navarrete, J.M., Puig, J., Villarroya, F., Ramos, R., Casadó-Anguera, V., Martín-García, E., Maldonado, R., Mayneris-Perxachs, J., Fernández-Real, J.M., 2023. Adipose tissue coregulates cognitive function. *Science Advances* 9, eadg4017. <https://doi.org/10.1126/sciadv.adg4017>
- Ordóñez, D.G., Lee, M.K., Feany, M.B., 2018. α -synuclein Induces Mitochondrial Dysfunction through Spectrin and the Actin Cytoskeleton. *Neuron* 97, 108-124.e6. <https://doi.org/10.1016/j.neuron.2017.11.036>
- Palanker, L., Tennesen, J.M., Lam, G., Thummel, C.S., 2009. *Drosophila* HNF4 regulates lipid mobilization and beta-oxidation. *Cell Metab* 9, 228–239.
<https://doi.org/10.1016/j.cmet.2009.01.009>
- Palm, W., Sampaio, J.L., Brankatschk, M., Carvalho, M., Mahmoud, A., Shevchenko, A., Eaton, S., 2012. Lipoproteins in *Drosophila melanogaster*—Assembly, Function, and Influence on Tissue Lipid Composition. *PLoS Genet* 8, e1002828. <https://doi.org/10.1371/journal.pgen.1002828>
- Palu, R.A.S., Chow, C.Y., 2018. Baldspot/ELOVL6 is a conserved modifier of disease and the ER stress response. *PLOS Genetics* 14, e1007557.
<https://doi.org/10.1371/journal.pgen.1007557>
- Paonessa, F., Evans, L.D., Solanki, R., Larriou, D., Wray, S., Hardy, J., Jackson, S.P., Livesey, F.J., 2019. Microtubules Deform the Nuclear Membrane and Disrupt Nucleocytoplasmic Transport in Tau-Mediated Frontotemporal Dementia. *Cell Reports* 26, 582-593.e5.
<https://doi.org/10.1016/j.celrep.2018.12.085>
- Parisi, M., Li, R., Oliver, B., 2011. Lipid profiles of female and male *Drosophila*. *BMC Research Notes* 4, 198. <https://doi.org/10.1186/1756-0500-4-198>
- Patel, A.A., Oztug Durer, Z.A., van Loon, A.P., Bremer, K.V., Quinlan, M.E., 2018. *Drosophila* and human FHOD family formin proteins nucleate actin filaments. *J Biol Chem* 293, 532–540.
<https://doi.org/10.1074/jbc.M117.800888>

- Patterson, K., Molofsky, A.B., Robinson, C., Acosta, S., Cater, C., Fischer, J.A., 2004. The Functions of Klarsicht and Nuclear Lamin in Developmentally Regulated Nuclear Migrations of Photoreceptor Cells in the *Drosophila* Eye. *MBoC* 15, 600–610. <https://doi.org/10.1091/mbc.e03-06-0374>
- Picard, C., Nilsson, N., Labonté, A., Auld, D., Rosa-Neto, P., Initiative, the A.D.N., Ashton, N.J., Zetterberg, H., Blennow, K., Breitner, J.C.B., Villeneuve, S., Poirier, J., Group, for the P.-A. research, 2022. Apolipoprotein B is a novel marker for early tau pathology in Alzheimer's disease. *Alzheimer's & Dementia* 18, 875–887. <https://doi.org/10.1002/alz.12442>
- Picelli, S., Björklund, Å.K., Reinius, B., Sagasser, S., Winberg, G., Sandberg, R., 2014. Tn5 transposase and tagmentation procedures for massively scaled sequencing projects. *Genome Res.* 24, 2033–2040. <https://doi.org/10.1101/gr.177881.114>
- Pick, S., Strauss, R., 2005. Goal-Driven Behavioral Adaptations in Gap-Climbing *Drosophila*. *Current Biology* 15, 1473–1478. <https://doi.org/10.1016/j.cub.2005.07.022>
- Pollak, C.P., Perlick, D., 1991. Sleep problems and institutionalization of the elderly. *J Geriatr Psychiatry Neurol* 4, 204–210. <https://doi.org/10.1177/089198879100400405>
- Poorkaj, P., Bird, T.D., Wijsman, E., Nemens, E., Garruto, R.M., Anderson, L., Andreadis, A., Wiederholt, W.C., Raskind, M., Schellenberg, G.D., 1998. Tau is a candidate gene for chromosome 17 frontotemporal dementia. *Ann Neurol* 43, 815–825. <https://doi.org/10.1002/ana.410430617>
- Prince, M., Wimo, A., Guerchet, M., Ali, G.-C., Wu, Y.-T., Prina, M., 2015. World Alzheimer Report 2015, The Global Impact of Dementia: An analysis of prevalence, incidence, cost and trends. *Alzheimer's Disease International, World Alzheimer Report.*
- R Core Team, 2021. R: A language and environment for statistical computing.
- Rasch, B., Born, J., 2013. About sleep's role in memory. *Physiol Rev* 93, 681–766. <https://doi.org/10.1152/physrev.00032.2012>
- Ries, A.-S., Hermanns, T., Poeck, B., Strauss, R., 2017. Serotonin modulates a depression-like state in *Drosophila* responsive to lithium treatment. *Nat Commun* 8, 15738. <https://doi.org/10.1038/ncomms15738>
- Ro, J., Harvanek, Z.M., Pletcher, S.D., 2014. FLIC: High-Throughput, Continuous Analysis of Feeding Behaviors in *Drosophila*. *PLoS One* 9, e101107. <https://doi.org/10.1371/journal.pone.0101107>
- Roh, J.H., Huang, Y., Bero, A.W., Kasten, T., Stewart, F.R., Bateman, R.J., Holtzman, D.M., 2012. Disruption of the Sleep-Wake Cycle and Diurnal Fluctuation of β -Amyloid in Mice with Alzheimer's Disease Pathology.

- Science Translational Medicine 4, 150ra122-150ra122.
<https://doi.org/10.1126/scitranslmed.3004291>
- Romero-Bueno, R., Ruiz, P. de la C., Artal-Sanz, M., Askjaer, P., Dobrzynska, A., 2019. Nuclear Organization in Stress and Aging. *Cells* 8.
<https://doi.org/10.3390/cells8070664>
- Rybak, J., Talarico, G., Ruiz, S., Arnold, C., Cantera, R., Hansson, B.S., 2016. Synaptic circuitry of identified neurons in the antennal lobe of *Drosophila melanogaster*. *J Comp Neurol* 524, 1920–1956.
<https://doi.org/10.1002/cne.23966>
- Sarkar, S., Olsen, A.L., Sygnecka, K., Lohr, K.M., Feany, M.B., 2021. α -synuclein impairs autophagosome maturation through abnormal actin stabilization. *PLoS Genet* 17, e1009359. <https://doi.org/10.1371/journal.pgen.1009359>
- Sbodio, J.I., Snyder, S.H., Paul, B.D., 2019. Regulators of the transsulfuration pathway. *Br J Pharmacol* 176, 583–593. <https://doi.org/10.1111/bph.14446>
- Scaffidi, P., Misteli, T., 2006. Lamin A-Dependent Nuclear Defects in Human Aging. *Science* 312, 1059–1063. <https://doi.org/10.1126/science.1127168>
- Schindelin, J., Arganda-Carreras, I., Frise, E., Kaynig, V., Longair, M., Pietzsch, T., Preibisch, S., Rueden, C., Saalfeld, S., Schmid, B., Tinevez, J.-Y., White, D.J., Hartenstein, V., Eliceiri, K., Tomancak, P., Cardona, A., 2012. Fiji: an open-source platform for biological-image analysis. *Nat Methods* 9, 676–682. <https://doi.org/10.1038/nmeth.2019>
- Schmid, E., Schinaman, J., Williams, K., Walker, D., 2023. Accumulation of F-actin drives brain aging and limits healthspan in *Drosophila*. *Res Sq* rs.3.rs-3158290. <https://doi.org/10.21203/rs.3.rs-3158290/v1>
- Schwartz, C., Fischer, M., Mamchaoui, K., Bigot, A., Lok, T., Verdier, C., Duperray, A., Michel, R., Holt, I., Voit, T., Quijano-Roy, S., Bonne, G., Coirault, C., 2017. Lamins and nesprin-1 mediate inside-out mechanical coupling in muscle cell precursors through FHOD1. *Sci Rep* 7, 1253.
<https://doi.org/10.1038/s41598-017-01324-z>
- Sen, P., Shah, P.P., Nativio, R., Berger, S.L., 2016. Epigenetic Mechanisms of Longevity and Aging. *Cell* 166, 822–839.
<https://doi.org/10.1016/j.cell.2016.07.050>
- Senthilan, P.R., Grebler, R., Reinhard, N., Rieger, D., Helfrich-Förster, C., 2019. Role of Rhodopsins as Circadian Photoreceptors in the *Drosophila melanogaster*. *Biology (Basel)* 8, 6. <https://doi.org/10.3390/biology8010006>
- Sexton, C.E., Bitan, G., Bowles, K.R., Brys, M., Buée, L., Maina, M.B., Clelland, C.D., Cohen, A.D., Crary, J.F., Dage, J.L., Diaz, K., Frost, B., Gan, L., Goate, A.M., Golbe, L.I., Hansson, O., Karch, C.M., Kolb, H.C., La Joie, R., Lee, S.E., Matallana, D., Miller, B.L., Onyike, C.U., Quiroz, Y.T., Rexach, J.E., Rohrer, J.D., Rommel, A., Sadri-Vakili, G., Schindler, S.E., Schneider,

- J.A., Sperling, R.A., Teunissen, C.E., Weninger, S.C., Worley, S.L., Zheng, H., Carrillo, M.C., 2024. Novel avenues of tau research. *Alzheimer's & Dementia* 20, 2240–2261. <https://doi.org/10.1002/alz.13533>
- Shwartz, A., Dhanyasi, N., Schejter, E.D., Shilo, B.-Z., 2016. The Drosophila formin Fhos is a primary mediator of sarcomeric thin-filament array assembly. *Elife* 5, e16540. <https://doi.org/10.7554/eLife.16540>
- Sirkis, D.W., Geier, E.G., Bonham, L.W., Karch, C.M., Yokoyama, J.S., 2019. Recent advances in the genetics of frontotemporal dementia. *Curr Genet Med Rep* 7, 41–52. <https://doi.org/10.1007/s40142-019-0160-6>
- Sonn, J.Y., Lee, J., Sung, M.K., Ri, H., Choi, J.K., Lim, C., Choe, J., 2018. Serine metabolism in the brain regulates starvation-induced sleep suppression in *Drosophila melanogaster*. *Proceedings of the National Academy of Sciences* 115, 7129–7134. <https://doi.org/10.1073/pnas.1719033115>
- Sotiropoulos, I., Galas, M.-C., Silva, J.M., Skoulakis, E., Wegmann, S., Maina, M.B., Blum, D., Sayas, C.L., Mandelkow, E.-M., Mandelkow, E., Spillantini, M.G., Sousa, N., Avila, J., Medina, M., Mudher, A., Buee, L., 2017. Atypical, non-standard functions of the microtubule associated Tau protein. *Acta Neuropathol Commun* 5. <https://doi.org/10.1186/s40478-017-0489-6>
- Sposito, T., Preza, E., Mahoney, C.J., Setó-Salvia, N., Ryan, N.S., Morris, H.R., Arber, C., Devine, M.J., Houlden, H., Warner, T.T., Bushell, T.J., Zagnoni, M., Kunath, T., Livesey, F.J., Fox, N.C., Rossor, M.N., Hardy, J., Wray, S., 2015. Developmental regulation of tau splicing is disrupted in stem cell-derived neurons from frontotemporal dementia patients with the 10 + 16 splice-site mutation in MAPT. *Human Molecular Genetics* 24, 5260–5269. <https://doi.org/10.1093/hmg/ddv246>
- Sterne, G.R., Otsuna, H., Dickson, B.J., Scott, K., 2021. Classification and genetic targeting of cell types in the primary taste and premotor center of the adult *Drosophila* brain. *eLife* 10, e71679. <https://doi.org/10.7554/eLife.71679>
- Stork, T., Bernardos, R., Freeman, M.R., 2012. Analysis of Glial Cell Development and Function in *Drosophila*. *Cold Spring Harb Protoc* 2012, pdb.top067587. <https://doi.org/10.1101/pdb.top067587>
- Strauss, R., Heisenberg, M., 1993. A higher control center of locomotor behavior in the *Drosophila* brain. *J Neurosci* 13, 1852–1861. <https://doi.org/10.1523/JNEUROSCI.13-05-01852.1993>
- Sun, J., Liu, C., Bai, X., Li, X., Li, J., Zhang, Z., Zhang, Y., Guo, J., Li, Y., 2017. *Drosophila* FIT is a protein-specific satiety hormone essential for feeding control. *Nat Commun* 8, 14161. <https://doi.org/10.1038/ncomms14161>
- Sun, X., Morozova, T., Sonnenfeld, M., 2006. Glial and Neuronal Functions of the *Drosophila* Homolog of the Human SWI/SNF Gene ATR-X (DATR-X) and the jing Zinc-Finger Gene Specify the Lateral Positioning of Longitudinal Glia

- and Axons. *Genetics* 173, 1397–1415.
<https://doi.org/10.1534/genetics.106.057893>
- Sun, Y., Yolitz, J., Wang, C., Spangler, E., Zhan, M., Zou, S., 2013. Aging Studies in *Drosophila melanogaster*. *Methods Mol Biol* 1048, 77–93.
https://doi.org/10.1007/978-1-62703-556-9_7
- Sunderhaus, E.R., Kretschmar, D., 2016. Mass Histology to Quantify Neurodegeneration in *Drosophila*. *JoVE* 54809.
<https://doi.org/10.3791/54809>
- Tellis, M.B., Kotkar, H.M., Joshi, R.S., 2023. Regulation of trehalose metabolism in insects: from genes to the metabolite window. *Glycobiology* 33, 262–273.
<https://doi.org/10.1093/glycob/cwad011>
- Thornton, C.A., Mulqueen, R.M., Torkenczy, K.A., Nishida, A., Lowenstein, E.G., Fields, A.J., Steemers, F.J., Zhang, W., McConnell, H.L., Woltjer, R.L., Mishra, A., Wright, K.M., Adey, A.C., 2021. Spatially mapped single-cell chromatin accessibility. *Nature Communications* 12, 1274.
<https://doi.org/10.1038/s41467-021-21515-7>
- Tiefenböck, S.K., Baltzer, C., Egli, N.A., Frei, C., 2010. The *Drosophila* PGC-1 homologue Spargel coordinates mitochondrial activity to insulin signalling. *The EMBO Journal* 29, 171–183. <https://doi.org/10.1038/emboj.2009.330>
- Ugrankar, R., Bowerman, J., Hariri, H., Chandra, M., Chen, K., Bossanyi, M.-F., Datta, S., Rogers, S., Eckert, K.M., Vale, G., Victoria, A., Fresquez, J., McDonald, J.G., Jean, S., Collins, B.M., Henne, W.M., 2019. *Drosophila* Snazarus regulates a lipid droplet population at plasma membrane-droplet contacts in adipocytes. *Dev Cell* 50, 557-572.e5.
<https://doi.org/10.1016/j.devcel.2019.07.021>
- Ugrankar-Banerjee, R., Tran, S., Bowerman, J., Kovalenko, A., Paul, B., Henne, W.M., 2023. The fat body cortical actin network regulates *Drosophila* inter-organ nutrient trafficking, signaling, and adipose cell size. *eLife* 12, e81170.
<https://doi.org/10.7554/eLife.81170>
- Villeponteau, B., 1997. The heterochromatin loss model of aging. *Experimental Gerontology, Proceedings of the Third International Symposium on the Neurobiology and Neuroendocrinology of Aging* 32, 383–394.
[https://doi.org/10.1016/S0531-5565\(96\)00155-6](https://doi.org/10.1016/S0531-5565(96)00155-6)
- Vinayagam, A., Kulkarni, M.M., Sopko, R., Sun, X., Hu, Y., Nand, A., Villalta, C., Moghimi, A., Yang, X., Mohr, S.E., Hong, P., Asara, J.M., Perrimon, N., 2016. An Integrative Analysis of the InR/PI3K/Akt Network Identifies the Dynamic Response to Insulin Signaling. *Cell Reports* 16, 3062–3074.
<https://doi.org/10.1016/j.celrep.2016.08.029>

- Volkenhoff, A., Weiler, A., Letzel, M., Stehling, M., Klämbt, C., Schirmeier, S., 2015. Glial Glycolysis Is Essential for Neuronal Survival in *Drosophila*. *Cell Metabolism* 22, 437–447. <https://doi.org/10.1016/j.cmet.2015.07.006>
- Wat, L.W., Chao, C., Bartlett, R., Buchanan, J.L., Millington, J.W., Chih, H.J., Chowdhury, Z.S., Biswas, P., Huang, V., Shin, L.J., Wang, L.C., Gauthier, M.-P.L., Barone, M.C., Montooth, K.L., Welte, M.A., Rideout, E.J., 2020. A role for triglyceride lipase brummer in the regulation of sex differences in *Drosophila* fat storage and breakdown. *PLOS Biology* 18, e3000595. <https://doi.org/10.1371/journal.pbio.3000595>
- Weaver, L.N., Ma, T., Drummond-Barbosa, D., 2020. Analysis of Gal4 Expression Patterns in Adult *Drosophila* Females. *G3 (Bethesda)* 10, 4147–4158. <https://doi.org/10.1534/g3.120.401676>
- Weston, L., Coutts, A.S., La Thangue, N.B., 2012. Actin nucleators in the nucleus: an emerging theme. *J Cell Sci* 125, 3519–3527. <https://doi.org/10.1242/jcs.099523>
- White, K.E., Humphrey, D.M., Hirth, F., 2010. The Dopaminergic System in the Aging Brain of *Drosophila*. *Front. Neurosci.* 4. <https://doi.org/10.3389/fnins.2010.00205>
- Winick-Ng, W., Rylett, R.J., 2018. Into the Fourth Dimension: Dysregulation of Genome Architecture in Aging and Alzheimer's Disease. *Front. Mol. Neurosci.* 11. <https://doi.org/10.3389/fnmol.2018.00060>
- Wolock, S.L., Lopez, R., Klein, A.M., 2019. Scrublet: Computational Identification of Cell Doublets in Single-Cell Transcriptomic Data. *cells* 8, 281-291.e9. <https://doi.org/10.1016/j.cels.2018.11.005>
- Wu, T., Deger, J.M., Ye, H., Guo, C., Dhindsa, J., Pekarek, B.T., Al-Ouran, R., Liu, Z., Al-Ramahi, I., Botas, J., Shulman, J.M., 2023. Tau polarizes an aging transcriptional signature to excitatory neurons and glia. *eLife* 12, e85251. <https://doi.org/10.7554/eLife.85251>
- Xu, H., Lee, S., Suzuki, E., Dugan, K.D., Stoddard, A., Li, H., Chodosh, L.A., Montell, C., 2004. A lysosomal tetraspanin associated with retinal degeneration identified via a genome-wide screen. *The EMBO Journal* 23, 811–822. <https://doi.org/10.1038/sj.emboj.7600112>
- Xu, K., DiAngelo, J.R., Hughes, M.E., Hogenesch, J.B., Sehgal, A., 2011. The Circadian Clock Interacts with Metabolic Physiology to Influence Reproductive Fitness. *Cell Metabolism* 13, 639–654. <https://doi.org/10.1016/j.cmet.2011.05.001>
- Yang, D., Wang, X., Zhang, L., Fang, Y., Zheng, Q., Liu, X., Yu, W., Chen, S., Ying, J., Hua, F., 2022. Lipid metabolism and storage in neuroglia: role in brain development and neurodegenerative diseases. *Cell & Bioscience* 12, 106. <https://doi.org/10.1186/s13578-022-00828-0>

- Yasuyama, K., Kitamoto, T., Salvaterra, P.M., 1996. Differential regulation of choline acetyltransferase expression in adult *Drosophila melanogaster* brain. *Journal of Neurobiology* 30, 205–218. [https://doi.org/10.1002/\(SICI\)1097-4695\(199606\)30:2<205::AID-NEU3>3.0.CO;2-9](https://doi.org/10.1002/(SICI)1097-4695(199606)30:2<205::AID-NEU3>3.0.CO;2-9)
- Young, M.D., Behjati, S., 2020. SoupX removes ambient RNA contamination from droplet-based single-cell RNA sequencing data. *GigaScience* 9, g1aa151. <https://doi.org/10.1093/gigascience/g1aa151>
- Yurgel, M.E., Shah, K.D., Brown, E.B., Burns, C., Bennick, R.A., DiAngelo, J.R., Keene, A.C., 2018. Ade2 Functions in the *Drosophila* Fat Body To Promote Sleep. *G3 (Bethesda)* 8, 3385–3395. <https://doi.org/10.1534/g3.118.200554>
- Zappia, M.P., Guarner, A., Kellie-Smith, N., Rogers, A., Morris, R., Nicolay, B., Boukhali, M., Haas, W., Dyson, N.J., Frolov, M.V., 2021. E2F/Dp inactivation in fat body cells triggers systemic metabolic changes. *eLife* 10, e67753. <https://doi.org/10.7554/eLife.67753>
- Zhao, P., Huang, P., Xu, T., Xiang, X., Sun, Y., Liu, Jingqi, Yan, C., Wang, L., Gao, J., Cui, S., Wang, X., Zhan, L., Song, H., Liu, Jingnan, Song, W., Liu, Y., 2021. Fat body Ire1 regulates lipid homeostasis through the Xbp1s-FoxO axis in *Drosophila*. *iScience* 24, 102819. <https://doi.org/10.1016/j.isci.2021.102819>
- Zheng, H., Yang, X., Xi, Y., 2016. Fat body remodeling and homeostasis control in *Drosophila*. *Life Sciences* 167, 22–31. <https://doi.org/10.1016/j.lfs.2016.10.019>
- Zhu, Y., Nern, A., Zipursky, S.L., Frye, M.A., 2009. Peripheral Visual Circuits Functionally Segregate Motion and Phototaxis Behaviors in the Fly. *Current Biology* 19, 613–619. <https://doi.org/10.1016/j.cub.2009.02.053>